Time evolution and steady states of dissipative quantum many-body systems

M.Sc. Vincent Raphael Overbeck

2018

Referent: Dr. Hendrik Weimer

Korreferent: Prof. Dr. Klemens Hammerer

Tag der Promotion: 28.05.2018

Abstract

The simulation of open quantum systems is an urgent but challenging task in theoretical physics. We apply a variational principle to calculate the steady state and the time evolution of open quantum systems. The variational approach is based on minimizing the trace norm of the density matrix and its time derivatives according to the quantum master equation. This approach allows us to reduce the problem of calculating the states of open quantum many-body systems to a modest number of variational parameters. We perform a variational analysis of the steady state of a dissipative transverse-field Ising model that preserves the Z_2- symmetry. An experimental realization of the model based on Rydberg atoms is suggested. We expand the variational norm with respect to a suitable order parameter corresponding to the Landau theory of closed quantum systems. It turns out that the phase diagram is significantly altered compared to its equilibrium counterpart, exhibiting inter alia a multicritical point. As the true steady state in general is outside of the variational class, we estimate the validity of the variational product state by including spatial inhomogeneities in the analysis. The underlying fluctuations are tightly connected to an effective temperature that is defined via the variational norm at the variational minimum. Knowing the effective temperature enables us to make use of the analogue of the Ginzburg criterion to calculate the upper critical dimension of the system. We also perform a perturbative one loop renormalization group analysis. Higher order terms of the expansion are considered as perturbations which lead to a shift of the position of the tricritical point compared to the product state result, with the shift decreasing exponentially with dimension.

The next chapter deals with the variational time evolution of a two-level dissipative Ising model based on product states and states that include nearest-neighbour correlations. The superiority of correlated states to product states we observe can be traced back to non-Markovian effects present at every time during the relaxation dynamics and even after the steady state is reached. We connect that non-Markovianity to a quantity that is easier accessible in experiments and that is based on the linear quantum entropy.

In the next chapter we analyse a liquid-gas transition of the steady state of the two-level model. In close analogy to the Ginzburg-Landau analysis of the multicritical regime, the time evolution now includes fluctuations whose strength is determined by the variational norm at the variational minimum. The resulting spatial inhomogeneities lead to qualitatively different dynamics compared to the homogeneous case. The efficiency of our variational approach allows us to calculate the time evolution of quite large systems, suppressing the influence of finite size effects.

In the last part of this thesis, we investigate the polarization transfer mechanisms between a Nitrogen Vacancy (NV) center and remote ^{13}C nuclei in diamond. Based on a NV- ^{13}C state mixing mediated by the hyperfine interaction, the polarization transfer can be observed close to the so-called ground state level anti crossing. We calculate the steady state polarization of the NV center and the nuclei and investigate the influence of the strength of the hyperfine interaction and the number of nuclei on it.

Abstract (deutsch)

Die computerbasierte Simulation von offenen Quantensystemen ist relativ anspruchsvoll. In dieser Arbeit werden wir ein Variationsprinzip anwenden, mithilfe dessen sich stationäre Zustände und die Zeitentwicklung offener Quantensysteme berechnen lassen. Dem Variationsprinzip liegt die Spur-Norm der Dichtematrix und ihrer Zeitableitung gemäß der Quanten-Mastergleichung zugrunde. Dieser Ansatz reduziert das Problem der Berechnung von Quantenzuständen von offenen Vielteilchensystemen auf einige wenige Parameter.

Wir führen eine variationelle Berechnung des stationären Zustandes eines dissipativen Ising-Modells durch, welches die Z_2- Symmetrie aufweist. Zudem beschreiben wir eine experimentelle Realisierung mithilfe von Rydberg Atomen. Unsere Vorgehensweise zur Berechnung des Phasendiagrammes entspricht der Landau-Theorie. Das Phasendiagramm weist qualitative Unterschiede im Vergleich zum Gleichgewichts-Ising Modell auf. So ist in diesem Phasendiagramm u.a. ein multikritischer Punkt enthalten. Um die Genauigkeit unseres Produktzustand-Ansatzes zu bestimmen, lassen wir Inhomogenitäten zu. Die zugrunde liegenden Fluktuationen können mit einer effektiven Temperatur in Verbindung gebracht werden, welche wiederum von der minimalen variationellen Norm bestimmt ist. Über diese effektive Temperatur lässt sich ferner das Ginzburg-Kriterium anwenden, mithilfe dessen wir die obere kritische Dimension bestimmen. Desweiteren führen wir eine Renormalisierungsgruppen-Analyse durch. Hierbei werden Terme höherer Ordnung der Entwicklung als Störung angesehen, welche zu einer Verschiebung des trikritischen Punktes aus der Landau-Theorie führen. Quantitativ fällt die Verschiebung exponentiell mit der Dimension ab.

Im nächsten Kapitel wird die variationelle Methode auf die zeitliche Entwicklung eines dissipativen Ising-Modells angewendet, zum einen basierend auf Produktzuständen, zum anderen basierend auf Zuständen, die Nächste-Nachbar-Korrelationen beinhalten. Die höhere Genauigkeit der korrelierten Zustände gegenüber Produktzuständen erklärt sich durch nicht-markovsche Effekte, die zu jedem Zeitpunkt der Evolution, auch nach Erreichen des stationären Zustandes, vorhanden sind. Außerdem wird ein Zusammenhang zwischen der nicht-Markovianität und eines Maßes der Quanteninformation hergestellt, welches experimentell leichter zu messen ist.

In dem nächsten Kapitel analysieren wir einen Phasenübergang erster Ordnung zwischen einer Gas- und einer Flüssigphase. Analog zur Ginzburg-Landau Theorie des stationären Zustandes werden Fluktuationen in die Zeitentwicklung eingefügt. Die entstehenden Inhomogenitäten führen zu einer qualitativ veränderten Zeitentwicklung verglichen mit homogenen Zuständen. Die Effizienz unserer variationellen Minimierung erlaubt es uns, relativ große Systeme zu berechnen.

Im letzten Teil dieser Arbeit wird die Polarisationsübertragung zwischen einem Nitrogen-vacancy (NV) center und entfernt liegenden ^{13}C Atomen in Diamant untersucht. Der Polarisationsübertrag basiert auf einer Mischung der Zustände des NV centers und der Kerne durch die Hyperfein-Wechselwirkung im Bereich des Ground State Level Anti Crossing. Wir berechnen die Polarisation des stationären Zustandes, welche von der Stärke der Hyperfein-Wechselwirkung und der Anzahl der Kerne abhängt.

Keywords

Open quantum systems

Offene Quantensysteme

Dissipative Rydberg gases

Dissipative Rydberg Gase

Quantum phase transitions

Quantenphasenübergänge

Contents

Contents

1. Introduction

No real physical system, whether quantum or not, can be totally decoupled from its environment. This fact makes the theory of open systems crucial in modern physics. As many of the concepts from quantum theory and statistical physics are based on the assumption of perfect isolation, the analysis of open quantum systems poses challenges. The interaction with the uncontrolled environment results in an infinite number of degrees of freedom, which makes the use of an effective theory necessary. This theory neglects all parts of the environment that are supposed to have no or a negligible effect on the evolution of the system of interest. For an accurate description of the state of the system, statistical ensembles of elements of the Hilbert space are needed rather than pure quantum states [1].

Experimental and simulation data indicates that the dynamics of open quantum systems exhibit features whose investigation could push the application of quantum mechanics. While quantum dissipation and accompanying phenomena like decoherence had long been considered an undesired process, dissipative quantum many-body systems offer new possibilites e.g. the controlled preparation of quantum many-body states [2–10]. Through the manipulation of atomic quantum gases, experimentalists reached a regime of strong interactions and controllable dissipation [11–15], providing the basis for such quantum state engineering.

Various approaches for the analysis and calculation of open quantum systems exist. Those methods used for quantum optics [16–19] usually differ from those used in condensed matter and chemical phyiscs [20–23]. There are some major challenges these approaches face: In closed systems, all thermodynamic quantities of interest can be derived from the partition function [24]. A corresponding concept is missing for open systems. Additionally, as in the equilibrium case, the dimensionality of the Hilbert space grows exponentially with the number of particles. Many calculations of dissipative many-body systems are based on mean-field approaches [4, 25–30], even though it has been shown that this ansatz is problematic for open quantum systems [31–33]. These controversies concern even the most simple model for a dissipative quantum many-body system, the dissipative Ising model [26, 31, 34, 35].

Another important aspect of the investigation of open quantum systems is non-Markovianity and its measurement. The assumption of non-Markovianity is based on simplifications that tend to lead to wrong predictions [1].

The natural dissipative element due to the radiative decay of the Rydberg state and the tunability of the interaction and dissipation of Rydberg atoms [36, 37] make ultracold Rydberg gases ideal candidates for the investigation of dissipative quantum many-body systems and the construction of an universal quantum simulator [38]. Rydberg atoms
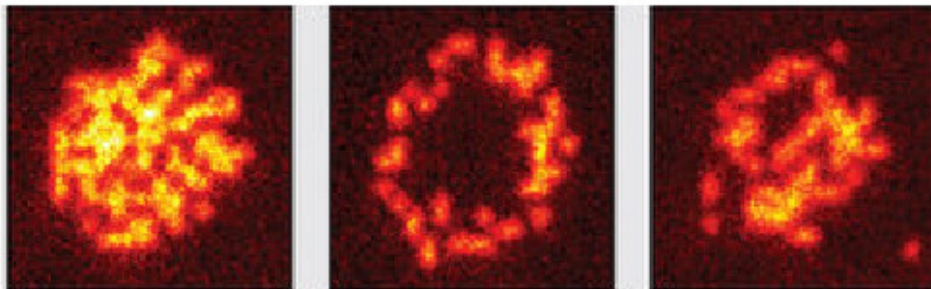
Figure 1.1.: Experimental visualisation of the interaction of dressed Rydberg atoms [64]. In the initial state, all atoms are distributed equally (left side). As the dynamics is highly influenced by long-range interactions, the atoms at the edge of the sample evolve differently, leading to inhomogeneous interference patterns (middle and right side).

are excited to the Rydberg state via a one or two-photon excitation, with their properties showing unusual strong scaling with the principal quantum number [36]. Techniques like Rydberg dressing make the lifetime and the interaction of Rydberg atoms even more controllable [39] and have various applications in theoretical works as well as in experiments [40, 41]. In experiments with Rydberg gases, the interplay of coherent dynamics and dissipation can be studied [42–45]. These dynamics exhibit features not known from equilibrium systems, such as interaction mediated laser cooling [37, 46], dissipative binding mechanisms [47, 48], and the stationary state undergoing phase transitions [12, 25, 26, 35, 49–55].

Another quantum system with dissipative elements are color centers, or defects, in diamond. Among these defects, especially Nitrogen-Vacancy centers consisting of a Nitrogen atom and a vacancy in the diamond structure, attracted much attention. They are promising candidates for various applications, e.g. in quantum photonic technologies [56–58], quantum information [59, 60] and electromagnetic field sensing [61–63].

In the first part of this thesis, we will use a generic variational principle for the analysis of dissipative quantum manby-body systems. The variational principle first arised with Hamilton's principle of stationary action in classical mechanics [65]. Since then, variational approaches have been commonly used e.g. for the minimization of an energy functional to calculate the ground state of a quantum system [66]. Based on a suitable norm of the density matrix and its time derivative, our variational approach reduces computationally intractable problems to just a few variational parameters allowing us to calculate the steady state as well as the time evolution of dissipative Ising models. In both cases, we perform a detailed analysis of the properties of the underlying dynamics and also compare the results for different variational classes. A focus will be on dissipative phase transitions that the steady state undergoes.

In the second part of the thesis, we study the effects of the hyperfine interaction mediated state mixing of an NV center and ^{13}C nuclei in diamond on the transition spectra. Beside the hyperfine interaction, our model includes radio frequency irradiation acting on the NV center and the nuclei and laser illumination as the dissipative process.

1.1. Structure of the thesis

In the following chapter of this thesis, the theoretical concepts, i.e. the mathematical and physical fundaments of the topics presented in this thesis, are described. Among these are the calculus of variations, physical properties of Rydberg atoms, the theory of phase transitions, the foundations of open quantum systems, and, tightly connected to the latter, quantum measures for entropy and non-Markovianity. Additionally, we present an introduction to NV centers in diamond and its electronic properties.

In the third chapter "Variational principle for open quantum systems", we will introduce the method that is used for the analysis of the systems we investigate in this thesis, namely the variational principle, for the steady state and the time evolution. We also present a specific example of how to use it.

The fourth chapter "Multicriticality of the non-equilibrium steady state" deals with spontaneous symmetry breaking in Ising models. In the first part of that chapter, we briefly present the common Ising model in closed quantum systems and its most important properties. Then, we analyse the multicritical properties of the steady state of a dissipative Ising model via the variational principle presented in the previous chapter. In the second part of the chapter, we estimate the validity of the variational product state ansatz by including fluctuations and by performing a renormalization group analysis.

In the fifth chapter we analyse another dissipative Ising model that does not exhibit the Z_2 symmetry. We apply the variational principle of the time evolution, that has been explained in the second part of chapter 3, and compare the evolution based on different variational classes.

The sixth chapter "First order liquid-gas transition" deals with a liquid-gas transition of the two-level dissipative Ising model. Here, we show results of the variational analysis concerning the steady state undergoing a liquid gas transition. In the second part of this chapter, we combine the method of the fluctuation-analysis presented in the fourth chapter with the variational time evolution presented in the fifth chapter. We investigate the properties of the time evolution close to the transition via adding fluctuations to the variational solution.

In the seventh part "Spin bath polarization in nitrogen-vacancy centers", we describe the Hamiltonian of the NV-^{13}C system and the mixing of states close to the Ground state level anti crossing (GSLAC). Finally, we show the steady state polarization of the NV center and the ^{13}C nuclei.

2. Theoretical concepts

In this chapter, we provide the theoretical basis of the work presented in this thesis. In the first part, we introduce the mathematical and physical basis for the variational principle. In the next section, Rydberg atoms and their most important properties are presented. The part 'Open quantum systems' deals with the quantum mechanical description of systems coupled to an uncontrolled environment and the derivative of the quantum master equation. The chapter provides a mathematical definition of (non-)Markovianity. Furthermore, a quantity that measures non-Markovianity in open quantum systems is introduced. In the last part of this chapter, we describe the electronic structure of Nitrogen-Vacancy centers in diamond and briefly explain the ground state state level anti crossing phenomenon.

2.1. Variational principle

Arising with Bernoulli's problem of the brachistochrone, the calculus of variations deals with finding extrema of functionals, i.e. functions of elements of the function space [67]. In this chapter we will introduce the variational principle and its applications in theoretical physics, especially in quantum mechanics. Then, we give a mathematical description of matrix norms on which the functional used in this thesis is based.

2.1.1. Variational principle in classical and quantum mechanics

In classical mechanics, the calculation of the trajectory of a system is based on the minimization of the action S which can be written as [68]

$$S[q] = \int_a^b L(t, q(t), \dot{q}(t)) dx. \tag{2.1}$$

with the Lagrange function L, the time t and the trajectory $q(t)$ and its time derivative $\dot{q}(t)$. Hamilton's principle states that the configuration $\{t, q, \dot{q}\}$ of the system is realized such that the action is stationary (i.e. minimal) and thus fullfils

$$\delta S \equiv 0. \tag{2.2}$$

with the infinitessimal change δS of the action. For a proper choice of the Langrange function, the resulting Euler-Lagrange equations correspond to Newton's equation of motion.

This kind of variational approach and Hamilton's principle of stationary action also finds applications in fields such as electrodynamics and thermodynamics [69].

In a closed quantum system described by a Hamiltonian H, the true ground state can be approximated via a variational approach. The crux of that approach is the minimization of the energy functional [70]

$$E[\Psi] = \frac{\langle \Psi | H | \Psi \rangle}{\langle \Psi | \Psi \rangle}. \tag{2.3}$$

To be explicit, the trial state Ψ depends on intrinsic parameters, which are varied during the minimization process. The true ground state is approximated by the wave function Ψ_0 following from the parameter configuration that leads to the lowest value of the energy-functional, with $E[\Psi_0]$ being the upper bound for the true ground state energy. Variational methods are also used for the computational investigation of quantum many-body phyiscs. One famous example from condensed matter physics is the density functional theory (DFT) [71]. In the scope of DTF theory, the energy is regarded as a functional of the electron density. The minimization of the energy functional leads to the ground state energy, the corresponding electron density comes from the self-consistent solution of the Kohn-Sham equations. Other examples of the application of the variational principle are the matrix product state formalism [72] and machine learning [73].

2.1.2. The trace norm and trace distance

The norm of vectors can be generalized to a norm of matrices. In this thesis, the functional of the variational principle is given as such a matrix norm. A matrix norm fullfils the axioms of vector norms. i.e. the semi positive definitness, linearity and the triangular inequality. Let $\mathcal{K}$ be a field of real or complex numbers. If a vector norm $||x||_V$ of the vector x, $x \in \mathcal{K}^n$, is given, the common induced norm (or operator norm) of the matrix $A \in \mathcal{K}^{m \times n}$ is defined as [74]

$$||A|| = \sup_{x \neq 0} \frac{||Ax||_V}{||x||_V}. \tag{2.4}$$

Another possibility of defining the norm of a matrix is via the singular values. The Schatten norms are important representatives of such norms. The Schatten p-norm is defined as

$$||A||_p = \left(\sum_{i}^{\min\{m,n\}} \varsigma_i^p \right)^{1/p}. \tag{2.5}$$

Here, the ς_i denote the singular values of A. The Schatten norm is unitarily invariant, i.e.

$$||A||_p = ||UAV||_p \tag{2.6}$$

for any unitary matrices U and V. In particular, the Schatten norm is invariant under the unitary transformation $A \to UAU^\dagger$. For $p = 2$, we get the so called Frobenius norm which corresponds to the induced matrix norm if A is a rank-one matrix or a zero matrix. For $p = \infty$, we have the spectral norm, which corresponds to the absolute value of the largest singular value of A. The case $p = 1$ leads to the so called trace-norm or nuclear norm and can be written as

$$||A||_1 = \text{Tr}\{\sqrt{A^\dagger A}\}. \tag{2.7}$$

If A is hermitian, the trace norm corresponds to the sum of the absolute value of the eigenvalues of A, i.e.

$$||A||_1 = \text{Tr}\{|A|\}. \tag{2.8}$$

Among the Schatten norms, the trace norm is the only norm fullfilling the condition

$$||A|| = ||\kappa A||/\kappa. \tag{2.9}$$

with $\kappa > 0$.

The properties of the trace norm makes it an appropriate candidate for applications in quantum mechanics, particularly in quantum information theory. The trace distance D of two different quantum states represented by ρ and σ is given by [75]

$$D = \frac{1}{2}||\rho - \sigma||_1. \tag{2.10}$$

This trace distance tells us about the distinguishability of the two states [76]. The mathemical properties and the physical meaning of the trace norm makes it the norm of choice for our variational analysis.

2.2. Phase transitions

Matter exists in different thermodynamics phases that have different physical and chemical properties. The phases can be classified for example by the aggregate conditions of water or the magnetization of a solid (ferromagnetic and paramagnetic). Since the fundament for the theory of statistical mechanics and the thermodynamics of phase transitions has been laid by Gibbs [77, 78], scientific research has produced at least a partial understanding of phases and phase transitions in both classical and quantum systems. Classical phase transitions can be understood as being driven by temperature fluctuations, whereas quantum phase transitions are driven by quantum fluctuations and strictly speaking can only accur at zero temperature $T = 0$ K [79]. Mathematically, phase transitions are tightly connected to singular behaviour of a thermodynamic quantity. Ehrenfest classified phase transitions by the quantities that show discontinuity, resulting in numbering the different kinds of phase transitions as first order, second order etc. [80]. In modern research of phase transitions, one

distinguishes only between first oder transitions and continuous transitions. In this chapter, we will give a brief overview of the concepts of the classical theory of phase transitions and then switch to its quantum counterpart and explain important concepts and methods of quantum phase transitions.

2.2.1. Classification of phase transitions

In classical thermodynamics, a large number of properties of a thermodynamic system can be drived from the partition function Z. It reads [81]

$$Z = \sum_i e^{-\beta H(s_i)} \tag{2.11}$$

with the Hamiltonian H of the system configuration s_i and $\beta = 1/k_B T$, where k_B is the Boltzmann constant and T is the temperature. The so called internal energy U can be derived from the partition function via the derivative to β and reads

$$U = -\frac{\partial \log Z}{\partial \beta}. \tag{2.12}$$

Then, the Helmhotz free energy A is defined as

$$A = U - TS = -\beta \log Z \tag{2.13}$$

with the entropy S. A thermodynamic system aims to minimize the free energy. Phase transitions occur if the free energy becomes non-analytic.

According to the Ehrenfest classification, the order of the phase transition corresponds to the lowest order of the derivative of the free energy that shows a discontinuity. So at a first order transition this concerns first order derivatives like the entropy and the volume, for a second order transition the response functions like the compressibility and the specific heat show a discontinuous jump [82].

Modern classifications of phase transitions include only two types of phase transitions: First order transitions and continuous transitions. A general description is given in [83]. Consider the bulk free energy density F_B and generalized couplings K_i of the system. If F_B is non-analytic and at least one derivative $\partial F_B/\partial K_i$ is discontinuous one speaks of a first order transition.

If F_B is non-analytic while all first derivatives are continous one speaks of a continuous transition.

2.2.2. Quantum phase transitions

Thermal fluctuations vanish at zero temperature, instead quantum fluctuations arising from the uncertanity principle dominate [79]. Figure (2.1) shows an example of quantum and classical phase transitions in a phase diagram: The second order phase transition line terminates at a critical point at a critical $g = g_c$ and $T = 0K$, where the phase
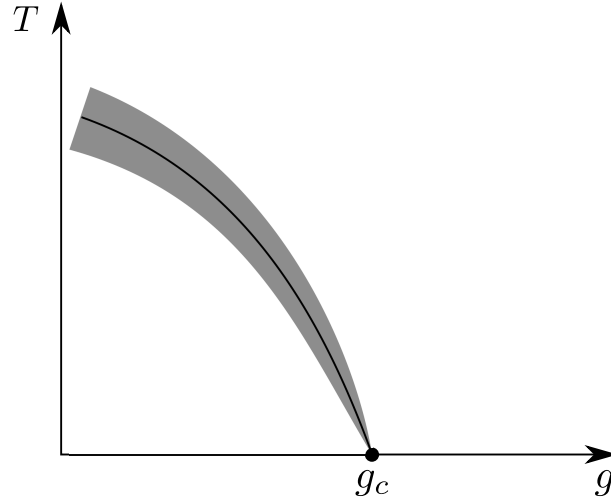
Figure 2.1.: For $T = 0K$ there is a quantum phase transition at $g = g_c$. For $T > 0$, there is a continuous transition that terminates at the quantum critical point. In the shaded region, the classical theory of phase transitions can be applied.

transition is purely quantum. In the immediate area of a quantum critical point, one can study the interplay of quantum and thermal fluctuations. In this case, thermal fluctuations dominate the shaded region around the transition line and the classical theory of phase transitions can be applied. Another more advanced example of the coexistence of a quantum and a classical phase transition in one phase diagram is the Bose-Hubbard-Model [84], where at $T = 0K$, there is a quantum phase transition between a superfluid phase and a Mott insulator. For $T > 0K$, there is a superfluid - normal fluid transition.
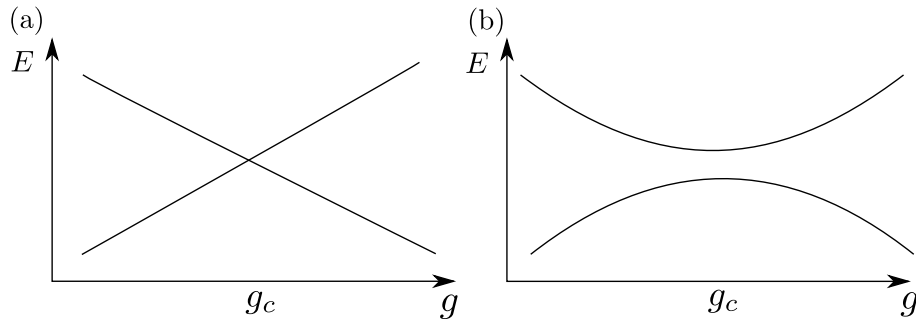
Figure 2.2.: (a): Level crossing of the two lowest eigenenergies of the Hamiltonian $H = H_0 + gH_1$ causing a non-analyticity at $g = g_c$. (b): More common case of an avoided level crossing in a finite system if $[H_0, H_1] \neq 0$.

Corresponding to the classical case, a phase transition occurs in a quantum system if the ground state energy becomes non-analytic. Consider the Hamiltonian

$$H = H_0 + gH_1 \tag{2.14}$$

with the coupling constant g and H_0 and H_1 not depending on g. If H_0 and H_1 commute, there can be a level crossing of the two lowest eigenenergies, which means an excited states becomes the ground state when passing a critical $g = g_c$ [79]. In the more general case of H_0 and H_1 not commuting, there will be an avoided level crossing, see Fig. (2.2 (b)). If we let the system size go to infnity, however, the gap closes leading to a nonanalyticity of the ground state energy.

2.2.3. Landau Theory

Landau's approach to the description of phase transitions is based on the concept of spontaneous symmetry breaking [85]. In more recent work, other classes of phase transitions were discovered, like for instance topological transitions [86]. Landau constructed a generalized mathematical theory making use of the similarities between phase transitions of very different systems. Crucially, a quantity called the order parameter Ψ is introduced to express the status of the symmetry in the system.
In the case of a system described by the classical Ising model, an appropriate order parameter is the magnetization. The low temperature phase has a finite magnetization meaning that the symmetry of the Hamiltonian (invariance under flip of all spins) is broken [79].
Another example of a broken symmetry expressed by an order parameter is the solid phase of matter, where the rotational and translational symmetry are broken. Here, one uses the amplitude of the density wave as the order parameter.
The transition to a superfluid happens when the gauge symmetry of the quantum Hamiltonian is broken. For a strong interacting system, the corresponding order parameter is given by the expectation value of the annihilation operator $\psi(r)$ [87].
In Landau theory, the free energy can be expressed via an expansion in the order parameter $\Psi(\mathbf{r})$, which exhibits a spatial dependence due to for instance thermal fluctuations. As a result, we can regard the free energy F as a functional depending on $\Psi(\mathbf{r})$ and write

$$F = \int d\mathbf{r}\, A + Bh(\mathbf{r})\Phi(\mathbf{r}) + C\Phi(\mathbf{r})^2 + D\Phi(\mathbf{r})^4 + E\left[\nabla\Phi(\mathbf{r})\right]^2. \tag{2.15}$$

The cubic term mostly vanishes due to the presence of a symmetry. The first order term, however, is assumed to decrease more rapid than any other term in the expansion approaching the critical point. The free energy funtional F is then minimized via a variational approach and one gets the ordinary equation [88]

$$0 = h(\mathbf{r}) + (C/B)\Phi(\mathbf{r}) + 4(D/B)\Phi(\mathbf{r})^3 + 2(E/B)\nabla^2\Phi(\mathbf{r}) \tag{2.16}$$

that can be solved with respect to the order parameter. Landau theory claims that this most probable state minimizing the free energy functional is the true state. Landau theory is on the same level as mean field theory as it ignores all fluctuations around this most probable state.

As explained in the following section, the universality class does not only depend on the symmetry of the order parameter, but also on the spatial dimension. The second criterion of equal spatial dimension is not fully included in Landau's theory, but still the gradient term in Eq. (2.15) connects the thermodynamics to the spatial dependence.

2.2.4. Critical exponents and universality

Close to a phase transition, a system can be characterized by its scaling limit. The scaling limit is reached either by sending small lengths, like the lattice spacing in a lattice, to zero while holding 'large' lengths, like the correlation length determinig for example the decay of ground state correlations, fixed. The other way is sending the correlation length to infinity, holding the lattice spacing constant [79]. Close to a critical point with the critical value g_c of a generalized coupling g, the charateristic length scale ξ of a system, diverges as

$$\xi^{-1} = \Lambda |g - g_c|^{\nu}, \tag{2.17}$$

that is, the system is governed by its long range physics. Here, ν is a critical exponent and Λ is an inverse length scale. Approaching the critical point, an observable Θ vanishes as

$$\Theta = \Theta_0 |g - g_c|^{z\nu} \tag{2.18}$$

That behaviour of Θ is valid for both sides of the critical point $g > g_c$ and $g < g_c$. Combining Eq. (2.17) and (2.18), we can directly connect the observable Θ to the length scale ξ close to the transition via

$$\Theta \propto \xi^{-z} \tag{2.19}$$

with the dynamic critical exponent z.

Crucially, the scaling limit is independent of the microscopic properties of the system. In the context of a phase transition, this means that the value of the critical exponent $z\nu$ is often independent of the microscopic properties of the model that is under consideration. This phenomenon is often refered to as universality [79].

Famous examples are the curve of the liquid/gas coexistence of a fluid and the magnetization of an Ising antiferromagnet. In both cases, the temperature T plays the role of the coupling. Surprisingly, the experimentally measured critical exponents for the density difference and the magnetization, respectively, are the same in both cases, even though the microscopic properties of the systems could not be more different.

This independence of the critical exponent from microscopic details lead to the definition of so called universality classes. An universality class contains physical systems exhibiting the same critical exponents. Even though the microscopic details of these systems within a universality class can differ largely, they have three things in common: Either forces are short ranged for all members or not, the symmetry group of the Hamiltonian and the dimensionality [83].

Tightly connected to the concept of universality classes is the concept of the critical dimension: Above the upper critical the mean-field predicted exponents become correct [89] as in high dimensionality, correlations are negligible.
Below the lower critical dimension fluctuations become strong and destroy the ordered phase. As a consequence, there is no phase transition.

2.3. Markovian processes

Originating in stochastic mathematics, the investigation of Markovianity of processes became an issue of great interest also in fields like condensed matter physics and quantum optics. A Markovian process is characterized by the indenpendence of the future evolution from the past behaviour of the process, i.e. predictions can be done solely on basis of the current state and do not become better even if taking the past evolution into account. Examples of non-Markovian behaviour in physical systems are scattering processes in a solid or a damped harmonic oscillator [1, 90].
Connected to the emergent research on open quantum systems, see next chapter, the characterization and measurement of (non-)Markovianity has become an important task, as in open quantum systems, the information flow between the system and its environment has to be taken into account, creating the basis for non-Markovian effects. Thus, the assumption of Markovian behaviour is in general done on the cost of drastic simplifications. Not surprisingly, the actual time evolution of quantum systems differs qualitatively from predictions based on the assumption of a Markovian time evolution [1].
It is well knwon that non-Markovianity is closely connected to the concept of quantum correlations and entanglement [91–93]. However, various approaches of measuring (non-)Markovianity exist, some of which are related to a generalization of the quantum master equation [94], linear maps [95], the increase of distinguishability (measured by the trace distance) between two evolving states [96, 97], the divisibility property [98] or the Fisher information [99, 100].
In this chapter, we will give a mathematical definition of Markovianity. We will draw a connection to non-Markovian behaviour in physical systems and find a measure of the degree of non-Markovianity based on a generalization of the quantum master equation.

2.3.1. Markovian stochastic processes

The property of (non-) Markovianity is usually related to a stochastic process $X(t)$, that is, a map

$$X : \Omega \times T \to \mathbb{R}. \tag{2.20}$$

Here, Ω is the sample space containing all possible events $\omega \in \Omega$ and T can be intepreted as an intervall of the real time axis. Mathematically, a stochastic process

$X(t)$ is called Markovian if it obeys [1]

$$\mu(X(t) \in B | X(t_m) = x_m, ..., X(t_1) = x_1) = \mu(X(t) \in B | X(t_m) = x_m) \tag{2.21}$$

for all Borel sets B and for all $m = 1, 2, 3, ...$ with the ordered set of times, $t_1 < t_2 < ... < t_m < t$. Here, $\mu(A)$ is the probability of the event A. Definition (2.21) tells us that the probability for $X(t) \in B$ is the same either under the condition that the system realized to $x_1, x_2, ..., x_m$ before or under the solely condition that the system realized to x_m at time t_m. Thus the probability just depends on the latest realization and is independent of the past. One might speak of rapid decrease of memory effects. The prime example of a Markovian process is the so called Wiener process or Brownian motion, that is, a continuous stochastic process with independent increments obeying the normal distribution [101].

2.3.2. Measure of Non-Markovianity

Our approach to the measurement of non-Markovianity is based on a generalization of the quantum master equation, which largely follows the work of [94].
The time evolution in the most general case can be written in the form [102]

$$\dot{\rho} = \Lambda_t[\rho] = \sum_k A_k(t) \rho B_k^\dagger(t), \tag{2.22}$$

with the linear map Λ_t acting on ρ. Expanding Λ_t eventually leads to a generalized form of the quantum master equation given by [94]

$$\frac{d}{dt}\rho = -i[H(t), \rho] \tag{2.23}$$
$$+ \sum_{k=1}^{d^2-1} \gamma_k(t) \left(L_k(t) \rho L_k^\dagger(t) - \frac{1}{2}\{L_k(t) L_k^\dagger(t), \rho\} \right).$$

For a detailed derivation see App. (C). Here d is the dimension of the state space. The generalized time dependent jump operators $L_k(t)$ are orthonormalized according to

$$\text{Tr}[L_k(t)] = 0, \qquad \text{Tr}[L_j^\dagger(t) L_k(t)] = \delta_{jk}. \tag{2.24}$$

The Hermitian operator $H(t)$, the effective decay rates $\gamma_k(t)$, and the $L_k(t)$'s are time dependent and differ from their counterparts in the Master equation in Markovian Lindblad form according to Eq. (2.57). Crucially, the generalized decay rates $\gamma_k(t)$ can become negative during the time evolution, reversing previous decay processes. This leads to the definition of non-Markovianity: If and only if one or more of the $\gamma_k(t)$ is negative, the time evolution is non-Markovian.
A quantitative measure for the degree of non-Markovianity is given by the sum of all negative generalized decay rates, which reads [94]

$$f(t) = \frac{1}{2} \sum_{k=1}^{d^2-1} [|\gamma_k(t)| - \gamma_k(t)]. \tag{2.25}$$

The challenge of the analysis is to transform the effective time evolution into the shape of (2.24) and calculate the generalized decay rates $\gamma_k(t)$.

2.4. Open quantum systems

An open quantum system is a quantum system coupled to an uncontrolled environment. For the description of such systems, the Schroedinger equation is not appropriate. Furthermore, the state of the open quantum system will in general not be a pure state in Hilbert space, but rather a mixed state. This results in the definition of measures for quantum entropy, giving information about the degree of mixture and irreversibility of the quantum dynamics. In the following chapter, we will describe an approach of investigating open quantum systems via a Markovian master equation approach. Doing so, we will first give a definition of the density matrix that is used to describe mixed states of quantum systems. In the second part of the chapter, we will derive an equation of motion for the density matrix that includes the coupling of the system of interest to the uncontrolled environment. In the last part, two different measures of quantum entropy, describing to which extend a state is mixed, are introduced.

2.4.1. Pure and mixed states

For the statistical formulation of quantum mechanics, e.g. for calculating expectation values, one uses the so called density matrix. In its most easiest form, we can express the density matrix as

$$\rho = |\Psi\rangle\langle\Psi| \tag{2.26}$$

where $|\Psi\rangle \in \mathcal{H}$ is an element (pure state) of the Hilbert space. The density matrix is unique for a physical state, while the ket of the state that can be written as $\exp(i\theta)|\Psi\rangle$, with the arbitrary phase $\theta \in [0, 2\pi)$.
Some important properties of the density matrix stem from the trace function. The trace of an operator O, i.e. of a map $O : \mathcal{H} \to \mathcal{H}$, is given by [103]

$$\mathrm{Tr}\{O\} = \sum_{k=1}^{d}\langle a_k|O|a_k\rangle \tag{2.27}$$

with the complete orthonormal basis $|a_k\rangle$ of the d-dimensional Hilbert space $\mathcal{H}$.
With this definition of the trace, the mean value of an operator O can be expressed as

$$\langle O\rangle = \langle\Psi|O|\Psi\rangle = \mathrm{Tr}\{\rho O\}. \tag{2.28}$$

In a more general case, one can consider a system consisting of several ensembles, each described by a vector in the Hilbert space $|\Psi_k\rangle$. In that case, the expectation value of an operator reads $\langle O\rangle = \sum_k \lambda_k\langle\Psi_k|O|\Psi_k\rangle$ and it is then convenient to define the density matrix as

$$\rho = \sum_k \lambda_k|\Psi_k\rangle\langle\Psi_k| \tag{2.29}$$

so that $\langle O \rangle = \mathrm{Tr}\{\rho O\}$ holds. Here, the λ_k's can be understood as the weights of each ensemble [1] with

$$\sum_k \lambda_k = 1. \tag{2.30}$$

Moreover, the density matrix fulfills

$$\mathrm{Tr}\{\rho^2\} \leq \mathrm{Tr}\{\rho\} = 1 \tag{2.31}$$

where the equal sign holds if and only if the system is in a pure state according to Eq. (2.26). Furthermore, the density matrix is hermitian and positive, i.e.

$$\rho^\dagger = \rho; \quad \rho \geq 0. \tag{2.32}$$

Diagonalizing ρ and expressing it in terms of eigenstates and eigenvalues leads to the same form of ρ as shown Eq. (2.29), with λ_k the eigenvalues and $|\Psi_k\rangle$ the orthonormalized eigenstates.

2.4.2. Composite systems and the partial trace

Consider a composite system of two Hilbert spaces $\mathcal{H} = \mathcal{H}_A \otimes \mathcal{H}_B$. In certain cases, one might be rather interested in the properties of one subsystem, and thus aims to get rid of the degrees of freedom of the second subsystem. This can be achieved through the partial trace function. The partial trace over the subsystem B is a linear map $\mathrm{Tr}_B : G(\mathcal{H}) \to G(\mathcal{H}_A)$, where $G(\mathcal{H})$ is the space of operators acting on $\mathcal{H}$. It can be explicitly expressed as [75]

$$\mathrm{Tr}_B\{|a\rangle\langle a'| \otimes |b\rangle\langle b'|\} = |a\rangle\langle a'| \mathrm{Tr}_B\{|b\rangle\langle b'|\}. \tag{2.33}$$

Here, $|a\rangle, |a'\rangle$ and $|b\rangle, |b'\rangle$ are generic vectors of the Hilbert spaces $\mathcal{H}_A$ and $\mathcal{H}_B$, respectively.
In the next step, we apply the partial trace to the density matrix. A general expression for the density matrix ρ_{AB} acting on $\mathcal{H}$ is given by

$$\rho_{AB} = \sum_{ijkl} c_{ijkl} |a_i\rangle\langle a_j| \otimes |b_k\rangle\langle b_k| \tag{2.34}$$

with $c_{ijkl} = \langle a_i b_k | \rho_{AB} | a_j b_l \rangle$. Here, the a_i form a complete orthonormal basis of $\mathcal{H}_A$ and correspondingly for the b_i and $\mathcal{H}_B$.
Applying the partial trace operation according to Eq. (2.33) to ρ_{AB}, we get

$$\mathrm{Tr}_B\{\rho_{AB}\} = \mathrm{Tr}_A\{\rho_{AB}\} = \sum_{ijk} c_{ijkl} |a_i\rangle\langle a_j|. \tag{2.35}$$

2.4.3. Liouville-von Neumann equation

A vector in Hilbert space obeys the Schroedinger equation

$$i\frac{d}{dt}|\Psi_k(t)\rangle = H(t)|\Psi_k(t)\rangle \tag{2.36}$$

with the Hamiltonian $H(t)$ and $\hbar = 1$. Letting a time evolution operator $U(t, t_0)$ act on the state, we have

$$U(t, t_0)|\Psi_k(t_0)\rangle = |\Psi_k(t)\rangle. \tag{2.37}$$

It is then easy to show that the time evolution operator also obeys the Schroedinger equation as the Hilbert space vector.

One can generalize that formalism to the time evolution of the density matrix introduced in chapter (2.4.1) and get the Liouville-von-Neumann equation for the time dependent density matrix [1]

$$\frac{d}{dt}\rho(t) = -i[H(t), \rho(t)]. \tag{2.38}$$

In analogy to the Liouville formalism in classical statistical mechanics, one often rewrites Equation (2.38) as

$$\frac{d}{dt}\rho(t) = \mathcal{L}\rho(t), \tag{2.39}$$

with the Liouville superoperator $\mathcal{L}$ that maps the operator $\rho(t)$ to its time derivative. Via the unitary transformation of an explicitly time dependent operator $A(t)$ according to

$$A_H(t) = U(t, t_0)^\dagger A(t) U(t, t_0) \tag{2.40}$$

one can shift the time dependence from the density matrix to the operators, which is the so called Heisenberg picture. Both the Schroedinger and the Heisenberg picture follow from the more general interaction picture, where the dynamics is governed by the von Neumann equation for the interaction picture density matrix [1].

2.4.4. Markovian quantum master equation

The following considerations follow to large extends the reference [1]. Consider a system that is composed of a subsystem of interest S and the environment E coupled to S. While the whole system $S + E$ still follows unitary, Hamiltonian dynamics, the open system S has different properties due to the interaction and therefore energy transfer with the environment E. The corresponding Hilbert space has a tensor product structure according to

$$\mathcal{H} = \mathcal{H}_S \otimes \mathcal{H}_E \tag{2.41}$$

where $\mathcal{H}_S$ and $\mathcal{H}_E$ are the Hilbert spaces of the system S and E, respectively. The Hamiltonian of the composed system can be expressed as

$$H = H_S \otimes I_E + I_S \otimes H_E + H_I, \tag{2.42}$$

with H_S being the Hamiltonian of the open system S, H_E the Hamiltonian of the environment E and H_I the interaction term between these two parts. One can express
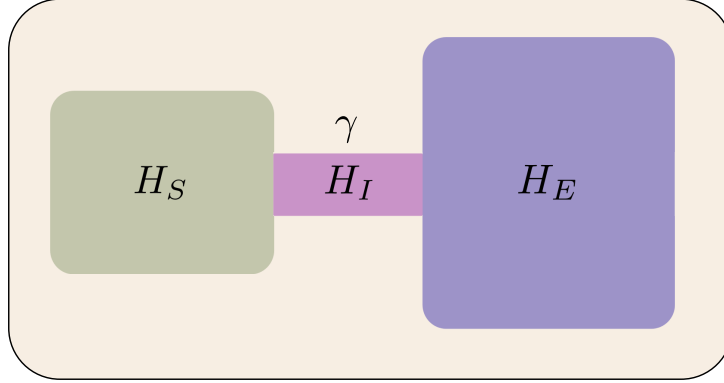
Figure 2.3.: Scheme of an open system and the coupling to its environment: The system of interest S described by the Hamiltonian H_S is coupled to its environment E (a heat bath for instance) via the interaction Hamiltonian H_I.

the density matrix of the composed system in the form

$$\rho = \rho_S \otimes \rho_E + C_{SE} \tag{2.43}$$

where C_{SE} stands for the correlation between S and E. Consequently, the density matrix of the subsystem S can be written as

$$\rho_S = \text{Tr}_E\{\rho\} \tag{2.44}$$

where Tr_E is the partial trace over all degrees of freedom of the environment E. The composed system $S + E$ evolves unitarily and therefore obeys the von Neumann equation introduced in the previous chapter (2.4.3). In the same spirit of tracing out the environment from ρ, we can write the time evolution of the density matrix of the open system S as

$$\frac{d}{dt}\rho_S(t) = -i\text{Tr}_E[H(t), \rho(t)], \tag{2.45}$$

For the next step, we assume that correlations between the systems S and E can be neglected and therefore equation (2.43) can be written as a product of ρ_S and ρ_E. The transformation of the open system from the initial time $t = 0$ to $t > 0$ can be written in the form

$$\rho_S(t) = Tr_E\{U(t,0)\rho_S(t) \otimes \rho_E(t)U^\dagger(t,0)\} = V(t)\rho_S(0). \tag{2.46}$$

2. Theoretical concepts

The map $V(t)$ replaces the unitary time evolution of the composed system $\rho_S \times \rho_E$, that was governed by the evolution operators $U(t, t_0)$. We can write

$$V(t)\rho_S(0) = \sum_{\mu\nu} \Omega_{\mu\nu}(t)\rho_S\Omega_{\mu\nu}(t). \tag{2.47}$$

Here, $\Omega_{\mu\nu}(t)$ is defined by

$$\Omega_{\mu\nu}(t) = \sqrt{\lambda_\nu}\langle\Phi_\mu|U(t,0)|\Phi_\nu\rangle \tag{2.48}$$

with λ_ν being the eigenvalues and Φ_ν being the eigenstates of ρ_E. It can be shown that $V(t)$ is a positive and trace-preserving map and, for markovian time evolution, fullfils the semigroup property [1]

$$V(t_1)V(t_2) = V(t_1 + t_2) \quad t_1, t_2 > 0 \tag{2.49}$$

and therefore represents a quantum dynamical semigroup. We continue expressing the semigroup in terms of a linear map $\mathcal{L}$ as

$$V(t) = e^{\mathcal{L}t}, \tag{2.50}$$

where now $\mathcal{L}$ takes the position of a generator of the semigroup. Equation (2.50) directly leads to

$$\frac{d}{dt}\rho_S = \mathcal{L}\rho_S. \tag{2.51}$$

The above Equation follows the structure of formula (2.39). The superoperator $\mathcal{L}$ can be considered as an generalization Liouville operator introduced in Equation (2.39). Consider the Liouville space of the N-dimensional Hilbert space $\mathcal{H}_S$ with the orthonormal basis operators F_i, $i \in \{0, 1, ..., N^2\}$ and F_0 being the identity. We express the $\Omega_{\mu\nu}$ from formula (2.47) as

$$\Omega_{\mu\nu}(t) = \sum_i^{N^2} F_i\text{Tr}_S\{F_i\Omega_{\mu\nu}(t)\}. \tag{2.52}$$

Inserting the latter into Eq. (2.47), we get

$$V(t)\rho_S = \sum_{i,j=1}^{N^2} c_{ij}(t)F_i\,\rho_S F_j^\dagger \tag{2.53}$$

with

$$c_{ij}(t) = \sum_{\mu\nu} \text{Tr}_S\{F_i\Omega_{\mu\nu}(t)\}\text{Tr}_S\{F_i\Omega_{\mu\nu}(t)\}^*. \tag{2.54}$$

Inserting the expression (2.53) into the derivative of ρ_S, that according to Eq. (2.51) can be written as

$$\mathcal{L}\rho_S = \lim_{\varepsilon \to 0} \frac{1}{\varepsilon} \{V(\varepsilon)\rho_S - \rho_S\} \tag{2.55}$$

we get the standard form of the generator

$$\mathcal{L}\rho_S = -i[H, \rho_S] + \sum_{i,j=1}^{N^2-1} a_{ij} \left(F_i \, \rho_S F_j^\dagger - \frac{1}{2}\{F_j^\dagger F_i \, , \rho_S\} \right). \tag{2.56}$$

with $a_{ij} = \lim_{\varepsilon \to 0} \frac{c_{ij}}{\varepsilon}$. Diagonalizing (a_{ij}) leads to the diagonal form of the generator that reads

$$\mathcal{L}\rho_S = -i[H, \rho_S] + \sum_{k=1}^{N^2-1} \gamma_k \left(A_k \rho_S A_k^\dagger - \frac{1}{2}\{A_k^\dagger A_k, \rho_S\} \right). \tag{2.57}$$

The γ_k, which are the eigenvalues of (a_{ij}), are the decay rates. The corresponding A_k operators given in terms of a linear combination of the F_i are usually refered to as Lindblad or jump operators in Lindblad form. The first part consisting of the commutator of ρ_S and the Hamiltonian stands for the coherent dynamics.

2.4.5. Quantum entropy

Analogously to classical systems, one can define a quantum entropy measure providing information about the degree of uncertainity present in a quantum system. In the definition of these measures, the classical probability distributions are replaced by the density operator ρ. In the following, we will briefly give the definition and most important properties of two common measures of entropy in a quantum system.

Von Neumann entropy One quite common measure of entropy in quantum information is the von Neumann entropy. It is defined via the density matrix ρ of a system and reads [104]

$$S(\rho) = -\text{Tr}\{\rho \ln \rho\}. \tag{2.58}$$

Expressing ρ by its spectral decomposition

$$\rho = \sum_i p_i |\phi_i\rangle\langle\phi_i| \tag{2.59}$$

we can rewrite the von Neumann entropy as [75]

$$S(\rho) = -\sum_i p_i \ln p_i \tag{2.60}$$

which is a more useful expression for concrete calculations This corresponds to the Shannon information entropy [1] for a distribution that maps an integer number i to a probability p_i: $i \rightarrow p_i$. In a mixture made of pure states $|\phi_i\rangle$ that are weighted with the corresponding probabilities p_i, $S(\rho)$ describes the uncertainity about the realization of a particular state of the ensemble.

Important properties of the von Neumann entropy are the semi-positive definiteness, $S(\rho) \geq 0$. The equal sign holds if and only if the system is in a pure state. Furthermore the von Neumann entropy is invariant under a unitary transformation of the Hilbert space. One can also define an upper bound given by $S(\rho) \leq \ln\{D\}$, with D being the dimension of the Hilbert space. The von Neumann entropy reaches its maximum value if and only if the system is in the maximally mixed state $\rho = I/D$.

Consider a system ρ_{ij} with subsystems $\rho_i = \text{Tr}_j\{\rho_{ij}\}$ and $\rho_j = \text{Tr}_i\{\rho_{ij}\}$. The von Neumann entropy is always smaller than the sum of the entropy of the subsystems, i.e.

$$S(\rho_{ij}) \leq S(\rho_i) + S(\rho_j). \tag{2.61}$$

We can interpret this in the way that the uncertainity about the system grows by looking at the single subsystems as the information contained in the correlation between i and j is lost.

Linear entropy   Another measure of quantum entropy is given by the linear entropy, that reads [1]

$$S_l(\rho) = \text{Tr}\{\rho - \rho^2\} = 1 - \text{Tr}\{\rho^2\}. \tag{2.62}$$

This functional is also a measure for the purity of states with the limits

$$0 \leq S_l(\rho) \leq 1 - \frac{1}{D}. \tag{2.63}$$

According to Eq. (2.62), the linear entropy is zero if and only if the system is in a pure state. S_l reaches its highes possible value for a maximally mixed state [1].

2.5. Rydberg atoms

Atoms that are highly excited with the electron being in a state with a high principal quantum number $n >> 10$ are so called Rydberg atoms [105]. The excited electrons are weakly bound (almost ionized) to the core of the atom. This reults in a strong interaction between excited atoms, leading to phenomena such as the Rydberg-blockade [106] and its counterpart, the Rydberg-antiblockade [107], see Fig. (2.4).

This behaviour makes Rydberg atoms to promising candidates in applications of quantum simulation and quantum information. For example, the Rydberg blockade mechanism can be used for the construction of two-qubit gates [38]. Also an experimental implementation of a Controlled-NOT gate has been succesfully demonstrated [108]. In the followingsections, we will review the most important properties of Rydberg atoms.
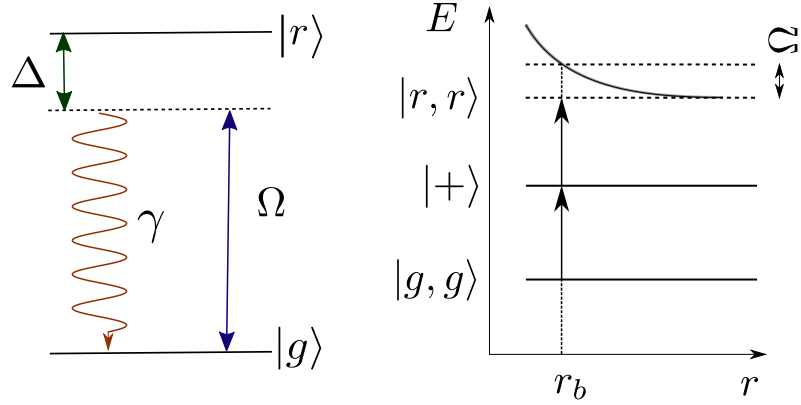
Figure 2.4.: Left side: Simplified scheme of a Rydberg atom: The ground state $|g\rangle$ is coupled to the excited Rydberg state $|r\rangle$ with a Rabi frequency Ω. The Rydberg state can be detuned with the detuning Δ and decays with the decay rate γ. Right side: Mechanism of the Rydberg blockade. The system is described by the $|g, g\rangle$ state (both atoms are in the ground state), the $|+\rangle = (|gr\rangle + |rg\rangle)/\sqrt{2}$-state and the doubly excited $|r, r\rangle$-state. The latter is driven out of resonance if the distance of the atoms is smaller than r_b, the so called Rydberg blockade radius.

2.5.1. Rydberg wavefunctions

For large orbital quantum numbers l, an electron in the Rydberg state essentially sees the atom core as a point charge, so that the trajectory and the binding energy of the electron corresponds to those of a hydrogen atom. For low l, however, the electron gets close to the core and the electron feels the unscreened charge of the core. Therefore, the total energy is surpressed compared to the hydrogen energy levels. The eigenenergies of the Rydberg state read [109]

$$E_n = -\frac{-R_y}{(n - \delta_l)^2} \tag{2.64}$$

with the principal quantum number n and the Rydberg constant $R_y = 109737.315685/\text{cm}$. Here, δ_l is the quantum defect depending on l. The Schrödinger equation with an $1/r$ Coulomb potential of the hydrogen atom can be seperated into an angular and a radial part. The full solution are wave functions of the form

$$\Psi_{nlm}(r, \phi, \theta) = \frac{\psi_{lm}(\phi, \theta)f(r)}{r} \tag{2.65}$$

with the spherical harmonic function $\psi_{lm}(\phi, \theta)$ solving the angular part and the solution of the radial part $f(r)$. Note that there is another independent solution of the radial equation $g(r)$ which we will use later on.

In the case of e.g. an alkali atom, the potential of the electron close to the core is lower than in the case of a hydrogen atom due to the multiple charge of the nucleus.

Consequently, the $1/r$ potential of the hydrogen atom is replaced by an effective potential $V_{eff}(r)$ with a lower potential for small distances r between atom core and electron [105]. The corresponding Schrödinger equation is still seperable into a angular and a radial part. The modification of the potential leads to a phase shift τ to the radial part of the hydrogen atom. Accordingly, the radial function $f(r)$ of the hydrogen atom is replaced by

$$\rho(r) = f(r)\cos(\tau) - g(r)\sin(\tau) \tag{2.66}$$

Finally, the full wave function of theRydberg state reads [105]

$$\Psi_{nlm}(r,\phi,\theta) = \frac{\psi_{lm}(\phi,\theta)\left[f(r)\cos(\pi\delta_l) - g(r)\sin(\pi\delta_l)\right]}{r} \tag{2.67}$$

with $\delta_l = \tau/\pi$. Note that the wave function (2.67) is only valid for $r > r_0$, where the Na potential V_{eff} and the $1/r$ Coulomb potential are equivalent.

2.5.2. Van-der-Waals interaction

Assuming the distance between two Rydberg atoms to be much larger than the principal quantum number of the atoms times the Bohr radius, i.e. $R \gg na_0$, the leading term of interaction potential is the dipol-dipol interaction that can be written as [110]

$$V_{dd} = e^2/R^3 \left(\mathbf{a} \cdot \mathbf{b} - 3a_z b_z\right). \tag{2.68}$$

Here, $\mathbf{a}$ and $\mathbf{b}$ is the position of the Rydberg electron of the atom $\mathbf{A}$ and $\mathbf{B}$, respectively, with respect to the atom core. We suppose that both atoms are in the state nlj, where n is the principal quantum number, l is the azimuthal quantum number and j is the total angular momentum quantum number. The dipole-dipole interaction then leads to the reaction

$$nlj + nlj \rightarrow n_s l_s j_s + n_t l_t j_t. \tag{2.69}$$

According to the dipol selection rules, we have $l_s, l_t = l \pm 1$ and $j_s, j_t = j \pm 0, 1$. In the case of Rubidium around the $|60_{p/s}\rangle$ state, for example, the coupling between the $|60p_{3/2}60p_{3/2}\rangle$ state and the $|60s_{1/2}61s_{1/2}\rangle$ state dominates [109]. The energy difference bewteen the initial and the final states is called the Förster defect F given by

$$F = E(n_s l_s j_s) + E(n_t l_t j_t) - 2E(nlj). \tag{2.70}$$

In the case of large distances R, a nonzero Förster defect leads to a van der Waals like interaction in second order of V_{dd} with an $1/R^6$ dependence. For small distances up to 5μm, the interactions become resonant with the electronic levels and show a $1/R^3$ dependence. Between these limits, the van der Waals interaction leads to a mixing of

the hyperfine structure of the two levels. If the fine structure is not affected by the interaction, the degenerate van der Waals Hamiltonian can be written as [110]

$$H_{vW} = \frac{C_6}{R_6} \sum_{m_s m_t} \mathcal{M}^\dagger |m_s m_t\rangle \langle m_s m_t| \mathcal{M} \tag{2.71}$$

where the operator $\mathcal{M}$ includes the angular mommentum properties of V_{dd}. The C_6 coefficient reads

$$C_6 = \sum_{n_s n_t} \frac{e^4}{-\delta_{st}} (R_{nl}^{n_s l_s} R_{nl}^{n_t l_t})^2. \tag{2.72}$$

with $R_{nl}^{n'l'} = \int dr P_{n'l'}(r) r P_{nl}(r)$ and the radial wave functions $P_{nl}(r)$. Applying H_{vW} to the two-atom eigenstate $|\phi\rangle$, we get

$$H_{vW}|\phi\rangle = \frac{C_6}{R^6} D_\phi |\phi\rangle. \tag{2.73}$$

with the van der Waals potential $\frac{C_6}{R^6} D_\phi$. The eigenvalues D_ϕ of the $\mathcal{M}^\dagger \mathcal{M}$ operator usually range from 0 to 1. Having several channels contributing to the interaction, the corresponding H_{vW} for each channel must be added together before being diagonalized [109].

2.5.3. Dressed states

The investigation of Rydberg atoms is limited by the short lifetime of the Rydberg state. For a Rydberg state with a principal quantum number of $n = 50$ one has a lifetime of around 100μs [105]. A quantum many-body system, however, needs more time to reach equilibrium. Through the so-called dressing of a Rydberg atom, one achieves the admixture of the ground state and the Rydberg state, leading to a longer lifetime and the possibility to e.g. tune the dipolar coupling between two atoms. A general description of an atom that is dressed by laser light is given in [111]. Here, we consider a Hamiltonian of the form

$$H = \varepsilon_R |r\rangle\langle r| + (\Omega \cos(\omega_L t)|g\rangle\langle r| + h.c.) \tag{2.74}$$

with the highly excited Rydberg state $|r\rangle$, the ground state $|g\rangle$ and the corresponding energy difference ε_R. The laser parameters are the Rabi frequency Ω and the frequency ω_L of the laser light. Shifting to the rotating frame of the Hamiltonian, and applying a rotating wave approximation, as explained in App. (F.2) for another example, leads to

$$H = \Delta|r\rangle\langle r| + \Omega/2 \left(|g\rangle\langle r| + h.c.\right), \tag{2.75}$$

where Δ is the detuning with $\Delta = \varepsilon_R - \omega_L$. In the case of Rydberg atoms, one usually uses a weak dressing $\Omega \ll \Delta$. Consequently, the eigenstates of the Hamiltonian can be written as a dressed state $|s\rangle$ given by

$$|s\rangle = |g\rangle + \frac{\Omega}{2\Delta}|r\rangle \tag{2.76}$$

The decay rate of the dressed state can be calculated by [39]

$$\gamma = \frac{\Omega^2}{4\Delta^2}\gamma_r$$

with γ_r being the decay rate of the Rydberg state. For example, if the dressed state has a 1% share of the Rydberg state, the lifetime of the dressed state $\tau = 1/\gamma$ is extended to about 10ms. In such a situation, the interaction given by [40, 112]

$$V = \frac{\Omega^4}{8\Delta^3}\left(1 + (r/\xi_0)^6\right)$$

is still strong enough to study many-particle physics. Here, we use $\xi_0^6 = C_6/2|\Delta|$ with the van-der-Waals coefficient C_6. Rydberg dressing has become a common tool for the investigation of many-body interactions [39, 113] and quantum magnetism [114, 115]. In recent years, the technique of Rydberg dressing has also been succesfully applied a number of experiments [41, 64, 116].

2.6. Nitrogen-Vacancy centers in diamond

Color centers observed in diamonds are lattice defects that have a unique absorption and emission spectra. These defects lead to fascinating coloration of diamonds and thus have been intensively studied [117]. The Nitrogen vacancy (NV) center has a special position among these color centers due to its outstanding properties, like read out and control of the ground state of the spin at room temperature [118] and long coherence times of the spin states of several ms [119–121]. Possible applications range from quantum computing [122–126] to magnetometry [127, 128].
In a Nitrogen vacancy center, one Carbon atom is replaced by a Nitrogen atom, and an adjacent Carbon atom is removed, causing a vacancy, see Fig (2.5). One can further distinguish between a neutral NV center NV^0 with electron spin $S = \frac{1}{2}$ in the ground state and a negative NV center NV^- with total electron spin of $S = 1$ [129, 130]. The NV^0 compromises five electrons from the bounds to the neighbouring electrons (three electrons from the dangling bond to the carbon atoms, two from the nitrogen atom). The NV^- inherits an additional electron from the lattice [117]. As the NV^- exhibits some interesting features like the measurability via electron paramagnetic spin resonance due to its paramagnetic ground state [118] and the C_3v-symmetry, scientific research usually refers to this kind of NV center. In the following, NV will refer to NV^-.

2.6.1. Optical and electronic properties

The NV defect including the Nitrogen atom, the vacancy and the three neighbouring carbon atoms of the vacancy exhibit the C_3v-symmetry. i.e. invariance under a $\frac{2\pi}{3}$ rotation around the vertical symmetry axis [131]. The transformation under operations such as rotations and reflections provide information about the electronic states of the NV center [132].
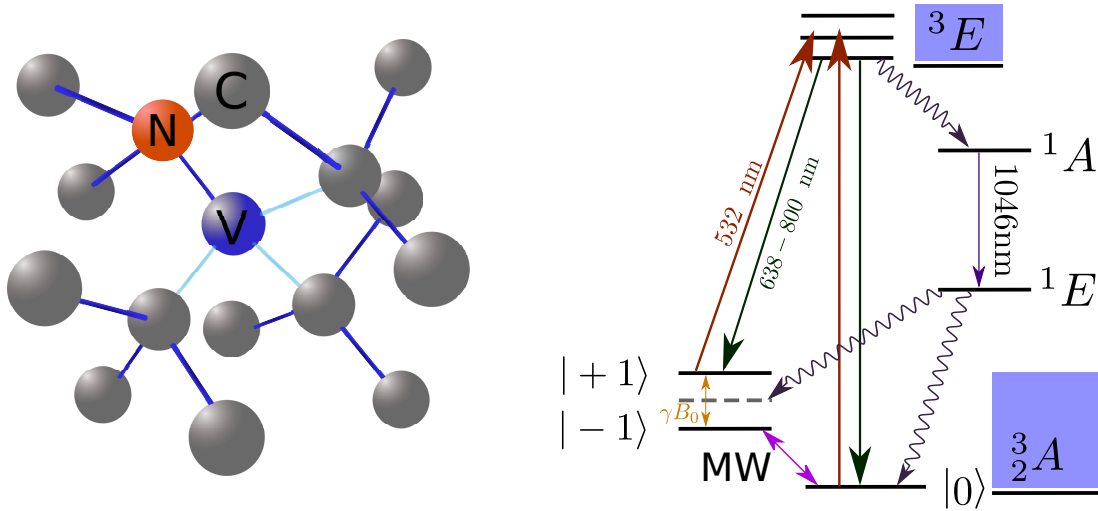
Figure 2.5.: Left side: An NV center consisting of a Nitrogen atom (N) and a vacancy (V) with sourrounding carbon atoms (C) in the diamond structure. There is a lone pair of electrons, i.e. unbonded valence electrons, indicated by the line between the nitrogen atom and the vacancy. Right side: Level scheme of an NV^- center with the ^3_2A triplet state as the ground state and the triplet ^3E excited state. The sublevels are $|0\rangle$ and $|\pm 1\rangle$, denoted here for the ground state. NV centers show strong absorption of green at light at 532 nm, the relaxation to the phonon sidebands at $650-800$ nm. The relaxation also happens through the singlet metastable states ^1A and ^1E via ISC. An external field B_0 lifts the degeneracy of the $|\pm 1\rangle$ states.

The electronic states of the NV center consist of a $^3A_2$ triplet ground state [133, 134], a $^3E_2$ triplet excited state [131] and the singlet metastable states ^1A and ^1E, see Fig. (2.5). The states of the triplets can be given as eigenstates of the S_z operator with $m_s = 0$; $m_s = \pm 1$ and the corresponding eigenstates $|0\rangle$ and $|\pm 1\rangle$. The degeneracy of the $m_s = 0$ and $m_s = \pm 1$ states is lifted by a zero field splitting with $D = 2.87$ GHz for the ground state and $D = 1.27$ GHz for the excited state [135].
NV centers show strong absorption for 532nm, light with this wavelength excites the NV from the ground state to the electronically and vibronically excited states. Phonon assisted relaxation then brings it back to the electronically excited states.
The excited electron can decay to the ground state by fluoresence, i.e. the emission of a photon. The zero phonon line between the ground state and the excited state is 637 nm or 1.945 eV [136]. If there is energy lost to the vibration of the lattice, the fluoresence ranges from $650-800$ nm.
The electrons in the excited state can also cross over to the metastable ^1A-state via inter-system crossing (ISC). The ISC between the ^3E state and the ^1A state is spin orientation dependent, with lifetimes of $\tau = 23$ ns for the $|0\rangle$ state and $\tau = 12.7$ ns for the $|\pm 1\rangle$ state [135]. This transition is called shelving, and the metastable states ^1A and ^1E are also called 'shelving' states. The singlet states have an infrared emission

band of 1046 nm. The decay from the ^1E state to the ^3A ground state also happens via inter-state crossing. The lifetime for this process is $\tau = 300$ ns [137]. Due to this higher decay rate of the $|\pm 1\rangle$ state, the transition is spin non-conserving, flipping $|\pm 1\rangle \leftrightarrow |0\rangle$. As a result, the NV center is polarized into the $|0\rangle$ state, with polarization up to 90% [138]. The long lifetime of the shelving state allows applications concerning single spin readout. As the $|\pm 1\rangle$ states go through the spin non-conserving, non-radiative relaxation process more often, they have a weaker fluorescence [122].

Due to the Zeeman effect, the degeneracy of the $|\pm 1\rangle$ states is lifted if an external magnetic field B_0 is applied along the NV symmetry axis. Using microwave irradiation, one can trigger ground state transitions $|0\rangle \leftrightarrow |-1\rangle$ or $|0\rangle \leftrightarrow |+1\rangle$ with the Rabi frequency $\Omega = \gamma_e B_1$. Here, γ_e is the gyromagnetic ratio of the NV electronic spin and B_1 is the component of the MW excitation that is perpendicular to the NV symmetry axis. This cycling transition between the spin-substates lowers the fluoresence of the NV center, raising possibilites to measure the NV resonance via the Optical Detected Magnetic Resonance [139].
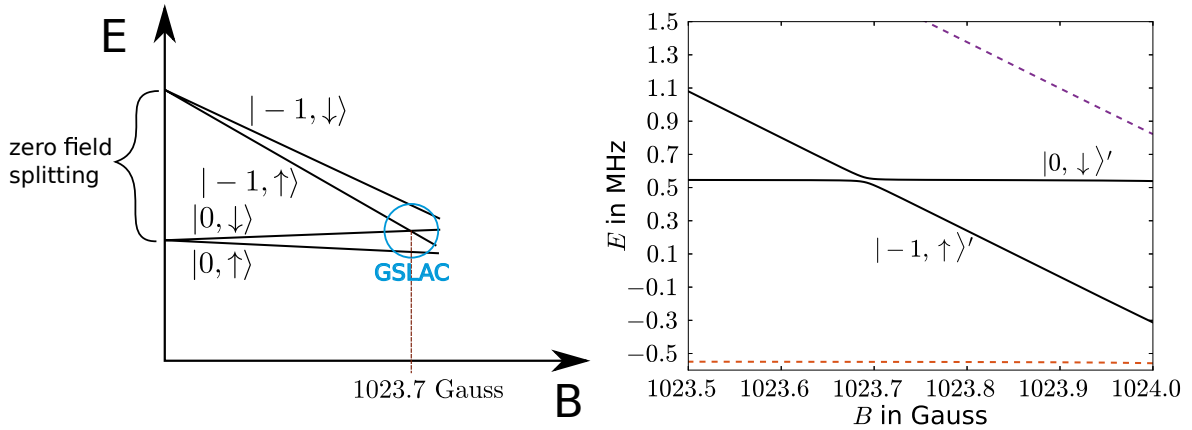
Figure 2.6.: Sketch of the energy of the eigenstates in a NV-^{13}C nucleus system, where $|0\rangle$ and $|-1\rangle$ refer to the NV ground states and $|\uparrow\rangle$ and $|\downarrow\rangle$ to the spin 1/2 states of the ^{13}C nucleus. At around $B = 1023.7$ Gauss, the states get mixed and there is a level-anticrossing. The circle indicates the area close to the GSLAC shown on the right side. In this region, the $|0,\downarrow\rangle$ and $|-1,\uparrow\rangle$ become mixed and therefore are labeled $'$.

Ground state level anticrossing   A ground state level anti-crossing (GSLAC), see right side of Fig. (2.6), was first discovered in NV centers in diamond in [140]. It occurs if the $|0\rangle \leftrightarrow |-1\rangle$ transition of the NV center and the transition of the nucleus become resonant. The transition frequency of the NV transition is given by $\gamma_e B_0 - D$, and that one of the nucleus by $\gamma_n B_0$. Here, γ_e is the gyromagnetic ratio of the electronic spin and γ_n the gyromagnetic ratio of the nucleus. D is the zero field splitting. The condition for

resonance then reads

$$D - \gamma_e B_G = \gamma_n B_G. \tag{2.77}$$

Inserting the values of $\gamma_e/2\pi = 2.802\text{MHz/Gauss}$, $\gamma_n/2\pi = -10.705e^{-4}\text{MHz/Gauss}$ and $D = 2870\text{GHz}$, we get $B_G = 1023.7\text{Gauss}$. If B_0 is close to B_G, the states of the NV center and the nucleus becoming highly mixed due to the hyperfine interaction. In this situation, the polarization of the NV center affects the polarization of the nucleus and vice versa.

3. Variational principle for open quantum systems

In this chapter, we will review the variational principle for the steady state [141] and extend it to the time evolution of open quantum systems. This is analogous to the variational principle for closed quantum systems, where an energy functional is minimized to find the ground state. In our approach, the energy is replaced by a trace norm based variational norm of the density matrix and its time derivative. Additionally, we show a concrete example of its application to a dissipative transverse field Ising model.

3.1. Variational principle for the steady state

In the first part of this chapter, we will describe the variational principle to calculate the non-equilibrium steady state. For the concrete calculation, we will construct an upper bound of the variational norm that has a compact form and allows us to reduce the complexity of the variational minimization.

3.1.1. Upper bound of the variational norm

In the scope of the variational principle a trial state ρ is taken. The underlying time derivative $\dot{\rho} = \mathcal{L}(\rho)$ is given according to the quantum master equation (2.57). The true steady state is approximated by that state ρ^{var} which minimizes the trace norm of $\dot{\rho}$, i.e. [141]

$$\rho^{var} = \arg_\rho \min ||\dot{\rho}||, \tag{3.1}$$

with $||...||$ being the trace norm, see chapter (2.1.2). In the following, $||\dot{\rho}||$ will be called the variational norm. Due to limitations in our variational manifold, the variational norm will in general not be equal to zero at the variational minimum, as it is the case for the true steady state. In the most simple case, the varitional class is restricted to product states that can be written as

$$\rho = \prod_i \rho_i, \tag{3.2}$$

3. Variational principle for open quantum systems

with the single site density matrix $\rho_i = \mathrm{Tr}_{i\!/}\{\rho\}$, where $\mathrm{Tr}_{i\!/}\{x\}$ is the partial trace over all sites except site i. The time derivative of a product state can be expressed as

$$\dot{\rho} = \sum_i \mathcal{R}\dot{\rho}_i + \sum_{\langle ij \rangle} \mathcal{R}\dot{C}_{ij}. \tag{3.3}$$

Here, $\mathcal{R}$ is the superoperator transforming the identity at site i, $\mathbb{1}_i$, to the density matrix ρ_i and C_{ij} is the correlation between site i and j with the time derivative $\dot{C}_{ij}$. From Eq. (3.3), we can already see the difference between the variational approach and mean-field decoupling: Even though our variational manifold is restricted to product states, the derivative contains correlations C_{ij} stemming from the interaction terms in the Hamiltonian. These are not considered in mean-field theory at all, where only the first term of the right side of (3.3) is set to zero. In contrast to other common numerical procedures like a Runge-Kutta algorithms, the Liouvillian is applied only one time to the product state within the variational principle, creating only the lowest order of correlations. For the actual minimization, we use an upper bound of the variational norm which reads

$$||\dot{\rho}|| \leq \sum_{\langle ij \rangle} ||\dot{\rho}_{ij}||. \tag{3.4}$$

In a translational invariant system, the sum over neighbouring sites gives a constant factor. Consequently, in such systems it is even sufficient to minimize the variational norm of a single bond $||\dot{\rho}_{ij}||$. For a detailed derivation of the upper bound of the variational norm see App. (A).
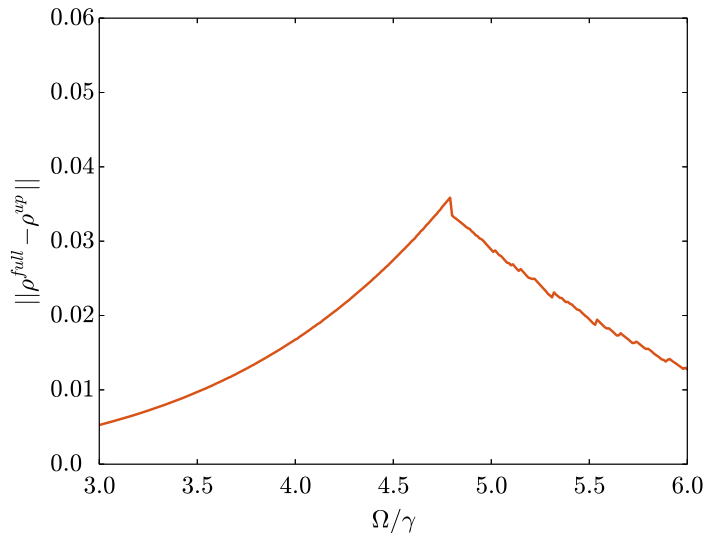

Figure 3.1.: Trace norm of the difference of the variational states ρ^{full}, which is gained by minimizing $||\dot{\rho}||$, and ρ^{up}, for which the upper bound $\sum_{\langle ij \rangle} ||\dot{\rho}_{ij}||$ was minimized.

To validate the accurateness of minimizing the upper bound instead of the full variational norm $||\dot{\rho}||$, we can consider a small system for which the variational minimization (3.1) is still evaluable. In this case, we consider a two dimensional dissipative Ising model on a 2×2-lattice. The Hamiltonian reads

$$H = \frac{\Omega}{2} \sum_i \sigma_x^{(i)} + \frac{V}{4} \sum_{\langle ij \rangle} \sigma_z^{(i)} \sigma_z^{(j)} \tag{3.5}$$

with the transverse field Ω and the interaction strength V. The dissipative part is governed by the jump operators $c_i = \sqrt{\gamma} \sigma_-^{(i)}$. In the basis where σ_z is diagonal, the Pauli matrices σ_μ are given by

$$\sigma_x = \begin{pmatrix} 0 & 1 \\ 1 & 0 \end{pmatrix}; \quad \sigma_y = \begin{pmatrix} 0 & -i \\ i & 0 \end{pmatrix}; \quad \sigma_z = \begin{pmatrix} 1 & 0 \\ 0 & -1 \end{pmatrix}. \tag{3.6}$$

We can then calculate the steady state according to (3.1) and by minimizing the upper bound given by Eq. (3.4). As a suitable distance between the two variational states, we calculate the trace distance (i.e. the trace norm of the difference of the two variational states). The result is shown in Fig. (3.1).

In the case of this small system, the deviation between the two states is relatively low. For larger system sizes, one finds that the scaling of the variational norm $||\dot{\rho}||$ is independent of the variational class and the model that is investigated. For a non-interacting model, one can explicitly show the $\propto \sqrt{N}$ dependence of the variational norm by making usage of the central limit theorem, where N is the number of particles [142].

Correlated variational trial states including nearest neighbour correlations can be written in the form

$$\rho^{corr} = \rho^{prod} + \sum_{\langle ij \rangle} \mathcal{R} C_{ij} + \sum_{\langle ij \rangle \neq \langle kl \rangle} \mathcal{R} C_{ij} C_{kl} + ..., \tag{3.7}$$

where ρ^{prod} is the product state given by Eq. (3.2). Applying the Liouvillian to ρ^{corr}, the interactions terms in the Hamiltonian generate higher orders of correlations, leading to the upper bound including three-site subsystems. We get

$$||\dot{\rho}^{corr}|| \leq \sum_{\langle ijk \rangle} ||\dot{\rho}_{ijk}^{corr}||. \tag{3.8}$$

Again, for a translational invariant system, the sum reduces to a constant factor and there is a single three-site minimization problem.

3.1.2. Application of the variational principle

Concretely, the variational minimization according to Eq. (3.1) can be done as follows: We parametrize the one-site density matrix ρ_i via

$$\rho_i = \frac{1}{2} + \sum_{\mu \in \{x,y,z\}} \alpha_\mu^{(i)} \sigma_\mu^{(i)} \tag{3.9}$$

3. Variational principle for open quantum systems

with the variational parameters

$$\left(\alpha_x^{(i)}, \alpha_y^{(i)}, \alpha_z^{(i)}\right) = \left(\langle\sigma_x^{(i)}\rangle, \langle\sigma_y^{(i)}\rangle, \langle\sigma_z^{(i)}\rangle\right),$$

where the σ_μ, $\mu \in \{x, y, z\}$, are the pauli matrices. Restricting our variational class to product states, the reduced two-site density matrix ρ_{ij} is given as the product of the single-site density matrices

$$\rho_{ij} = \rho_i \otimes \rho_j. \tag{3.10}$$

The trial state ρ_{ij} consists of six variational parameters, three per lattice site. We consider a dissipative Ising model with the Hamiltonian according to Eq. (3.5) and the quantum jump operators $c_\kappa = \sigma_-^\kappa$ acting on site κ. According to the master equation (2.57), we can then construct the α_μ-dependent time derivative of ρ_{ij}

$$\dot{\rho}_{ij}(\{\alpha_\mu\}) = \mathrm{Tr}_{i\!\!/j\!\!/}\{\dot{\rho}\} = -i[H_\mathrm{int} + H_\mathrm{loc} + H_\mathrm{eff}, \rho_{ij}] \tag{3.11}$$
$$+ \gamma \sum_{\kappa \in \{i,j\}} \left(c_\kappa \rho_{ij} c_\kappa^\dagger - \frac{1}{2}\{c_\kappa c_\kappa^\dagger, \rho_{ij}\}\right).$$

Here, $\mathrm{Tr}_{i\!\!/j\!\!/}\{\dot{\rho}\}$ means that all sites except i and j, which form our subsystem of interest, are traced out. The single parts of the Hamiltonian in formula (3.12) read

$$H_\mathrm{loc} = \frac{\Omega}{2}\left(\sigma_x^{(i)} + \sigma_x^{(j)}\right) \tag{3.12}$$
$$H_\mathrm{int} = \frac{V}{4}\sigma_z^{(i)}\sigma_z^{(j)}$$
$$H_\mathrm{eff} = \frac{V}{4}(2d-1)\left(\langle\sigma_z^{(k)}\rangle\sigma_z^{(i)} + \langle\sigma_z^{(l)}\rangle\sigma_z^{(j)}\right).$$

The trace operation over the interaction with the neighbouring sites k and l lead to the mean-field like terms in H_eff, see also Fig. (3.2). Calculating the derivative of ρ_{ij} according to Eq. (3.12) and taking the trace norm we get $||\dot{\rho}_{ij}||$. For the final constrained minimization procedure with respect to the variational parameters

$$\arg_{\rho_{ij}(\{\alpha_\mu\})}\min\{||\dot{\rho}_{ij}||\}, \tag{3.13}$$

efficient numerical algorithms exist, for example in the Scientific Computing Tools for Python library [143–145].
Including correlations in the variational manifold demands more variational parameters. We can express a correlated density matrix in terms of variational parameters and pauli matrices as

$$\rho_{ij}^{corr} = \frac{1}{4} + \sum_{\mu,\nu \in \{x,y,z\}} \alpha_{\mu\nu}\sigma_\mu^{(i)} \otimes \sigma_\nu^{(j)}, \tag{3.14}$$

where again the $\alpha_{\mu\nu}$ denote the variational parameters. Here, the correlation between site i and j is taken into account according to $\rho_{ij}^{corr} = \rho_i \otimes \rho_j + C_{ij}$. In principle, it is

Figure 3.2.: Visualisation of the two-dimensional lattice. Each Rydberg atom (represented by the blue dots) occupies one site of the lattice with a lattice spacing a. A single bond consists of two atoms at sites i and j, each interacting with its adjacent atoms at sites k and l, respectively.

possible to include even higher-order or long-range correlations, if the ansatz for the variational state is modified accordingly. Even though this will make the calculation more complicated, the basic idea of the variational principle remains unchanged. The construction of the variational norm $||\dot{\rho}_{ijk}||$ for correlated states works accordingly to the product-state case. For a single bond ρ_{ij}^{corr}, we have nine variational parameters in the case of correlated states according to Eq. (3.14) compared with six in the case of product states. Consequently, we have higher computational cost finding the minimum of the variational norm.

3.2. Variational principle for the time evolution

In the previous chapter, we reviewed the variational principle for calculating the non-equilibrium steady state. We also aim for calculating the relaxation dynamics of the open quantum system taking place before steady state is reached. For that reason we will replace the norm of the time derivative used for calculating the steady state by the norm of an integration expression. Analogue to the steady state case we will construct an upper bound of the variational norm for the variational classes of product states and nearest-neighbour correlations. We also want to stress that the technique proposed here is similar to other variational approaches based on matrix product states [146–148].

3.2.1. Variational norm of the time evolution

In the most simple case, the integration of the quantum master equation can be done by the common Euler method, where $\rho(t + \tau)$ is given by

$$\rho(t + \tau) = \rho(t) + \tau \mathcal{L}\left(\rho(t)\right) + O(\tau^2) \tag{3.15}$$

with integration step size τ.

3. Variational principle for open quantum systems

We can further minimize the integration error due to the finite size of τ by using the implicit midpoint method [149]. As the Liouvillian $\mathcal{L}$ is linear, we can write the integration expression in implicit midpoint form as

$$\rho(t+\tau) = \rho(t) + \frac{\tau}{2}\mathcal{L}\left[\rho(t) + \rho(t+\tau)\right] + O(\tau^3). \tag{3.16}$$

Using this integration method, we have an integration error of the order of τ^3, compared with τ^2 in the case of the euler integration.

Accordingly, we use the implicit midpoint method to define the variational norm D for the time evolution as

$$D \equiv \left|\left|\rho(t+\tau) - \rho(t) - \frac{\tau}{2}\mathcal{L}\left[\rho(t) + \rho(t+\tau)\right]\right|\right|_1. \tag{3.17}$$

Here, $\rho(t+\tau)$ denotes the trial state, parametrized by the variational parameters. The true state $\rho(t+\tau)$ is then approximated by the variational state $\rho^{var}(t+\tau)$ that minimizes the functional D, i.e.

$$\rho^{var}(t+\tau) = \arg_{\rho(t+\tau)}\min\{D\}. \tag{3.18}$$

Given an initial state $\rho_0 = \rho(t = t_{min})$, the time evolution in an intervall $[t_{min}, t_{max}]$ is calculated by interating over time in τ- steps and minimize D with respect to $\rho(t+\tau)$ in each iteration. The variational result $\rho^{var}(t+\tau)$ is the initial state $\rho(t)$ for the next iteration and so forth.

The largest share of the error of this integration process will in general be rooted in the limitation of the variational manifold. The value of the variational norm at the variational minimum is a measure for this error. On the other hand, the error originating from the finite integration step τ is small in comparison.

Finally, we want to stress that integration schemes such as the common Runge Kutta method [150] generate higher order of correlations and are therefore more difficult to handle than our variational approach.

3.2.2. Upper bound

For the concrete calculation of the variational time evolution we use an upper bound of the functional D given by Eq. (3.17) which reads

$$D \leq \sum_{\langle ij \rangle} \left|\left|\rho_{ij}(t+\tau) - \rho_{ij}(t) - \frac{\tau}{2}\mathcal{L}[\rho_{ij}(t) + \rho_{ij}(t+\tau)]\right|\right|_1, \tag{3.19}$$

for product states. In a translational invariant system the problem is reduced to a single two-site problem.

If nearest-neighbour correlations are included in the variational manifold, the upper bound of the variational norm includes three sites

$$D \leq \sum_{\langle ijk \rangle} \left|\left|\rho_{ijk}(t+\tau) - \rho_{ijk}(t) - \frac{\tau}{2}\mathcal{L}[\rho_{ijk}(t) + \rho_{ijk}(t+\tau)]\right|\right|_1, \tag{3.20}$$

corresponding to the steady-state analysis. For the derivation of the upper bounds see App. (A). The parametrization of $\rho_{ij}(t + \tau)$ and $\rho_{ijk}(t + \tau)$ works analogue to the variational steady state analysis described in chapter (3.1.2).

4. Multicriticality of the non-equilibrium steady state

In the following chapter, we will investigate the critical properties of a dissipative Ising model that preserves the Z_2-symmetry.

In the first part, we will review the equilibrium quantum Ising model and show its most important results.

In the second part, we investigate a dissipative Ising model. The content of the subsections (4.4-4.6) are based on the publication [151]. Our analysis is based on the variational ansatz for product states described in chapter (3.1.1), from which we construct a Landau theory for open quantum systems. Effective classical theories using product states have been succesfully applied to the investigation of open quantum systems, e.g. in [35, 44, 54, 152, 153]. We identify one variational parameter as the order parameter describing the paramagnet-ferromagnet transition. We will show that the non-equilibrium steady state phase diagram includes, beside a continuous transition known from the equilibrium Ising model, a first order transition and a tricritical point. As our variational manifold is limited to product states, we will verify in detail the accurateness of our ansatz by estimating the strength of fluctuations via a Ginzburg-Landau analysis and renormalization group corrections.

4.1. The equilibrium Ising model

The many-particle Ising model is one of the most basic models of statsitical physics. In two dimensions, it exhibits a continuous ferromagnetic transition, which is , next to the condensation of steam or freezing of water, one of the most famous examples for a phase transition [154].

The Hamiltonian of the quantum mechanical equivalent of the transverse field Ising model is written in terms of operators, in this case pauli matrices $\sigma^{(i)}_{\{x,y,z\}}$, and reads

$$H = -\Delta \sum_i \sigma_x^{(i)} - J \sum_{\langle ij \rangle} \sigma_z^{(i)} \sigma_z^{(j)} \tag{4.1}$$

with the interaction strength J and the transverse magnetic field Δ.

The $\sigma_z^{(i)} \sigma_z^{(j)}$ part of the Hamiltonian has the ± 1 eigenvalues with the corresponding spin states $| \uparrow \rangle_i$ and $| \downarrow \rangle_i$. Without the off-diagonal σ_x-part, the quantum Ising model thus reduces to its classical counterpart. The transverse field, however, perturbs the magnetic

order. The expectation value of σ_z will serve as the order parameter, defining the status of order and symmetry in the system.

The symmetry properties of the Hamiltonian play a crucial role concerning the investigation of phases and phase transitions. We see that the Z_2 transformation

$$\sigma_z^{(i)} \to -\sigma_z^{(i)}; \quad \sigma_x^{(i)} \to \sigma_x^{(i)}, \tag{4.2}$$

that is generated by the application of the σ_x operator to each site ("spin flip"), leaves the Ising Hamiltonian invariant. In a phase, where the ground state is not left invariant under the $\prod_i \sigma_x$ transformation, this symmetry is not present anymore, one speaks of spontaneous symmetry breaking [79]. These considerations will be crucial in the identification of the different phases of the Ising model and their transition into one another.

With regard to the paramter Δ, we can basically distinguish betweent two different cases: In the leading order of $\Delta \gg J$, the ground state is given by

$$|0\rangle = \prod_i (|\uparrow\rangle_i - |\downarrow\rangle_i) \equiv \prod_i |\leftarrow\rangle_i \tag{4.3}$$

with the corresponding -1 eigenvalue of σ_x. From definition (4.3), we can readily see that $\langle 0|\sigma_z^{(i)}|0\rangle = 0$, i.e. in this parameter regime, we are in the unordered phase. Correlations between different sites i and j vanish as $\langle 0|\sigma_z^{(i)}\sigma_z^{(j)}|0\rangle = \delta_{ij}$. An expansion in $1/\Delta$ gives [79]

$$\langle 0|\sigma_z^{(i)}\sigma_z^{(j)}|0\rangle \propto e^{-|r_i - r_j|/\xi}, \tag{4.4}$$

i.e. they remain short-ranged. Here, ξ corresponds to the correlation length introduced in (2.17).

In the opposite case of $\Delta \ll J$, the σ_z part of the Hamiltonian with the corresponding eigenvalues and eigenstates dominates. For $\Delta = 0$, we get the degenerate ground state

$$|\uparrow\rangle = \prod_i |\uparrow\rangle; \quad |\downarrow\rangle = \prod_i |\downarrow\rangle. \tag{4.5}$$

Regarding these ground states, one immediately notices that the Z_2 symmetry is broken as the transformation does not leave the ground state invariant, but instead maps one ground state into the other one. Also the correlations behave different compared to the large Δ-case. Assuming a small g perturbation leads to

$$\lim_{|x_i - x_j| \to \infty} \langle 0|\sigma_z^{(i)}\sigma_z^{(j)}|0\rangle = n^2. \tag{4.6}$$

Accordingly, the order parameter is given by $\langle 0|\sigma_z|0\rangle = \pm n$ with n being the spontaneous magnetization. Due to the finite value of the order paramater, we are in the ordered phase. At some critical value $\Delta = \Delta_c$, there is the phase transition between the ordered and the unordered phase, transforming the power law of correlations according to (4.4) into (4.6) in a nonanalytic way with respect to Δ, as indicated in Fig. (4.1).

Figure 4.1.: On top: Continous transition between the paramagnetic and the ferromagnetic phase according to the transverse field Ising model with the transverse field Ω and the single-spin energy Δ. The picture below shows the degenerate ground states of the ferromagnet.

4.2. A Z_2 symmetric dissipative Ising model

In the dissipative Ising model studied in the previous chapter (3.1.2) with the variational approach, the Z_2 symmetry of the Hamiltonian is broken externally due to the Lindblad terms in the master equation. In the following, we will study an Ising model in which the dissipation acts in the eigenbasis of the transverse field, leading to an invariance of the master equation with respect to the Z_2 transformation. The transverse field Ising Hamiltonian reads

$$H = \Delta \sum_i \sigma_z^{(i)} - J \sum_{\langle ij \rangle} \sigma_x^{(i)} \sigma_x^{(j)}, \qquad (4.7)$$

with the transverse field in z-direction with strength Δ and interaction strength J. The Z_2-transformation [32]

$$\sigma_x \to -\sigma_x \qquad \sigma_y \to -\sigma_y \qquad (4.8)$$

leaves the master equation invariant as the Lindblad part is bilinear in the Lindblad operators $c_i = \sigma_-$. The overall sign is unchanged and we have a global Z_2 symmetry, which then might be spontaneously broken in a ferromagnetic phase. Calculations of this model have already been done by a Keldysh approach, where findings indicate that the continous transition becomes instable for sufficiently large dissipation rates [32]. We will investigate phase transitions of the steady state of the model via our variational principle.
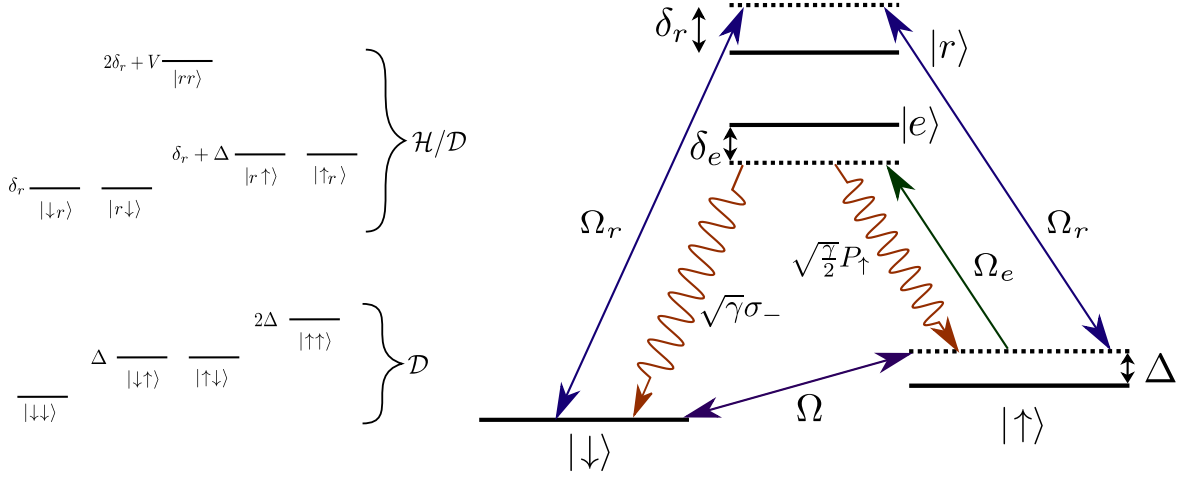
Figure 4.2.: Left side: Eigenstates of H_0, where each atom has a level scheme shown on the right side. We also denoted the corresponding eigenenergies and the subspaces of the Hilbert space the eigenstates belong to. Right side: The spin configurations $|\uparrow\rangle$ and $|\downarrow\rangle$ form the ground state manifold, the Rydberg state $|r\rangle$ is dressed with Rydberg dressing δ_r. Both dissipation processes are realized via the $|e\rangle$-state.

4.3. Level scheme

For the experimental realization of the Z_2-preserving dissipative Ising model, we use a level scheme of dressed Rydberg atoms with the Rydberg state being weakly admixed to the ground state. In the level scheme we propose, the states $|\uparrow\rangle$ and $|\downarrow\rangle$ correspond to the ground states are coupled to the Rydberg state $|r\rangle$ with a Rabi frequency Ω_r. Additionally, the ground states are coupled to each other via a frequency Ω, see Fig. (4.2). This admixing of the Rydberg state to the ground states allows us to effectively integrate out the Rydberg state using a perturbative approach. We assume that the full Hamiltonian of the two-atom system can be written as

$$H = H_0 + H_1 \tag{4.9}$$

with the perturbative part H_1. We divide the Hilbert space into two subspaces, the model space $\mathcal{D}$ [155], which contains the low-energy eigenstates of H_0, namely all possible combinations of the $|\uparrow\rangle$ and $|\downarrow\rangle$-states, and the complementary high energy subspace $\mathcal{H}/\mathcal{D}$ containing the Rydberg state $|r\rangle$, see Fig. (4.2). H_1 represents the coupling between the low-energy and the high-energy states, i.e. it contains all Ω_r-terms. Here, we expand the full Hamiltonian H in Ω_r/δ_r up to $k-$th order via Lindgren's perturbation theory for almost degenerate states [156]. A more detailed description of that procedure can be found in App. (D). The resulting effective Hamiltonian $H_{\text{eff}}^{(k)}$ acts on the $\mathcal{D}$-subspace eigenstates $|\Psi^\mathcal{D}\rangle$ of H_0 as

$$H_{\text{eff}}^{(k)}|\Psi_n^\mathcal{D}\rangle = E_n^{(k)}|\Psi_n^\mathcal{D}\rangle \tag{4.10}$$

with the eigenenergies $E_n^{(k)}$ being the exact eigenenergies of H_0 up to the k-th order of Ω_r/δ_r. In the most general case, the effective Hamiltonian can be written in terms of Pauli matrices as

$$H_{\text{eff}} = \Delta \sum_i \sigma_z^{(i)} + \Omega' \sum_i \sigma_x^{(i)} - \sum_{ij} J_{ij}\sigma_x^{(i)}\sigma_x^{(j)} \ + \ \text{const.} \tag{4.11}$$

The parameters Δ and Ω' of the Hamiltonian contain the parameters from the level scheme according to Fig. (4.2). We can get rid of the Z_2 symmetry breaking σ_x-term by changing the coupling Ω of the two ground states. Note that H_{eff} is only Hermitian up to $k-$th order of Ω_r/δ_r. Here, we expand to the fourth order and find that for $\Omega_r = \delta_r/10$ and $\Delta \sim |J_{\langle ij\rangle}| \sim \Omega_r^4/\delta_r^3$, the σ_x-term is strongly suppressed compared to the σ_z- and $\sigma_x\,\sigma_x$-terms. The Rydberg interaction strength V, on the other hand, has to be fixed at a value small enough to justify our cut off beyond nearest-neighbour interactions. We found $V = 3\,\delta_r$ as a reasonable value. The dissipative terms $\sim \sigma_-$ in the Liouvillian of the master equation are realized by optical pumping from the spin-up into the spin-down state. The corresponding atomic states in the case of ^{87}Rb are $|\uparrow\rangle = |5S_{1/2}, F = 2, m_F = 2\rangle$, $|\downarrow\rangle = |5S_{1/2}, F = 2, m_F = 1\rangle$, and $|e\rangle = |5P_{3/2}, F = 3, m_F = 2\rangle$. For this choice, we have an additional dephasing into the $|\uparrow\rangle$ state. The corresponding jump operator $P_\uparrow = |\uparrow\rangle\langle\uparrow|$ preserves the Z_2 symmetry and is also weaker than the dissipative spin flip. [157].

4.4. Landau theory for open quantum systems

Following the description in chapter (3.1.2) for a translationally invariant system, we parametrize the product state density matrix $\rho_{ij} = \rho_i \otimes \rho_j$ with $\rho_i \equiv \rho_j$ via the variational parameters

$$\alpha = (\langle\sigma_x\rangle, \langle\sigma_y\rangle, \langle\sigma_z\rangle) \equiv (\phi, c\phi, \lambda). \tag{4.12}$$

The non-analyticity is contained in ϕ. Consequently, the seperation of c and ϕ in the σ_y-coefficient makes c an analytic function. We identify ϕ as the order parameter which has a finite value in the ferromagnetic (ordered) phase. Then, the time derivative $\dot\rho_{ij}$ is given by the master equation, where we use the Z_2-preserving dissipative Ising model with the Hamiltonian (4.7) and the jump operators $c_i = \sqrt{\gamma}\sigma_-^{(i)}$. The variational minimization with respect to the trial state ρ_{ij} is applied according to

$$||\dot\rho_{ij}|| \rightarrow \min. \tag{4.13}$$

In the region of interest, the variational state gained via the numerical minimization of $||\dot\rho_{ij}||$ is close to purity with $\alpha^2 = 1$. Therefore we set λ to $\lambda^2 = 1 - \phi^2 - (c\phi)^2$ in our analytic calculation and keep ϕ and c as variational parameters. We can now begin with the analysis in close analogy to Landau theory for equilibrium systems. Compared to the Landau expression for closed systems introduced in Eq. (2.15), the energy functional is replaced by the variational norm. As we assume a homogeneous system, there is no

spatial dependence of the order parameter and we drop the gradient term. Finally the expansion of the variational norm $||\dot\rho_{ij}||$ in the order parameter $\phi = \langle\sigma_x\rangle$ up to sixth order leads to

$$||\dot\rho_{ij}|| = u_0 + u_2\phi^2 + u_4\phi^4 + u_6\phi^6. \tag{4.14}$$

The coefficients u_n are functions of the parameters of the Hamiltonian as well as of the coordination number $z = 2d$ and the variational parameter c. The full expression of the coefficients is given in App. (E). We can now see the advantage of separating c from ϕ in the σ_y- coefficient: Any non-analytic behaviour is contained in ϕ, whereas c and the coefficients u_n are smooth functions. Accordingly, we can classify the phase transition by the behaviour of ϕ. A discontinuous jump of ϕ indicates a first order transition, whereas a discontinuity of the derivative is connected to a second order transition. The analytic part c of the variational parameters can be determined directly from the following considerations: Far away from a phase transition, the variational norm is dominated by the ϕ^2-term of the expansion. Consequently, the variational solution is found by minimizing the u_2 coefficient with respect to c, which results in

$$c = \frac{J\gamma z}{(\gamma/2)^2 + 4\Delta^2}. \tag{4.15}$$

The order parameter ϕ, which is left as an independent variational parameter, determines the phase of the steady state: For a finite value of ϕ, there is an ordered phase with a broken Z_2 symmetry, whereas for $\phi = 0$, there is an unordered phase.

4.5. Spontaneous symmetry breaking of the variational steady state

The possible different kinds of phase transitions of a ϕ^6 theory according to Eq. (4.14) are known: They range from a continuous transition to a first order transition, which would be an extension to the phase diagram known from the equilibrium case, and a tricritical point, where the lines of first and second order meet. For the second order transition, we have the condition [158]

$$u_2 = 0; \quad u_4 > 0. \tag{4.16}$$

The behaviour of the variational norm at the second order transition is shown at the left side of Fig. (4.3). The global minimum of the variational norm at $\phi = 0$ in the paramagnetic phase is turned into two symmetric minima, indicating a second order transition. The condition for the first order transition is $||\dot\rho_{ij}|| = 0$ and $\partial||\dot\rho_{ij}||/\partial\phi = 0$. Solving these equations with respect to u_2, one gets

$$u_2 = \frac{|u_4|}{6u_6}; \quad u_4 < 0. \tag{4.17}$$
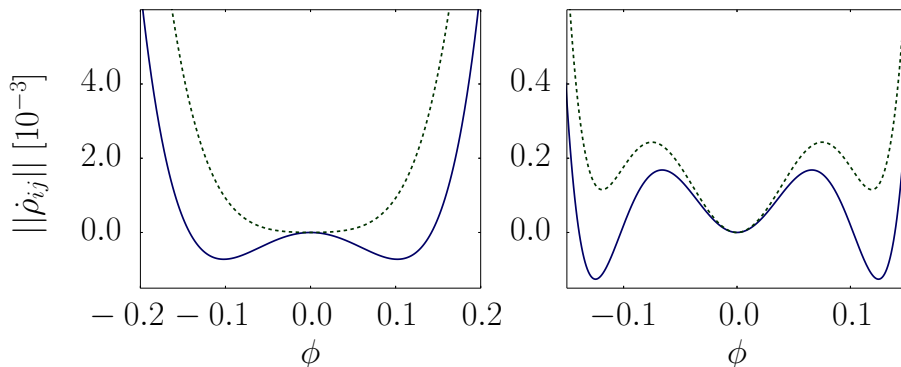
Figure 4.3.: Expansion in the variational norm $||\dot{\rho}_{ij}||$ to the sixth order in ϕ over ϕ in the paramagnetic (dashed) and the ferromagnetic (solid) phase. One notices that close to the second order transition (left), there is single minimum at $\phi = 0$ in the PM phase, which is transformed into two symmetric minima in the FM phase. Close to the first order transition (right) there are three distinct local minima. The global minimum moves from the minimum at $\phi = 0$ in the PM phase to the minima at finite ϕ in the FM phase.

We see that in the case of a first order transition, u_4 becomes negative and the ϕ^6-term becomes relevant for the stability of the expansion of the variational norm. Close to the first order transition, there are three different minima (right side of Fig. (4.3). At the transition, the global minimum is shifted from $\phi = 0$ in the paramagnetic phase to $\phi \neq 0$ in the ferromagnetic phase. First and second order line meet at the tricritical point, which accordingly fullfils $u_2 = 0$; $u_4 = 0$. The non-equilibrium steady state phase diagram exhibits all these phenomena, see Fig. (4.4). We can conclude that adding dissipation to the dynamics significantly alters the phase diagram, including the appearance of a first order transition and a tricritical point. In addition to that, the order parameter behaves as $\phi \sim \pm(-u_2/3u_6)^{1/4}$ in the tricritical regime, which means that we have a critical exponent of $1/4$ instead of $1/2$ known from the equilibrium Ising phase diagram.

4.6. Fluctuations of the system

The construction of the Landau expansion in chapter (4.5) is based on product states. The true steady state will deviate from this product state as indicated by the finite value of the variational norm at the variational minimum. In this chapter, we will address the question how strong fluctuations influence the system and at which point they lead to a breakdown of the product state ansatz. In the first part, we will introduce spatial inhomogeneities. Then, we will make use of Ginzburg's criterion to calculate the upper critical dimension, that tells us at which dimension the product state solution becomes self-consistent at the tricritical regime.
In the second part, corrections of the Landau coefficients are calculated via a
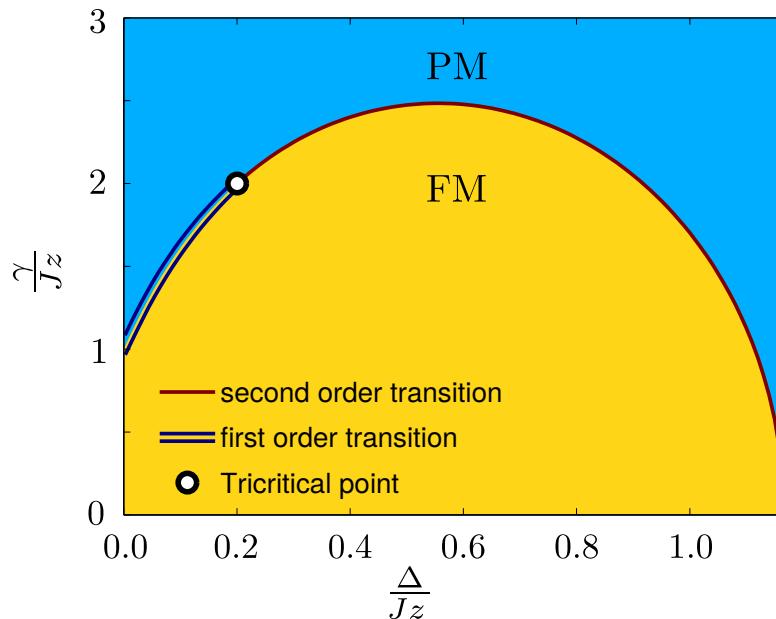
Figure 4.4.: Steady state phase diagram of the three-dimensional dissipative Ising model. We find a first order and a second order transition between ferromagnetic (FM) and paramagnetic (PM) phases. First and second order line meet at a tricritical point.

renormalization group analysis. In the last part, we analyze the behaviour of the variational solution for infinite spatial dimensions. In this limit, there are no correlations and the variational approach becomes equivalent to mean field theory.

4.6.1. Spatial inhomogeneities

Fluctuations will generally produce spatial inhomogeneities. Including spatial inhomogeneities in our analysis means that the value of the order parameter ϕ_i depends on the site i. According to Eq. (3.4), the variational norm of an inhomogeneous lattice consists of a sum over the bonds ρ_{ij}. An expansion of the variational norm leads to

$$D = \sum_{\langle ij \rangle} ||\dot{\rho}_{ij}|| = \sum_{\langle ijkl \rangle} \frac{J}{2} (z-1) (\phi_i - \phi_k)^2 + \frac{J}{2} (z-1) (\phi_j - \phi_l)^2 + J'(\phi_i - \phi_j)^2 \quad (4.18)$$

$$+ \sum_{\langle ij \rangle} \left[u_0 + u_2 \phi_i^2 + u_4 \phi_i^4 + u_6 \phi_i^6 \right].$$

Here, the coefficients u_n correspond to the coefficients of the expansion (4.14) from the homogeneous case. Due to the inhomogeneities, there are additional terms of the form $\sim (\phi_i - \phi_k)^2$ with neighbouring sites i and k. The coefficient J' is given by

$$J' = -\frac{J}{4} + \frac{\left(\frac{\gamma}{4}\right)^2 + \Delta^2}{4J} + \frac{J\gamma^2}{\gamma^2 + 16\Delta^2}. \quad (4.19)$$

For a finite value of ϕ_i, there is also a σ_x and a σ_y component of the one-site density operator ρ_i according to the ansatz (4.12) and the eigenbasis of ρ_i is not just the σ_z eigenbasis. Consequently, the coupling J' also depends on γ and Δ beside the interaction strength J. In the long wavelength limit, we have $\phi_i - \phi_k = \phi_j - \phi_l = \phi_i - \phi_j$, and after factoring out the coordination number z we arrive at

$$D = \sum_{\langle ij \rangle} z \left[\frac{J}{2} \left(1 - \frac{1}{z} \right) + \frac{J'}{z} \right] (\phi_i - \phi_j)^2 + \sum_i z \left[u_0 + u_2 \phi_i^2 + u_4 \phi_i^4 + u_6 \phi_i^6 \right]. \quad (4.20)$$

We see that even in the presence of spatial inhomogeneities, the variational norm can be written in a relatively compact form, allowing us to further analyse its behaviour near to criticality.

Taking the continuum limit of the variational norm according to Eq. (4.20) the $(\phi_i - \phi_j)$ term transforms to a gradient and the summation over the sites becomes an integral over the spatial variable x. This leads to

$$D[\Phi] = z \int d^d x \; u_0 + v_2 (\nabla \Phi)^2 + u_2 \Phi^2 + u_4 \Phi^4 + u_6 \Phi^6. \quad (4.21)$$

with the gradient coefficient v_2 given by

$$v_2 = \left[\frac{J'}{z} + \frac{J}{2} \left(1 - \frac{1}{z} \right) \right] a^2. \quad (4.22)$$

4.6.2. Ginzburg's criterion

In this section, we will apply the so-called Ginzburg criterion to analyze the strength of fluctuations and at which point they lead to a breakdown of the product state ansatz. We consider the continuum limit of the variational norm according to Eq. (4.21) as a Ginzburg-Landau functional [159]. The squared length scale of correlations can be calculated via

$$\xi^2 = v_2 / 2|u_2|. \quad (4.23)$$

The order parameter ϕ from the previous section is the spatial average of the fluctuating field $\Phi(x)$. The mean square deviation of the field reads [159]

$$\langle [\phi - \Phi]^2 \rangle = \frac{T_{\text{eff}}}{2 v_2} \xi^{2-d} w^d. \quad (4.24)$$

Here, w is the reduced patch version of the Yukawa potential and $\langle ... \rangle$ stands for the averaging over different realizations of the Gaussian fluctuations.

The next step is to evaluate the quantities appearing on the right side of Eq. (4.24) to find an analytic expression for the strength of fluctuations related to the variational solution.

The fluctuations in our system exhibit thermal statistics [32] due to the existence of a dynamical symmetry [54] and therefore can be characterized by an effective temperature

4. Multicriticality of the non-equilibrium steady state

T_{eff}. This effective temperature is directly connected to the variational norm of the product state solution as the variational norm measures the fluctuation-induced deviation of the true steady state from the variational state. Normalizing the variational norm by a factor of $z/2$ we get an intensive quantity, which reads

$$T_{\text{eff}} = \frac{z}{2} ||\dot{\rho}_{ij}||. \tag{4.25}$$

According to Eq. (4.25), the value of the effetive temperature is given by zJ at the Ising transition line, which corresponds to the result found via field-theoretical calculations within a Keldysh formalism [32]. We can now start to evaluate the mean square deviation of the order parameter field Φ at the tricritical point. At the $u_4 = 0$-line, the order parameter behaves as

$$\phi = \pm(-u_2/3u_6)^{1/4}. \tag{4.26}$$

Remarkably, the critical exponent of the order parameter becomes $\beta = 1/4$ rather than $1/2$, which indicates that there is a different universality class than in the case of the equilibrium Ising transition. Inserting the expressions of ξ^2 and T_{eff} in Eq. (4.24), we get

$$\frac{\langle [\phi - \Phi]^2 \rangle}{\phi^2} = \frac{\sqrt{3}}{4} w^d v_2^{-d/2} u_0 \sqrt{u_6} u_2^{(d-3)/2} \tag{4.27}$$

as the relative mean square deviation of ϕ. We can now see the special role of $d = 3$ dimensions: Approaching the tricritical point, i.e. $u_2 \to 0$, fluctuations will increase for $d < 3$. For $d > 3$, on the other hand, the u_2-exponent is positive and fluctuations decrease. So, in above 3 dimensions, our product state ansatz becomes self-consistent and the mean field exponents become correct. For the experimental case of three dimensions, there are logarithmic corrections of these exponents [160], which should not qualitatively change the results.

4.6.3. One loop renormalization-group corrections

So far, we neglected potentially influential renormalizations of the u_4-term, which can lead to large shifts of the position of the tricritial point. In this chapter, we will calculate the one-loop renormalization group corrections of the u_4 term. The renormalization group analysis combined with a perturbative treatment of higher order terms in a Ginzburg-Landau-Wilson functional allows us to calculate corrections of the position of the tricritial point systematically. In this sense it is an extension of the analysis of fluctuations done in the previous chapter.
As a starting point, the variational norm D

$$D[\Phi] = z \int d^d x \; u_0 + v_2 (\nabla \Phi)^2 + u_2 \Phi^2 + u_4 \Phi^4 + u_6 \Phi^6, \tag{4.28}$$

is considered equivalent to an effective Ginzburg-Landau-Wilson (GLW)-functional [161], where the higher order terms, in this case the Φ^6- term, are
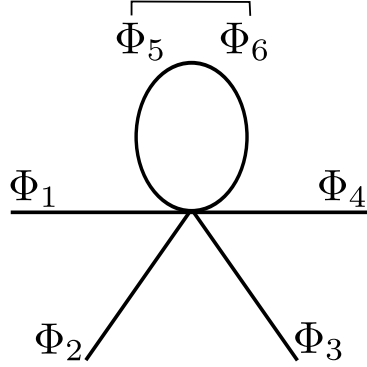
Figure 4.5.: One-loop correction of the u_4-term in the momentum space intergral. There are $\binom{6}{2}$ possibilities of contracting (the circle) two order parameter fields in a ϕ^6-term.

treated as a perturbation. Transforming the GLW-functional (4.28) into momentum space, one can apply the steps of the renormalization group, that is, modifying the length scale, rescaling and renormalization. Here, we use a differential RG transformation, obtaining differential equations for the renormized coefficients rather than recursion formulas [83]. We get to the linear flow equations [161]

$$\frac{du_2}{dl} = 2u_2 + c_1 u_4 + c_2 u_6 \tag{4.29}$$

$$\frac{du_4}{dl} = (4 - d)u_4 + c_3 u_6 \tag{4.30}$$

$$\frac{du_6}{dl} = (3 - d)u_6. \tag{4.31}$$

Of special interest is the renormalized $u_4(l)$-term as its fixed point characterizes the phase transition. The c_3-term is calculated as follows: Transformed into Fourier space, we can split up $D[\Phi(q)]$ into a part for which we have the familiar Gaussian solution:

$$D[\Phi]_0 = \int \frac{d\mathbf{q}}{(2\pi)^d} (u_2 + v_2 \mathbf{q}^2)\Phi_{\mathbf{q}}^2 + u_4 \Phi_{\mathbf{q}}^4. \tag{4.32}$$

and the higher order perturbative part

$$V = \frac{u_6}{(2\pi)^{5d}} \int d\mathbf{q}_1 d\mathbf{q}_2 d\mathbf{q}_3 d\mathbf{q}_4 d\mathbf{q}_5 \Phi_{\mathbf{q}_1}\Phi_{\mathbf{q}_2}\Phi_{\mathbf{q}_3}\Phi_{\mathbf{q}_4}\Phi_{\mathbf{q}_5}\Phi_{-\mathbf{q}_1-\mathbf{q}_2-\mathbf{q}_3-\mathbf{q}_4-\mathbf{q}_5} \tag{4.33}$$

that leads to deviations from the Gaussion solution. In Fig. 4.5, we show the origin of the $c_3 u_6$-term: Two order parameter fields in the momentum space integral V are contracted which leads to an additional fourth order term. The contraction of the perturbation V reads [161]

$$\langle \Phi_{\mathbf{q}_1}\Phi_{\mathbf{q}_2} \rangle = \frac{(2\pi)^d \delta^d(\mathbf{q}_1 + \mathbf{q}_2)}{2(u_2 + v_2 \mathbf{q}_1^2)}. \tag{4.34}$$

4. Multicriticality of the non-equilibrium steady state

Integrating out the contracted part in Eq. (4.33) we find for c_3

$$c_3 = \frac{2^{-d}15S_d}{\pi^2 v_2},\tag{4.35}$$

where S_d is the surface area of the d-dimensional unit sphere. The prefactor 15 stems from the number of possible contractions.

As a solution for the flow equations (4.29-4.31), we get

$$u_4(l) = u_4(0)e^{(\epsilon+1)l} + c_3 u_6(0)\left[e^{(\epsilon+1)l} - e^{\epsilon l}\right]\tag{4.36}$$

$$u_6(l) = u_6(0)e^{\epsilon l},\tag{4.37}$$

where $\epsilon = 3 - d$. The critical behaviour and the first order line of the system is determined by the fixed point u_i^* of the renormalization group transformation [83]. Choosing a suitable initial condition $u_2(0)$, the fixed point u_2^* corresponds to the Ising critical line.

There are three different cases for the fixed point of u_4: If $u_4^* = \infty$, the renormalized u_4 is positive and there is a continuous transition. For $u_4^* = -\infty$, we end up at a first order transition. The tricritial point in $d \geq 3$ is found for $u_4^* = 0$. Eq. (4.36) tells us that the value of the fixed point u_4^* depends on the sign of $u_4(0) + c_3 u_6(0)$. Consquently, the microscopic coupling constants $u_4(0)$ and $u_6(0)$ characterize the phase transition. Therefore we have a shift of the tricritial point from $u_4 = 0$ to $u_4 = -c_3 u_6$. For $d = 3$ dimensions, the renormalized tricritial point is located at $(\Delta/Jz, \gamma/Jz)_{\text{TC}} = (0.023, 0.35)$. The c_3 coefficient decreases exponentially with dimension and so does the shift of the tricritial point due to renormalization corrections.

4.6.4. Relation to mean-field theory

The mean-field equations for the time derivative of the Pauli operators read

$$\frac{d}{dt}\langle\sigma_x\rangle = -\frac{\gamma}{2}\langle\sigma_x\rangle - 2\Delta\langle\sigma_y\rangle\tag{4.38}$$

$$\frac{d}{dt}\langle\sigma_y\rangle = -\frac{\gamma}{2}\langle\sigma_y\rangle + 2\Delta\langle\sigma_x\rangle + 2zJ\langle\sigma_x\rangle\langle\sigma_z\rangle\tag{4.39}$$

$$\frac{d}{dt}\langle\sigma_z\rangle = -\gamma - \gamma\langle\sigma_z\rangle - 2zJ\Delta\langle\sigma_x\rangle\langle\sigma_y\rangle.\tag{4.40}$$

The expectation value of σ_x of the steady state with $\frac{d}{dt}\langle\sigma_x\rangle = \frac{d}{dt}\langle\sigma_y\rangle = \frac{d}{dt}\langle\sigma_z\rangle = 0$ is given by

$$\langle\sigma_x\rangle = \pm\Re\left\{\frac{\sqrt{\gamma^2 + 16zJ\Delta - 16\Delta^2}}{2\sqrt{2}zJ}\right\}\tag{4.41}$$

Expression (4.41) gives a second order transition at [32]

$$\gamma_c^2 - 16(zJ\Delta + \Delta^2) = 0.\tag{4.42}$$
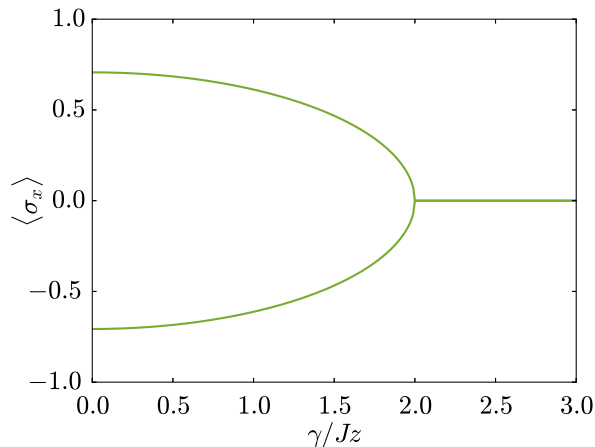
Figure 4.6.: Mean field solution for the order parameter $\phi = \langle\sigma_x\rangle$ for $\Delta/Jz = 0.5$ and $z = 6$. There is a continuous transition at γ_c given by Eq. (4.42). For $\gamma < \gamma_c$, we have two symmetric solutions of $\langle\sigma_x\rangle$ according to Eq. (4.41).
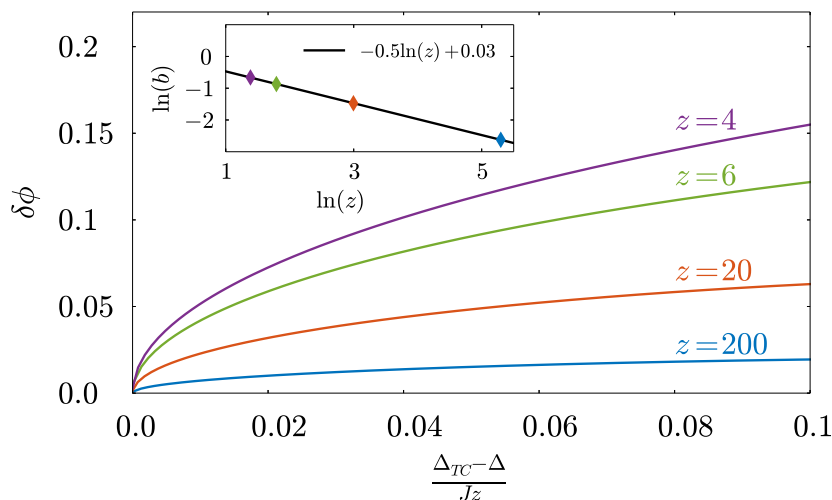
Figure 4.7.: Jump of the order parameter $\delta\phi$ versus $\frac{\Delta_{TC}-\Delta}{Jz}$ along the first order line for $z = 4, 6, 20$ and 200. Via double logarithmic fitting, we obtain the prefactor b from to Eq. (4.43). In the inset, the logarithm of b is plotted against the logarithm of z. The corresponding fit (solid line) confirmes the $b \propto 1/\sqrt{z}$ behaviour.

between the phases with $\langle\sigma_x\rangle = 0$ and $\langle\sigma_x\rangle \neq 0$, see Fig. (4.6). Crucially, $\langle\sigma_x\rangle$ shows no discontinuities within mean-field theory and thus there is no first order transition. Consquently, mean field theory predictions are qualitatively wrong even above the upper critical dimension. On the other hand, we know that in the limit of $z \to \infty$, correlations vanish and mean field theory becomes correct. One might expect the position of the tricritical point to converge towards $\Delta = 0$ in the limit of infinite

dimensions, so that there is no first order transition in the phase diagram anymore. In our variational analysis, however, we find that the formal solution of the tricritical point, that is, $u_2 = 0$; $u_4 = 0$ approaches $(\Delta/zJ, \gamma/zJ)_{TC} = (0.22, 1.66)$ in the limit of infinite dimensions. Instead, we find that the mean-field result is recovered in another way: The jump of the order parameter $\delta\phi$ at the first order transition can be expressed as

$$\delta\phi = b \left(\frac{\Delta_{TC} - \Delta}{Jz} \right)^{1/2}. \tag{4.43}$$

Fitting the jump of the order parameter along the first order transition line for several values of the spatial dimension $d = z/2$, we find that the prefactor b behaves as $b \propto 1/\sqrt{z}$, see Fig. (4.7). Consequently, the jump $\delta\phi$ is suppressed with increasing dimension. In the case of infinite dimensions, there is effectively no first order transition and the mean-field result is recovered. Incontrast to equilibrium systems, though, mean-field is qualitatively wrong for any finite dimension.

5. Time evolution of Rydberg gases

In this chapter, we will extend the variational analysis of the steady state to the time evolution of a driven-dissipative Rydberg gas. We integrate the quantum master equation within the variational manifold including both only product states and correlated states. Furthermore, we will investigate the intrinsic properties of the dynamics. We will apply a measure for the degree of non-Markovianity and draw a connection to a quantum information measure, which is more easy to handle experimentally. The results presented in this chapter are based on the publication [162].

5.1. Time evolution

We will first briefly introduce the Hamiltonian and the dissipative terms of the system under consideration. In the second part, we show results of the variational analysis of the time evolution introduced in chapter (3.2) and compare them to the full solution of the quantum master equation.

5.1.1. The Hamiltonian

We consider a many-particle system consisting of ultracold Rydberg atoms being placed on an optical lattice with one atom per lattice site. The interaction is van der Waals-like. As each atom is described by a two-level system with the ground state $|g\rangle$ and the Rydberg state $|r\rangle$, the Hamiltonian can be written in the spin $1/2$ formalism with the pauli matrices σ_μ. The ground state is represented by the spin down state, the excited rydberg state corresponds to the spin up state. Accordingly, the quantum jump operators $c_i = \sqrt{\gamma}\sigma_-^{(i)}$ appearing in the incoherent part of the master equation describe a spin flip from the excited state to the ground state with decay rate γ. In the rotating frame, the Hamiltonian is given by

$$H = \frac{g}{2}\sum_i \sigma_x^{(i)} + \frac{h}{2}\sum_i \sigma_z^{(i)} + \frac{V}{4}\sum_{\langle ij\rangle} \sigma_z^{(i)}\sigma_z^{(j)} \tag{5.1}$$

with the interaction strength V following from a repulsive van der Waals interaction, and the laser paramaters g corresponding to the transverse field $\Omega = g$, and the longitudinal field h, related to the detuning Δ by $h = \Delta + zV/2$. Our focus will be on the pure transverse field model with $h = 0$.
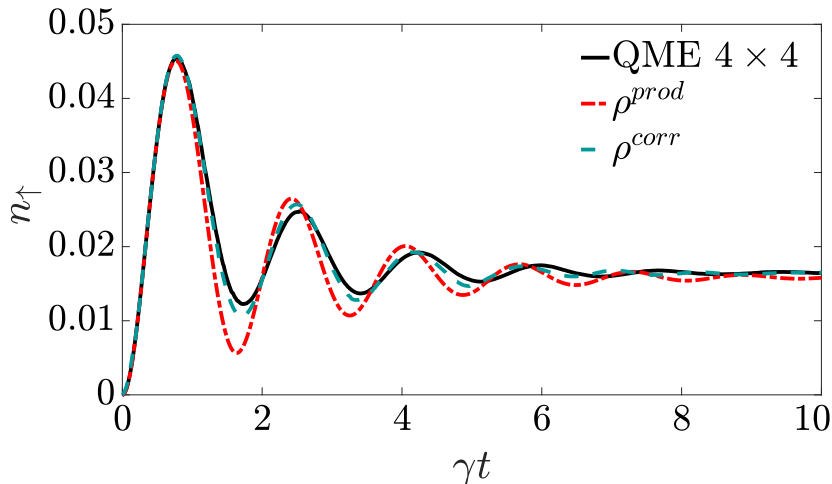
Figure 5.1.: We plot the Rydberg density n_r versus time for $h = 0$, $\Omega = \gamma$ and $V = 2\gamma$. The initial state with zero density corresponds to the electronic ground state. The calculation is done via the quantum trajectory method in a 4×4 lattice (solid), the variational method including correlations ρ^{corr} (dashed) and variational product states ρ^{prod} (dashed-dotted).

5.1.2. Time evolution based on different variational classes

Considering the Hamiltonian (5.1) and the dissipative terms with $c_i = \sqrt{\gamma}\sigma_-^{(i)}$, the time derivative of the density matrix ρ is given by the master equation (2.57). As variational states we use product states $\rho_{ij}^{prod} = \rho_i \otimes \rho_j$ and states including nearest neighbour correlations with $\rho_{ij}^{corr} = \rho_i \otimes \rho_j + C_{ij}$. In the case of product states and a homogeneous system, the variational norm

$$D = ||\rho_{ij}(t + \tau) - \rho_{ij}(t) - \frac{\tau}{2}\mathcal{L}[\rho_{ij}(t) + \rho_{ij}(t + \tau)]|||$$

is minimized with respect to $\rho_{ij}(t + \tau)$ and correspondingly for correlated states, as described in chapter (3.2). The initial state $\rho(t = 0)$ of the time evolution corresponds to the state of all atoms being in the electronic ground state (all spins pointing down). We compare the results of the variational analysis to the solution of the full quantum master equation calculated via a quantum trajectory method [163, 164]. As we can readily see from Fig. (5.1), it is worth accepting more variational parameters for correlated states and the resulting higher computational cost of the variational analysis: The correlated states ρ^{corr} quantitatively agree much better with the quantum trajectory solution than the product state solution ρ^{prod} does.

Iterating the time evolution calculation over different values of Ω and V with $h = 0$, we see that in certain parameter regimes, especially for large Ω and V, the deviation between the two methods becomes quite large, see Appendix (B). We can connect this behaviour to the presence of a first order liquid-gas transition close to this parameter

regime [141], where long-range correlations become important. Therefore our variational description including only nearest- neighbour correlations becomes less accurate. For a more accurate description the variational class has to be extended beyond nearest-neighbour correlations, at the cost of more variational parameters. In chapter (6), in which the liquid-gas transition is intensively studied, we choose another way and investigate the influence of classical fluctuations on the time evolution. On the other hand, the quantum trajectory method is limited to finite lattices (a 4×4 lattice in this case) which is increasingly problematic as finite size effects become stronger approaching the phase transition.

5.2. Properties of the time evolution

As we have seen in the previous chapter, the variational principle using correlated states delivers an appropriate description of the time evolution in the regime of small Ω/γ. In this chapter, we will thus concentrate on the properties of the variational solution for the correlated two-site subsystem ρ_{ij}^{corr}.

5.2.1. Non-Markovian behaviour

Through interactions of the subsystem of interest and its environment, further coherent and incoherent terms that are not included in the Markovian master equation according to Eq. (2.57) possibly emerge and influence the time evolution. For the two-site subsystem ρ_{ij}, the generic shape of the quantum master equation introduced in section (2.3.2) is given by

$$\frac{d}{dt}\rho_{ij} = -i[H(t), \rho_{ij}] \tag{5.2}$$
$$+ \sum_{k=1}^{d^2-1} \gamma_k(t) \left(L_k(t)\rho_{ij}L_k^\dagger(t) - \frac{1}{2}\{L_k(t)L_k^\dagger(t), \rho_{ij}\} \right),$$

If the time evolution is non-Markovian or not is determined by the values of the generalized dissipation rates $\gamma_k(t)$. Equivalently to the generalized master equation (5.2), we can write

$$\dot{\rho}_{ij} = \sum_{k,l=0}^{N-1} c_{kl} G_k \rho_{ij} G_l. \tag{5.3}$$

Here, the G_k operators stand for the tensor product of all possible combinations of Pauli matrices, so that $N = 16$. The $\gamma_k(t)$ are the eigenvalues of the decoherence matrix $\mathbf{d}$ with the entries $d_{kl} = c_{kl}$ for $k, l > 0$.
For one ρ_{ij} and its derivative $\dot{\rho}_{ij}$, Eq. (5.3) is highly under-determined, as the tensor $\mathbf{c}$ consists of N^2 4×4 matrices. In order to uniquely determine $c_{\alpha\beta}$, we solve the Eq. (5.3)

5. Time evolution of Rydberg gases
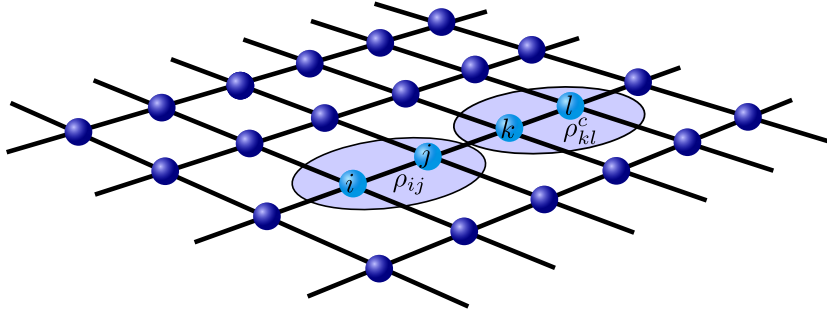
Figure 5.2.: Lattice structure for the calculation of the non-Markovianity $f(t)$. The variational state $\rho_{ij} \equiv \rho^{mn}$ is being iterated over a complete set of initial states. The environment interacting with the sites i and j is given by the solution to the time evolution of the system for correlated states ρ^c; see Fig. 5.1.

for each state of the full set of states

$$\rho^{00} = \frac{\sigma_0 \otimes \sigma_0}{4}; \quad \rho^{mn} = \frac{1 + \sigma_m \otimes \sigma_n}{4} \tag{5.4}$$
$$m, n \in \{0, x, y, z\}; \quad m + n \neq 0.$$

To compute $\dot{\rho}_{ij}(t)$, we take the ρ^{mn} as our initial variational states $\rho_{ij}(t)$. Then, we can variationally calculate $\rho_{ij}(t + \tau)$ and $\rho_{ij}(t + 2\tau)$, holding the surrounding sites fixed to ρ^{corr} from the time evolution of the previous chapter at the corresponding time, see Fig. (5.2). This way, we take the correlations contained in ρ^{corr} and its interaction with the
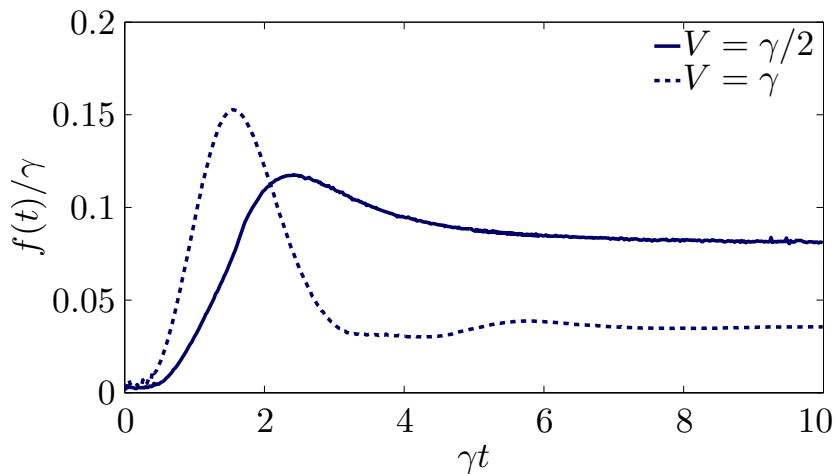
Figure 5.3.: Sum of negative generalized decay rates $f(t)$ for $V = \gamma/2$ (solid) and $V = \gamma$ (dashed). The Rabi frequency is $\Omega = \gamma$.

environment into account. The time derivative of ρ_{ij} is approximated according to

$$\dot{\rho}_{ij}(t+\tau) = \frac{\rho_{ij}(t+2\tau) - \rho_{ij}(t)}{2\tau} + O(\tau^3). \tag{5.5}$$

Iterating over all states in the set (5.4), we find a unique solution for the entries of the $c_{\alpha\beta}$-matrix and finally for the $\gamma_k(t)$ and for $f(t)$. The results for $f(t)$ that is calculated according to Eq. (2.25) are shown in Fig. (5.3). We see that for $\Omega = \gamma$, the non-Markovianity is always finite, remarkably even in the regime of the stationary state ("eternal non-Markovianity" , [94]). We are now able to understand the role of correlations for the time evolution: Neglecting correlations means neglecting non-Markovian behaviour that, however, plays a crucial role for the dynamics. This is the reason why the correlated variational states describe the time evolution quantitatively much better than simple product states.

5.2.2. Quantum linear mutual information

In the previous chapter we saw that the preparation of the lattice to measure the non-Markovianity is quite complicated, as we have to control the two site system independent from its environment and iterate over all 16 states $\rho^{m,n}$. The aim of this subchapter is drawing a connection between the non-Markovianity and a quantity of quantum information, which is easier accessable. While such a connection at a first glimpse seems pretty far-fetched, we will show that the so called quantum linear mutual information (QLMI) reproduces the bilinear dependence on the variational parameters of the variational norm.
The QLMI is defined by [165]

$$I = S_l(\rho_i \otimes \rho_j) - S_l(\rho_{ij}), \tag{5.6}$$

where $S_l(A)$ is the linear entropy given by Eq. (2.62). The QLMI can thus be interpreted as a measure of the strength of correlations, giving the difference of the entropy of the product state of sites i and j, $\rho_i \otimes \rho_j$, and the correlated state ρ_{ij}. For small interaction-values, we find a good agreement of the non-Markovianity and the QLMI, whereas for larger V, the two quantities deviate from each other. This behviour can be verified by expanding ρ_{ij} around product states and writing it as

$$\rho_{ij} = \rho_i \otimes \rho_j + \varepsilon A. \tag{5.7}$$

Here, ϵ is the expansion parameter and A is the product of any two Pauli matrices. Using the ansatz 5.7 we find the following expression for the QLMI:

$$I = \varepsilon \alpha_\kappa \alpha_\lambda + O(\varepsilon^2). \tag{5.8}$$

Remarkably, the QLMI is bilinear in the variational parameters α_μ. The non-Markovianity, on the other hand, is based on the variational solution ρ_{ij}^{var} following

from the minimization of D. We find that both the variational norm D and ρ_{ij}^{var} are bilinear in the variational parameters α, too. Consquently, the non-Markovianity shows the same behaviour with respect to the α as the QLMI.

If we take another measure of information, namely the von-Neumann mutual information I_{VN}, with $S = -\mathrm{Tr}\{\rho\ln\rho\}$, we arrive at

$$I_{\mathrm{VN}} = \varepsilon\,\mathrm{Tr}\{A\ln(\rho_i\otimes\rho_j)\} + O(\varepsilon^2), \tag{5.9}$$

which has a logarithmic dependence on the variational parameters. This is not consistent with the bilinear dependence of the variational norm and thus, unlike the QMLI, cannot give an accurate description of the non-Markovianity.
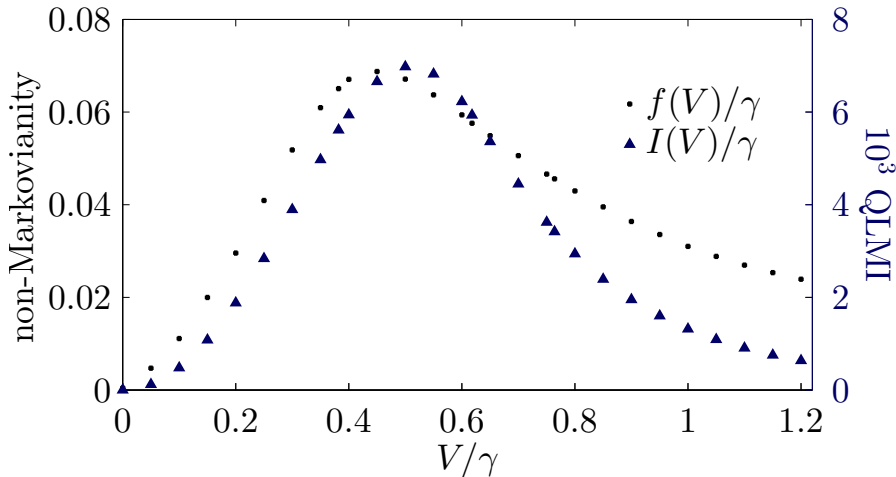
Figure 5.4.: Non-Markovianity f and the quantum linear mutual information (QLMI) I for $t \to \infty$ over the interaction strength V with $\Omega = \gamma$.

These considerations explain why, in the case of small V/γ, we find that the QLMI and only the QLMI deviates from the non-Markovianity just by a constant. In figure (5.4) we show the QLMI and the non-Markovianity of the steady state versus the interaction strength V. For larger V/γ, however, the variational steady state tends towards the pure state with all atoms in the electronic ground state as one sees in Figures (B.1) to (B.4). With regard to the expansion (5.8), this means that the variational parameters except α_z go to zero and the first order term vanishes, making the expansion in ε less accurate. Indeed, for $V > 0.6\gamma$, the QLMI decreases much faster than the non-Markovianity, leading to nontrivial deviations.

6. First order liquid-gas transition

In this section, we will perform a variational calculation of the steady state of a dissipative Ising model [141]. The steady state of that model has been intensively studied, and several predictions of the behaviour of the steady state have been made: Some works predict a bistable phase in the steady state phase diagram [26, 35, 166]. In one dimensional systems, numerical solutions of the full quantum master equation based on monte carlo simulations and exact diagonalization predict a unique solution [47, 166]. Also the existence of an antiferromagnetic phase has been claimed [31]. We will now review the model with the variational approach for the steady state [141, 142, 167] and the time evolution.

6.1. Steady state phase diagram

We calculate the steady state of the dissipative Ising model governed by the Hamiltonian (5.1) and the jump operators $c_i = \sqrt{\gamma}\sigma_-^{(i)}$ using the variational principle according to Eq. (3.1). Assuming a translationally inviariant system the variational minimization procedure reads

$$||\dot{\rho}_{ij}|| \to min \tag{6.1}$$

for product states and

$$||\dot{\rho}_{ijk}|| \to min \tag{6.2}$$

for correlated states (nearest-neighbour correlations). The time derivative of the density matrix $\dot{\rho} = \mathcal{L}\rho$ is given by the quantum master equation according to Eq. (2.57) with the Lindbladian $\mathcal{L}$. In the following chapters, the longitudinal field is assumed to be zero, i.e. $h = 0$.

In the equilibrium transverse field Ising model, the Z_2 symmetry is spontaneously broken in an ordered phase leading to a continuous transition between the unordered and the ordered phase. In the dissipative Ising model under consideration, this symmetry is broken externally in the quantum master equation even for $h = 0$ due to the dissipative terms. Counting the Rydberg excitations as particles, however, with the dissipation being considered as a particle loss process, it is possible to find the equivalent of the liquid-gas transition [168] if a corresponding symmetry arises.

For all values of the interaction strength V and the strength of the transverse field g, the variational analysis provides a unique steady state. The variational steady state can be identified either as a high density state (liquid state) with $n_\uparrow \sim 0.5$ or as a low density

6. First order liquid-gas transition

state (gas) with $n_\uparrow \sim 0.1$. Each of these variational states corresponds to a local minimum of the variational norm. Which of the minima has the lower variational norm depends on the parameters of the model.

For $V = 5\,\gamma$, we find a discontinuous jump of the Rydberg density at a critical value of $g_c = 4.5\,\gamma$ in the case of product states, whereas including nearest neighbour-correlations shifts the jump to $g_c = 5.9\,\gamma$, see left side of Fig. (6.1). Again, we compare the results of the variational analysis with the quantum trajectory method, that solves the full master equation on a 4×4-lattice. Due to the finite size of the system, we observe a rather smooth transition from the lattice gas to the lattice liquid. If we take the largest value of $\partial n_\uparrow / \partial g$ as a basis, the transition according to the quantum trajectory method takes place at $g_c = 5.5$.
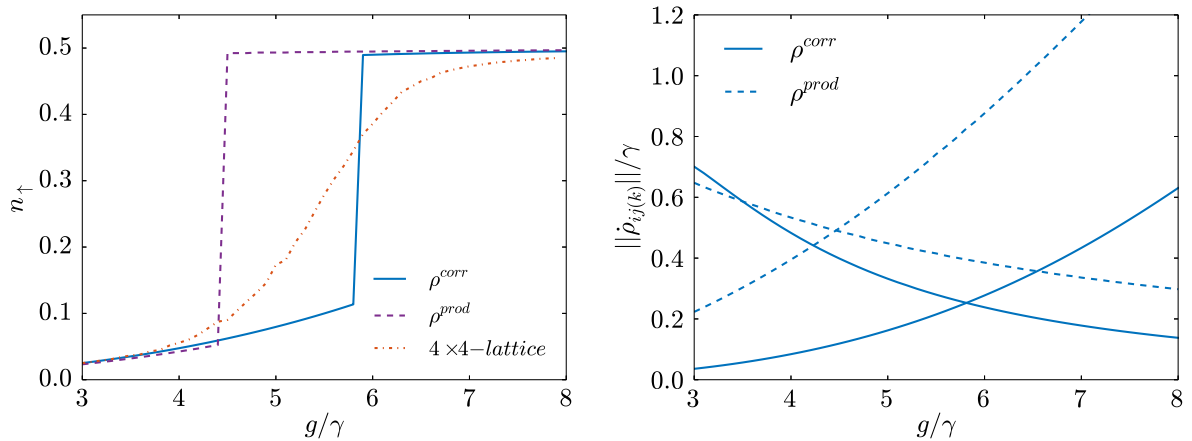
Figure 6.1.: Left side: Rydberg density of the steady state according to the variational principle for product states (dashed line), correlated state (solid line) and for the full solution of the master equation on a 4×4 lattice (dashed-dotted). Right side: Variational norm of the two local minima close to the first order transition again for product states (dashed) and correlated states (solid). In the case of product states, the variational norm corresponds to $||\dot{\rho}_{ij}||$, whereas for correlated states we have $||\dot{\rho}_{ijk}||$. Both figures are calculated at $V = 5\gamma$.

Analogously to equilibrium systems, this first order jump is accompanied by a level crossing of the underlying functional. In our analysis, the free energy functional is replaced by the variational norm. At the right side Fig (6.1), we show the variational norm of the lattice-gas state and the lattice-liquid state for product states and correlated states, repectively. For small g, the variational norm of the liquid is higher. As a consequence, the system prefers the lattice gas as the steady state. When g passes g_c, the variational norm of the lattice liquid becomes smaller than the norm of the gas state, and the system is in the high density state.

Evaluating the g-V phase diagram with the variational principle, we find the first order liquid-gas transition in an intervall of V. Analogously to the classical liquid-gas transition, the transition line ends in a critical point, as shown in the phase diagram
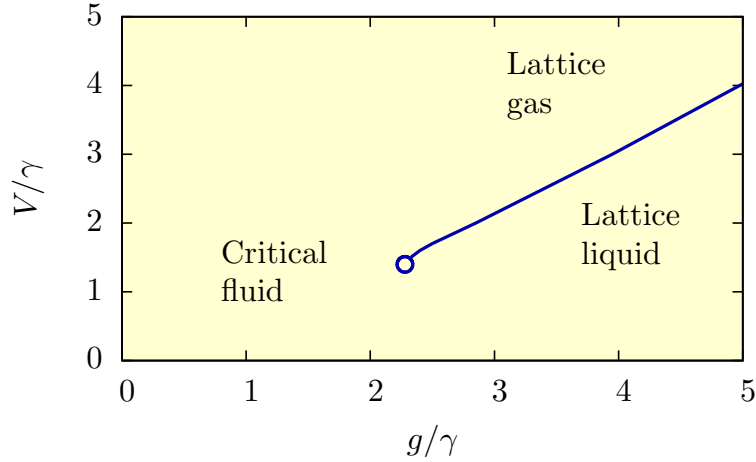
Figure 6.2.: Non equilibrium steady state phase diagram for $h = 0\gamma$ [141]. The first order transition between the lattice gas and the lattice liquid ends in a critical point.

(6.2). Around the critical point, that is located at $(g, V) = (2.28, 1.40)\gamma)$, the system forms a critical fluid [141].

For small interactions strength V, there is no non-analyticity according to perturbation theory in V and consequently no phase transition. Thus one can state that the interaction strength takes the role of the inverse temperature β of the classical liquid-gas transition.

6.2. Time evolution of inhomogeneous states

For a further investigation of the liquid-gas transition described in the previous chapter, we will look at the time evolution close to the transition. In chapter (5.1.2), we saw that including correlations in the variational manifold substantially increases the quality of the variational time evolution. Nevertheless, we also noticed that further improvements are required, especially in parameter regimes close to the liquid-gas transition and for higher values of the Rabi frequency. In this part of the thesis, we extend our variational analysis of product states via including fluctuation-induced spatial inhomogeneities of the lattice. This is done in the same way as it was done for the Ginzburg-Landau analysis in chapter (4.6.2), that allowed us to estimate the accuracy of the product state ansatz. We noticed that under certain conditions fluctuations lead to a breakdown of our product state ansatz.

The strength of these classical fluctuations is given by the variational norm at the variational minimum which in turn defines an effective temperature. In this chapter, we will investigate how such fluctuations influence the dynamics and if there are qualitative changes compared to the homogeneous case. Particularly in the regime of the first order liquid-gas phase transition [141, 142], we will find out which of the two local variational minima of the steady state is favoured by the inhomogeneous time evolution.

6.2.1. A master equation including noise terms

In order to include fluctuations in the analysis, we will now extend the master equation by noise terms of stochastic character. Following the general expression of a stochastic differential equation in the Itô formalism [169], the evolution of $\rho(t)$ is split into two parts and can be written as

$$d\rho = \mathcal{L}\{\rho(t)\}dt + \xi(t)dW(t). \tag{6.3}$$

where the first part on the right side is governed by the quantum master equation represented by the Liouvillian $\mathcal{L}$. This part is solved by the variational approach. Additionally, there is the stochastic Wiener process $W(t)$ and its time increment $dW(t) = W(t + \tau) - W(t)$. The strength of the noise is controlled via the time-dependent coefficient $\xi(t)$. Using $d\rho = \rho(t + \tau) - \rho(t)$ with the integration time step τ, we can rewrite Eq. (6.3) as

$$\rho(t + \tau) = \rho(t) + \mathcal{L}\{\rho(t)\}\tau + \xi(t)dW(t). \tag{6.4}$$

Assuming that the variational analysis solves the master equation, we can express $\rho(t + \tau)$ as

$$\rho(t + \tau) = \rho^{var}(t + \tau) + \xi(t)dW(t). \tag{6.5}$$

Having found the variational solution $\rho^{var}(t + \tau)$ that can be calculated as described in the previous chapter, we have to add the noise terms to get the full solution for the time increment.
The Wiener process $W(t)$ appearing in Eq. (6.3) is simulated by

$$W(t) = \sqrt{\tau} \sum_{t_j=0}^{t} Z_{t_j}, \tag{6.6}$$

where Z_{t_j} are random numbers obeying the standard normal distribution $\mathcal{N}(0, 1)$. Here, t_j is the time with the time increment $t_{j+1} - t_j = \tau$. Then, the differential of the Wiener process reads

$$dW(t) = W(t + \tau) - W(t) = \sqrt{\tau} Z_{t+\tau}, \tag{6.7}$$

i.e. it obeys the standard normal distribution. Accordingly, the prefactor $\xi(t)$ appearing the stochastic master equation (6.3) corresponds to the standard deviation of the noise terms.

6.2.2. Variational analysis of inhomogeneous states

For solving the variational part of the stochastic equation (6.3), we use product states, i.e. we make an ansatz according to Eq. (3.9) for the single site density matrix. The variational parameters then read

$$\underline{\alpha}^{(i)}(t) = \left(\alpha_x^{(i)}, \alpha_y^{(i)}, \alpha_z^{(i)}\right) = \left(\langle\sigma_x^{(i)}\rangle, \langle\sigma_y^{(i)}\rangle, \langle\sigma_z^{(i)}\rangle\right) \tag{6.8}$$

for $\rho_i(t)$ at site i.

In chapter (3.2.2) we found that, in a homogeneous lattice, a single bond ρ_{ij} is required for calculating the time evolution via the variational principle. For the inhomogeneous case, we variationally parametrize $\rho_{ij}(t + \tau)$ and perform the minimization with respect to $\rho_{ij}(t + \tau)$ according to

$$\sum_{\langle ij \rangle} ||\rho_{ij}(t + \tau) - \rho_{ij}(t) - \frac{\tau}{2} \mathcal{L}\left[\rho_{ij}(t) + \rho_{ij}(t + \tau)\right]||_1 \to min \qquad (6.9)$$

with the trace norm $||...||_1$ of the implicit midpoint integration term. Each bond ij has a different spin configuration and therefore gives another contribution to the variational norm. Using product states, however, we have $3N^2$ independent variational parameters in the case of a $N \times N$-lattice. Our goal here will be to calculate relatively large system sizes with $N = 8$ or even $N = 16$, resulting in a high computational effort for the minimization of each time step τ. Thus the calculation of the variational time evolution
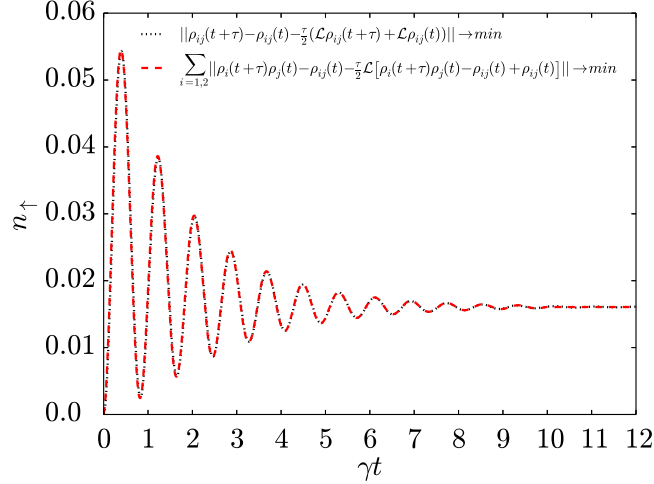
Figure 6.3.: Comparison of the time evolution of a two-spin system calculated via minimizing all variational parameters at once (dotted line) and via holding one spin constant and minimize the other one, respectively (dashed line). The calculation is done for the Hamiltonian (5.1) with $h = 0$, $\Omega = 2\gamma$ and $V = 4\gamma$ and the jump operator $c = \sigma_-$.

is intractable for the desired system sizes.

Our approach used here will be not to use equation (6.9) for the variational minimization, i.e. minimize the full variational norm with respect to the variational parameters of all lattice sites at once. Instead, we evolve each site from time t to $t + \tau$ via a minimization with respect to the parameters of that specific site, holding all other sites constant. The corresponding variational norm for a single site i then reads

$$D_i = \sum_j ||\rho_i(t + \tau)\rho_j(t) - \rho_{ij}(t) - \frac{\tau}{2} \mathcal{L}\left[\rho_{ij}(t) + \rho_i(t + \tau)\rho_j(t)\right]||_1 \qquad (6.10)$$

6. First order liquid-gas transition

with adjacent sites j and $\#j = 2d$. The minimization procedure accordingly reads

$$\rho_i^{var}(t + \tau) = \arg_{\{\rho_i(t+\tau)\}}\min\{D_i\}. \tag{6.11}$$

One iterates this single-site minimization procedure over each site i to evolve the system from time t to time $t + \tau$. Consequently, instead of minimizing $3N^2$ parameters at once, we perform N^2 independent minimizations with respect to 3 parameters for each minimization, making the variational solution computable also for larger system sizes. Due to the product state structure of our variational manifold, that procedure corresponds to the minimization of all variational parameters at once according to Eq. (6.9). Indeed we find no numerical deviation of the iterative minimization of the spins to the full minimization, see Fig.(6.3). That approach allows us to analyze relatively large system sizes, suppressing finite size effects.

6.2.3. Simple noise terms

In this section we show how to integrate the stochastic master equation (6.3) by including rather simple noise terms. In conformity with the seperation of $\rho(t)$ into a variational part and a noise part according to Eq. (6.5), we can split the coefficients of the pauli matrices $\alpha_\mu^{(i)}(t)$ into a variational part solving the quantum master equation
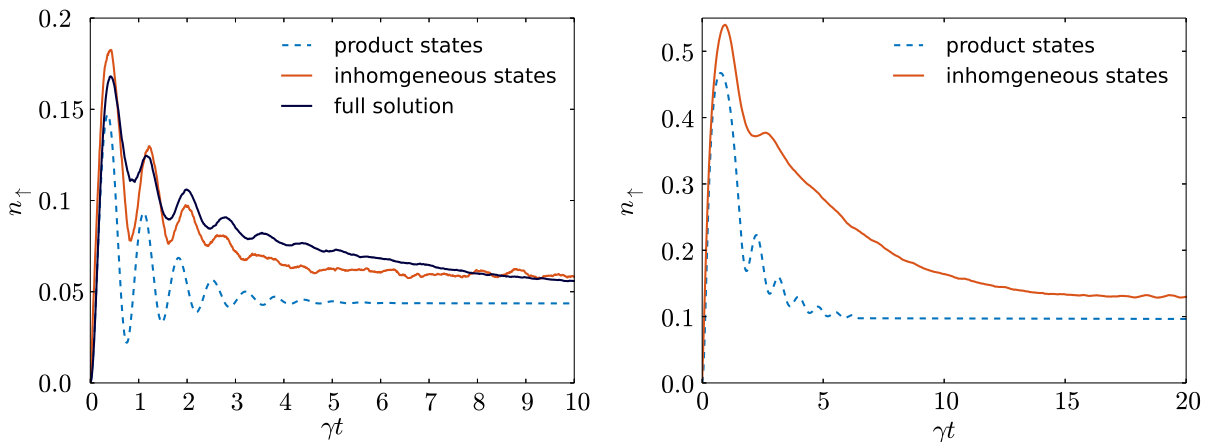
Figure 6.4.: The time evolution of the average Rydberg density of the lattice is shown. Left side: Comparison of the full solution of the QME with the variational solution (product states) and including noise terms (inhomogeneous states) for $g = 4\gamma$. These calculations were done on a 4×4 lattice. Right side: Time evolution of the homogeneous and the inhomogeneous state for $g = 5.6\gamma$ on a 16×16-lattice. We plot the Rydberg density averaged over all 256 sites. The calculations for both figures were done for $h = 0$ and $V = 5\gamma$, with the atoms being polarized into the electronic ground state as the intial state. The finite lattice has periodic boundary conditions. The Rydberg density of the inhomogeneous states were calculated by averaging over 10 trajectories.

and the noise part. Here, the quantum master equation part consists of the Hamiltonian (5.1) and the quantum jump operators $c_i = \sigma_-$ and the decay rate γ. A simple approach to add a noise term to the variational solution is given by

$$\alpha_\mu^{(i)}(t) = \alpha_\mu^{(i)var}(t) + \sqrt{\tau'}\left[D_i^{\min}Z_\mu^{(i)}(t)\right].\tag{6.12}$$

Here, $Z_\mu^{(i)}(t)$ is a standard normally distributed random number and the dimensionless $\tau' = \gamma\tau$. The strength of the noise term is controlled by the prefactor $\xi(t) = D_i^{\min}(t)$ which corresponds to the variational norm according to Eq. (6.10) at the variational minimum. According to Fig. (6.4), including noise terms leads to a qualitatively different time evolution compared to the variational product state solution. At a certain paramter regime, we see that the inhomogeneous variational solution agrees better with the full solution than the product state solution does, see left side of Fig. (6.4). Closer to the phase transition, one observes two different time scales of the inhomgeneous time evolution. For smaller times, there is a rather fast oscillation of the inhomogeneous state, which is also observed for the product state solution. At about $t = 4/\gamma$, however, a metastable state with a rather high Rydberg density arises. This state then decays exponentially on a longer time scale, see right side of Fig. (6.4). We can conclude that already this simple ansatz of taking fluctuations into account highly influences the time evolution and the steady state that is reached. Even though the comparison to the full solution of the quantum master equation looks quite promising, the question remains whether including this kind of classical fluctuations provide an accurate description of the time evolution and which role quantum fluctuations play in the system.

6.2.4. Differentiated Noise Terms

For the further investigation of the time evolution, we will use more differentiated noise terms than those described in the previous chapter (6.2.3). According to Eq. (6.5), we seperate the $\alpha_\mu^{(i)}(t)$ into a variational part and a noise part. The ansatz for the noise terms read

$$\alpha_\mu^{(i)}(t) = \alpha_\mu^{(i)var}(t) + \sqrt{\tau'}\Lambda\left(\varepsilon_\mu^{(i)}(t)Z_\mu^{(i)}(t) + \sum_{j,\,\nu}\varepsilon_{\mu\nu}^{ij}(t)Z_{\mu\nu}^{ij}(t)\right)\tag{6.13}$$

with adjacent sites j of site i, and the coefficients $\varepsilon_\mu^{(i)}(t) = \mathrm{Tr}\{\mathcal{D}_{\mathbf{i}j}(t)\sigma_\mu^{(i)}\sigma_0^{(j)}\}$ and $\varepsilon_{\mu\nu}^{ij} = \mathrm{Tr}\{\frac{(\mathcal{D}_{\mathbf{i}j}+\mathcal{D}_{i\mathbf{j}})}{2}\sigma_\mu^{(i)}\sigma_\nu^{(j)}\}$. Here, $\mathcal{D}_{\mathbf{i}j}(t)$ is the midpoint integration expression

$$\mathcal{D}_{\mathbf{i}j}(t+\tau) = \rho_i^{var}(t+\tau)\rho_j(t) - \rho_{ij}(t) - \frac{\tau}{2}\mathcal{L}\left[\rho_{ij}(t) + \rho_i^{var}(t+\tau)\rho_j(t)\right]\tag{6.14}$$

where $\rho_i^{var}(t+\tau)$ is that variational state that minimizes $D_i(t+\tau)$ according to Eq. (6.11). $\mathcal{D}_{i\mathbf{j}}(t)$ is defined accordingly with respect to site j and $\rho_j^{var}(t+\tau)$. This way we can connect a noise strength $\varepsilon_{\mu\nu}^{ij}$ with the corresponding contribution to $\mathcal{D}_{\mathbf{i}j} + \mathcal{D}_{i\mathbf{j}}$ in $\mu\nu$ direction.

6. First order liquid-gas transition
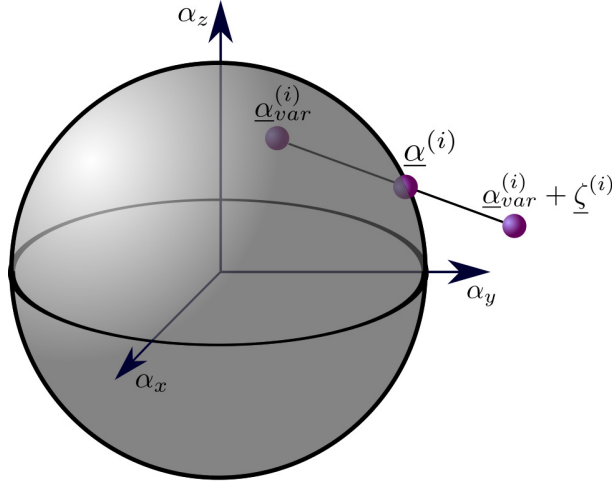
Figure 6.5.: Unit sphere in the $(\alpha_x, \alpha_y, \alpha_z)$- space of site i. Through the noise terms $\underline{\zeta}$, the variational solution $\underline{\alpha}_{var}^{(i)}$ can be driven out of the unit sphere, hurting the positivity of ρ_i. The final $\underline{\alpha}^{(i)}$ lays on that point of the connecting vector of $\underline{\alpha}_{var}^{(i)}$ and $\underline{\alpha}_{var}^{(i)} + \underline{\zeta}(t)$, that is on the border of the unit sphere, restoring the positivity.

The random numbers $Z_\mu^{(i)}(t)$ and $Z_{\mu\nu}^{ij}(t)$ obey the standard normal distribution. These random numbers are fixed to a link between adjacent sites i and j, i.e. the same random number $Z_{\mu\nu}^{ij}$ appears in the noise terms of the parameter $\alpha_\nu^{(j)}(t+\tau)$.

By adjusting the prefactor $\Lambda = \mathcal{K}\Lambda'$ we make sure that the effective noise strength is on the order of the variational norm at the variational minimum $\sum_j ||\mathcal{D}_{\mathbf{ij}}||$. Consequently, the normalization factor Λ' is determined according to

$$\Lambda' \left(\sum_\mu |\varepsilon_\mu^{(i)}| + \sum_{j,\ \mu\nu} |\varepsilon_{\mu\nu}^{ij}| \right) = \sum_j ||\mathcal{D}_{\mathbf{ij}}||. \tag{6.15}$$

The $\mathcal{K}$ factor will in general be larger than 1, as the random numbers $Z_{\mu\nu}^{ij}(t)$ partly compensate each other when being summed up. Additionally, the positivity constraint of $\rho^{(i)}$ effectively weakens the noise, as described in the next section.

Preservation of positivity The positivity of ρ_i^{var} can be guaranteed through the application of contraints to the variational minimization process. The noise terms

$$\zeta_\mu^{(i)} = \sqrt{\tau'}\Lambda \left(\varepsilon_\mu^{(i)}(t)Z_\mu^{(i)}(t) + \sum_{j,\ \nu} \varepsilon_{\mu\nu}^{ij}(t)Z_{\mu\nu}^{ij}(t) \right); \quad \underline{\zeta}^{(i)} = \left(\zeta_x^{(i)}, \zeta_y^{(i)}, \zeta_z^{(i)} \right), \tag{6.16}$$

however, may drive the final result into a forbidden region with $|\underline{\alpha}^{(i)}| > 1$.

In order to restore the positivity, $\underline{\alpha}^{(i)}(t+\tau)$ is shifted along the connection vector of $\underline{\alpha}_{var}^{(i)}$ and $\underline{\alpha}_{var}^{(i)} + \underline{\zeta}(t)$ to the border of the unit sphere in the $\underline{\alpha}^{(i)}$-space, see Fig (6.5). As this
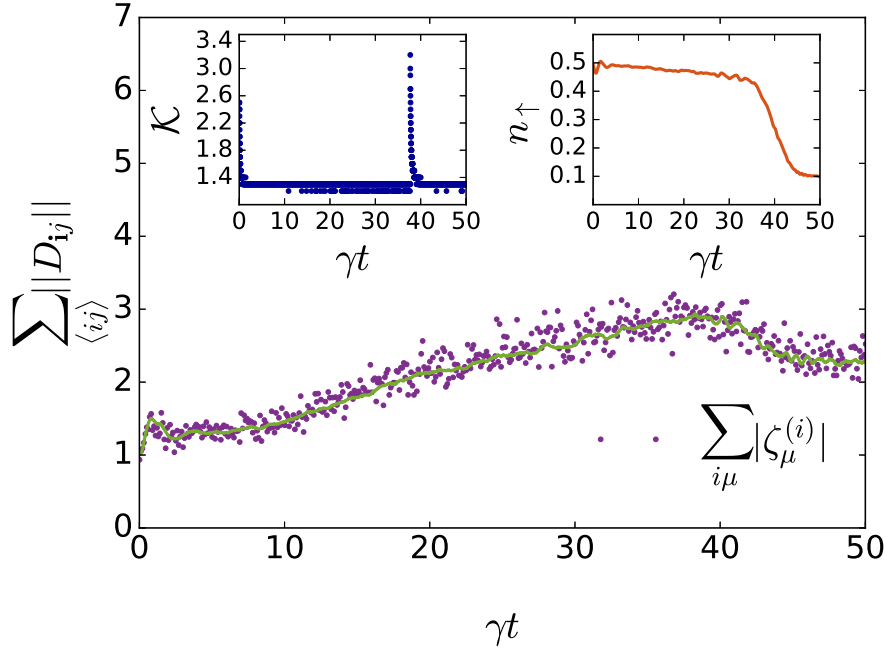
Figure 6.6.: The variational norm $\sum_{\langle ij \rangle} D_{\mathbf{i}j}$ (solid line) and the noise (dotted) versus time γt for $g = 5.7\gamma$. Insets: Value of $\mathcal{K}$ versus time and the corresponding time evolution of the Rydberg density $n_\uparrow$.

procedure effectively weakens the noise, the $\mathcal{K}$-factor defined in the paragraph below Eq. (6.13) will be in general larger than 1, such that the effective strength of the noise corresponds to the effective temperature determined by the variational norm. In Fig. (6.6), we plot the noise terms and the variational norm for $h = 5.7\gamma$ and $V = 5\gamma$. The factor $\mathcal{K}$ plotted in the inset is adjusted such that the noise is comparable to the variational norm and ranges from 1.2 to 3.5.

With regard to the full solution via quantum trajectories, we did not find a substantial improvement of the time evolution using these differentiated noise compared to the primitive noise terms presented in section (6.2.3). Still, these noise terms give rise to further interesting phenomena, as described in the next section.

6.2.5. Time evolution

In this chapter we show results with regard to the time evolution according to the stochastic master equation (6.3) with the noise terms introduced in chapter (6.2.4). The quantum master equation part of Eq. (6.3) is governed by the Hamiltonian (5.1) and the quantum jump operators $c_i = \sigma_-^{(i)}$. In the following, we calculate the time evolution of an 8×8 lattice with periodic boundary conditions. Due to the stochastic character of the noise processes, a Monte Carlo approach is appropriate. In concrete, several realizations of the time evolution are calculated. The observables like the Rydberg

density is gained via averaging over these realizations, or trajectories.

We calculate the time evolution of the average Rydberg density of the lattice in a purely transverse field model, i.e. $h = 0$, $V = 5\gamma$ and different values of g. Of particular interest for us is in which steady state the system ends up and if it depends on the choice of the initial state.

Electronic ground state as the inital state   In this first part the initial state is chosen such that all atoms are polarized into their electronic ground states, i.e. $n_\uparrow = 0$ for $t = 0$. For $g \leq 5.7\gamma$, the relaxation dynamics reaches the steady state that corresponds to the lattice gas in the phase diagram (6.2), with a low Rydberg density. For $g = 5.8\gamma$, however, the relaxation dynamics drives the system into the variational state with a higher Rydberg density, corresponding to the lattice liquid phase, see Fig. (6.7). So, according to the time evolution starting in the electronic ground state, the liquid-gas transition is located between $g = 5.8\gamma$ and $g = 5.7\gamma$. This is a shift compared to the critical value of $g_c = 4.5\gamma$ found via the variational steady state analysis based on product states [141].
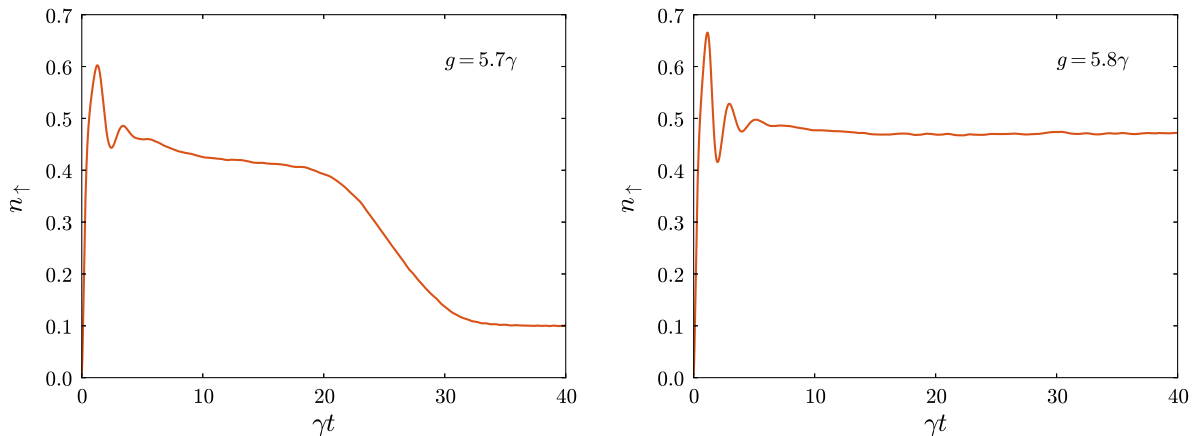
Figure 6.7.: The time evolution of the average Rydberg density of the lattice is shown for $g = 5.7\gamma$ (left side) and $g = 5.8\gamma$ (right side). In both cases, all atoms are polarized into the electronic ground state as the initial state. The Rydberg density was calculated by averaging over $n_{\text{traj}} = 10$ trajectories.

Variational steady state as the initial state   We will now calculate the time evolution starting from the lattice gas (low-density state) and the lattice liquid (high-density state), each state corresponding to a local minimum of the variational norm of the steady state, as described in chapter (6.1). For each value of g, we calculate the time evolution of 20 trajectories, with 10 trajectories starting from one of the two minima, respectively.

We see that up to a value of $g = 5.7\gamma$, the steady state that is reached for long times does not depend on the initial state. For $5.8\gamma \leq g \leq 7.4\gamma$, however, there is a region of bistability and the steady state that is reached indeed depends on the initial state.

For $g \leq 5.8\gamma$, the time evolution of the system prefers the low-density state, even if the time evolution starts at the variational minimum of the steady state corresponding to the high-density state.
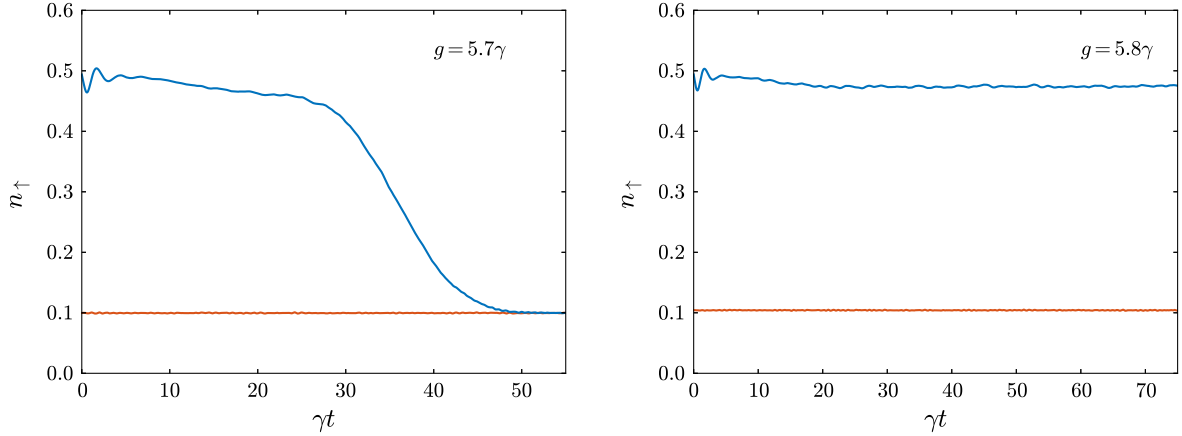
Figure 6.8.: Average Rydberg density of the lattice over time for $n_{\mathrm{traj}} = 10$ trajectories and $g = 5.7\gamma$ (left side) and $g = 5.8\gamma$ (right side). For both values of g, we start in the two distinct variational minima of the steady state. For $g = 5.7\gamma$, both time evolutions end up the same steady state. For $g = 5.8\gamma$, however, there is bistability.
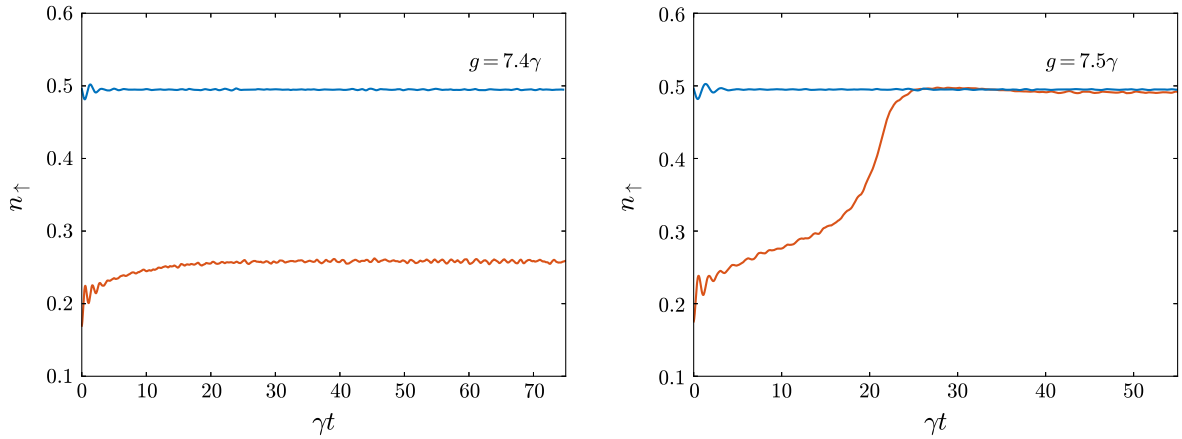
Figure 6.9.: The time evolution of the average Rydberg density of the lattice is shown. Left side: Time evolution starting from the two variational states for $g = 7.4\gamma$. Right side: Time evolution starting from the two variational states for $g = 7.5\gamma$.

For $g \geq 5.8\gamma$, the high-density steady state has the lower variational norm. Still, the time evolution does not reach this state if the system is initialized at the low-density state, see left side of Fig.(6.9). For $g = 7.4\gamma$, for example, the variational norm of the

state connected to a low Rydberg density is significantly higher than the norm of the high-density state. This leads to strong fluctuations included in the dynamics. The variational minimization, however, drives the system back into the low-density minimum. In that sense, one can say that our approach including classical fluctuations is biased towards the low-density, or lattice gas, state which leads to a relatively large bistable regime.

For $g \geq 7.5\gamma$ fluctuations of the low-density state are even stronger, and the system reaches the high-density state with a lower variational norm.

As a summary, we state that the time evolution of the semiclassical approach does not provide a unique steady state, which shows that quantum fluctuations are relevant for reproducing the correct steady state.

7. Spin bath polarization in nitrogen-vacancy centers

7.1. The Hamiltonian and laser illumination

For the description of the ^{13}C atoms we use a spin one-half representation with the Pauli matrices $I_\mu^{(j)}$ at site j and $\mu \in \{x, y, z\}$. The S_μ operators represent the NV's electron in spin one description. Here, we omit the $|1\rangle$ state, so that S_μ represents the $\{|0\rangle; |-1\rangle\}$-subspace. Close to the GSLAC condition, the Hamiltonian can be written as

$$H = D_G S_z^2 + B_0 \left(\gamma_e S_z + \gamma_n \sum_j I_z^{(j)} \right) + \sum_j SAI^{(j)} + 2B_1 \cos(\omega_{RF} t) \left(\gamma_e S_x + \gamma_n \sum_j I_x^{(j)} \right) \tag{7.1}$$

with the zero field splitting $D_G = 2.87$ GHz. The Zeeman effect concerning the ^{13}C atoms and the NV center contributes to the Hamiltonian with the gyromagnetic ratios of $\gamma_e = 2.802$ MHz/Gauss for the NV electron and $\gamma_n = -10.705 \cdot 10^{-4}$ MHz/Gauss for the nuclei. The interaction between the ^{13}C nuclei and the NV center is given in terms of a hyper-fine interaction $SAI^{(j)}$ with the hyperfine tensor A. Additionally, we have radio frequency irradation acting on both the NV center and the nuclei.

The hyperfine interaction is dominated by the Fermi contact interaction and the dipole interaction. In the following, we consider nuclei that are far away from the NV center, so that we only take the dipole interaction, i.e. the interaction due to the magnetic moment of the nucleus and the electron, into account. The full dipolar Hamiltonian consists of six parts, most of them can be neglected assuming a weak interaction strength, see App. (F.1). It turns out that the SAI-term in the Hamiltonian (7.1) can be replaced by

$$H_{hf} = a \left(2S_z I_z - \frac{1}{2}(S_- I_+ + S_+ I_-) \right) \tag{7.2}$$

for the hyper-fine interaction. Here, the interaction strength a reads

$$a = -\frac{\mu_0}{8\pi} \frac{\gamma_n \gamma_e h}{r^3} \tag{7.3}$$

with the permeability μ_0.

7. Spin bath polarization in nitrogen-vacancy centers

Transforming the Hamiltonian to the rotating frame and applying the rotating wave approximation under the assumption $B_1\gamma_e \ll \omega_{RF}$ leads to [170]

$$H = \Delta_e S_z + \Delta_n \sum_j I_z^{(j)} + \sum_j a_j \left(2 S_z I_z^{(j)} - S_x I_x^{(j)} - S_y I_y^{(j)} \right)$$
$$+ \frac{1}{\sqrt{2}} \Omega (S_x + \frac{\sqrt{2}\gamma_n}{\gamma_e} \sum_j I_x^{(j)}). \tag{7.4}$$

For the details of the transformation and the the rotating wave approximation see App. (F.2). Here, $\Delta_e = \gamma_e B_0 - D + \omega_{RF}$ is the off resonant irradiation of the $|0\rangle \leftrightarrow |-1\rangle$ transition and $\Delta_n = \gamma_n B_0 + \omega_{RF}$ is the off resonant nuclear transition. $\Omega = B_1\gamma_e$ is the Rabi frequency of the NV ground state transition.

Using the Hamiltonian H given by equation (7.4), the density matrix ρ obeys the quantum master equation

$$\frac{d}{dt}\rho = -i[H,\rho] + \Gamma\rho \tag{7.5}$$

with the laser illumination Γ acting as the dissipation. It can be expressed as

$$\Gamma = \frac{r_L}{\sqrt{2}} \left(S_+ \rho S_- - \frac{1}{2}(S_- S_+ \rho + \rho S_- S_+) \right). \tag{7.6}$$

This kind of dissipation only couples the NV's electron. In general, also the nuclei couple to dissipative terms via relaxation. The laser illumination drives the NV electron into its $|0\rangle$ state with a rate of r_L.

7.2. Steady state polarization

We will now let several ^{13}C nuclei interact with the NV center. The additional hfi terms of the Hamiltonian might lead to a shift of the double quantum and the NV transition with respect to w_{RF}. We calculate $\langle S_z \rangle$ and $\langle I_z \rangle$ of the steady state, where the latter is referring to the first nucleus or an average value of all nuclei.

As parameters, we choose a Rabi frequency of $\Omega = 0.1$ MHz and a magnetic field of $B = B_0 - 0.15$ Gauss. The rate of the laser illumination is $r_L^{-1} = 20$ μs. In Fig. (7.1) we plot the polarization of the NV center $\langle S_z \rangle$ and the polarization of the first nucleus $\langle I_z^{(1)} \rangle$ in a system with two nuclei. We vary the strength of the coupling to the second nucleus a_2 from $a_2 = 0$ to $a_2 = 100$ kHz.

We notice that the transition of the NV center is shifted slightly, from $w_{RF} = 1.5$ MHz for $a_2 = 0$ kHz to about $w_{RF} = 1.42$ MHz for $a_2 = 100$ kHz. The transition of the first nucleus is affected only very weakly by the change of the interaction strength. The peak remains at $w_{RF} \approx 1.1$ MHz, except for the highest value of a_2 (blue line). For this highest value of a_2, non trivial effects influence the polarization, and we get transitions of higher order in the spectrum.
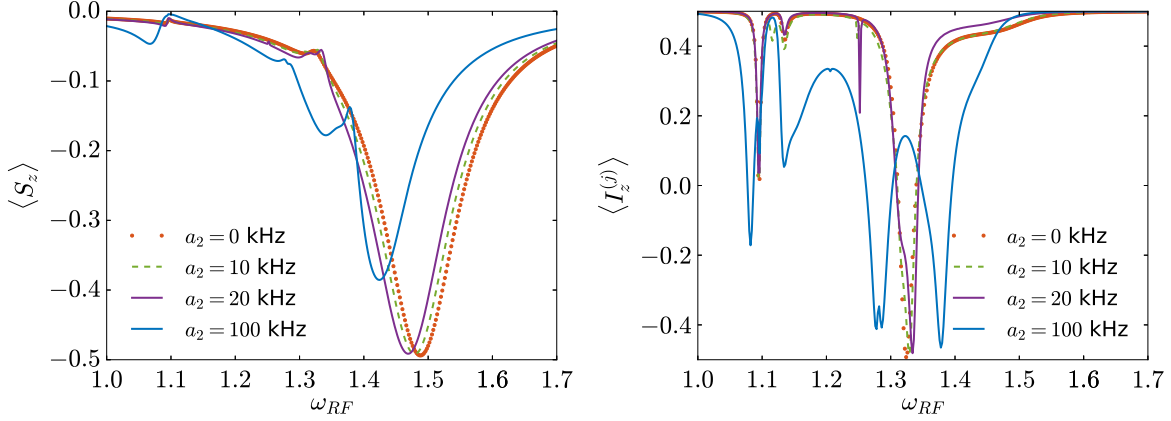
Figure 7.1.: Left side: Expectation value of S_z over w_{RF} for two ^{13}C nuclei and different values of hyper fine coupling a_2. The coupling to the first nucleus is set to $a_1 = 20$ kHz. Right side:Polarization $\langle I_z \rangle$ of the first nucleus with the same configuration as on the left side.
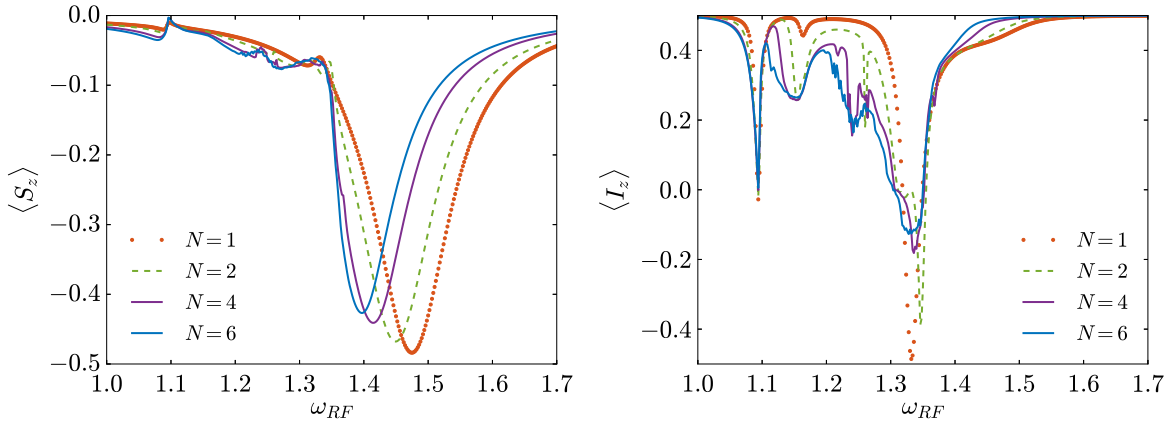
Figure 7.2.: The polarization $\langle S_z \rangle$ on the left side, and the average nuclear polarization $\langle I_z \rangle$ for one, two and four and six nuclei, respectively. The coupling strengths are 35, 30, 25, 20, 15 and 10kHz.

For a_2 up to 20kHz we notice a peak at about $w_{RF} = 1.33$ MHz. The corresponding transition is affecting both the NV center and the nuclei. In the following, we call it the double quantum transition. In Figure (7.2) on the left side, we plot the polarization $\langle S_z \rangle$ and the average nucleus polarization $\langle I_z \rangle$ versus the frequency ω_{RF}. We see an influence of the number of nuclei interacting with the NV center on the NV polarization, with the NV transition shifting to smaller values of ω_{RF}. As in the previous case, the single quantum transition of the nuclei is rather unaffected by the additional hyperfine terms. The double quantum transition is broadened and the value of the peak decreases with increasing particle number. For values of ω_{RF} between the single quantum and double quantum transition, we see new transitions appearing in the spectrum for the number of

nuclei $N \geq 4$. With increasing particle number, these new transitions become more broadened.

In Ref. [171] a related central spin model including hyperfine interaction and dissipation was investigated. The authors suggest NV centers in diamond interacting with ^{13}C nuclei as a possible experimental realization. The corresponding phase diagram inter alia exhibits a first and a second order transition between a low-effective temperature phase, where the nuclei are polarized in the direction of the electron dissipation, and a high-effective temperature phase, where the nucleus polarization is opposed to the electron dissipation.

As a result, we showed that due to the hyperfine interaction, the NV polarization affects the polarization of the sourrounding nuclei, laying the bases for an effective spin bath polarization. The particular transitions could be well identified in the spectra. Future theoretical work could include more nuclei in the analysis, what might lead to further interesting observations.

8. Summary and outlook

In this thesis, we investigated phase transitions and the time evolution of dissipative spin models, especially dissipative Ising models. For the analysis, we used a variational principle that is based on the minimization of the trace norm of the density matrix. Additionally, we investigated the polarization transfer in a spin system realized by an Nitrogen Vacancy center in diamond.

We investigated a dissipative Ising model exhibiting the Z_2- symmetry known from the equilibrium Ising model. We succesfully applied the analogue of the Landau theory to the open quantum system, expanding the variational norm in the order parameter. The phase diagram is significantly altered compared to the equilibrium case. Between the paramagnetic phase and the ferromagnetic phase, we found a first order as well as a second order transition, which meet at a tricritical point.

We varified the validity of our product state ansatz via a Ginzburg-Landau analysis. In the scope of this theory, we could define an effective temperature via the variational norm at the variational minimum as it is a measure of the strength of fluctuations. According to Ginzburg's criterion, we find that the upper critical dimension is the same as in the equilibrium system, namely $d = 3$. Above that dimension, the variational product state ansatz is self consistent. In the case of $d = 3$ dimensions, the corrections of the Landau exponents are logarithmic, suggesting the measurability of our results in experiments. We could also show that our approach is in line with mean-field theory in the limit of infinite dimensions, as the jump of the order paramater at the first order transition decreases with one over square root of the dimension. Additionally, we systematically calculated corrections of the Landau theory combining a renormalization group analysis with perturbation theory. It turned out that due to corrections of the fourth order term of the expansion, the position of the tricritical point is shifted. The size of the shift, however, decreases exponentially with growing dimension.

For the experimental realization of this model, we propose a level scheme with two ground states being coupled to the dressed Rydberg state.

Modifying the functional, the variational principle was applied also to the time evolution of a dissipative Ising model that does not exhibit the Z_2 symmetry. For the variational ansatz we used product states and correlated states, whereby the latter include nearest-neighbour correlations. We compared the results with the full solution of the quantum master equation calculated via a the quantum trajectory method. It turned out that including correlations in the variational manifold significantly improves the result. Over a large parameter regime, the time evolution of the full solution and of the correlated variational states agree very well. We could show that the worse performance of product states is based on non-Markovian effects. The time evolution of the

correlated variational two-site subsystem inheres non-Markovian behaviour that remarkably stays after the steady state is reached. We could show that for weak interactions, the non-Markovianity scales like the quantum linear mutual information, which is more easily accessible experimentally.

In the last part of this thesis, we investigated a first order transition of the two-level dissipative Ising model. Counting excitations as particles, this transition can be mapped onto a liquid-gas transition. The variational steady state analysis showed that there are two distinct variational minima, one corresponding to the gas state, the other one to the liquid state. We calculated the variational time evolution including classical fluctuations. As in the Ginzburg-Landau approach, these cause spatial inhomogeneities that qualitatively modify the time evolution. In a parameter regime close to the predicted transition point, we find a bistable regime, i.e. the steady state depends on the choice of the initial state of the time evolution.

As a summary of this first part of the thesis, we proposed a concept corresponding to the minimization of the free energy functional for open quantum systems. Our variational ansatz proved to be computationally very efficient, while the full knowledge of the variational parameters gave us detailed insight into the time evolution and the critical properties of dissipative Rydberg gases.

We noticed that the appropriateness of the results highly depend on the variational ansatz. In that sense, it might be worth extending the variational states beyond nearest-neighbour correlations to many-particle correlations in future works. The variational principle could furthermore be applied to other systems in the field of dissipative quantum systems. Also, the experimental progress in investigating dissipative quantum systems and and particularly Rydberg gases will continue. The Z_2-preserving dissipative Ising model investigated in this thesis is an obvious candidate for an experimental realization. The successful measurement of the tricritical point could then stimulate even more experimental and theoretical work and applications in that field.

In the second part of this thesis, we considered a dissipative spin model of an NV center in diamond, coupled to ^{13}C nuclei via hyperfine interaction. Close to the ground state level anti crossing, where the NV transition is in resonance with the transition of the nuclei, the polarization of the NV center and the nuclei effect each other. Beside the single quantum transition of the NV center and the nuclear spins, the effect of the double quantum transition can be identified in the polarization of the steady state. We investigated both the influence of the interaction strength and the number of nuclei to the transitions. We found that increasing the hfi strength between one nucleus and the NV center in an NV-two nuclei system shifts the NV transition with respect to the irradiation frequency, whereas the effects on the nuclear transition are quite weak. The polarization of the double quantum transition is slightly reduced by an increasing interaction strength. We also calculated the polarization of the NV center and the nuclei for a one-, two-, four- and six-nuclei system. Again we observe a shift of the NV transition with respect to the irradiation frequency. The double quantum transition is rather broadened and in the case of more particles, higher order transitions emerge. The polarization transfer in Nitrogen vacancy centers in Diamond have already been

proofen useful for the realization of radio frequency free detection and polarization transfer. The mechanisms of NV-bath polarization investigated here lay the basis for further applications of NV centers like quantum state engineering.

For future work, it might be interesting to study the effect of more nuclei interacting with the NV center. Due to its computational efficiency, the variational principle for open quantum systems is a candidate for this purpose.

A   Upper bound of the trace norm of the master equation

In this chapter, we will give a detailed calculation of the upper bound of the trace norm functional that is used for the variational procedure concerning the steady state in chapter (4) and for the time evolution in chapter (5). We will further distinguish between variational classes consisting of product states and variational classes including nearest-neighbour correlations. The first part "Steady state" part follows the analysis presented in [142]. The second part extends the calculation of the upper bound to the time evolution.

A.1. Steady state

A.1.1. Product states

We start with a product state ansatz for the density matrix, i.e.

$$\rho^{prod} = \Pi_i \rho_i. \tag{A.1}$$

Differentiating ρ^{prod} with respect to time according to the quantum master equation, one gets [142]

$$\dot{\rho}^{prod} = \sum_i \mathcal{R}\dot{\rho}_i + \sum_{\langle ij \rangle} \mathcal{R}\dot{C}_{ij}. \tag{A.2}$$

Here, C_{ij} accounts for the correlation between sites i and j that is generally created by interactions terms in the Hamiltonian or correlated jump operators. Taking the trace norm of Eq. (A.2) we get

$$||\dot{\rho}^{prod}|| = ||\sum_i \mathcal{R}\dot{\rho}_i + \sum_{\langle ij \rangle} \mathcal{R}\dot{C}_{ij}|| \tag{A.3}$$

We now get an upper bound of the trace norm by pulling out the i-sum and making use of the triangle inequality:

$$||\dot{\rho}^{prod}|| \leq \sum_i ||\mathcal{R}\dot{\rho}_i + \sum_{\langle j \rangle} \mathcal{R}\dot{C}_{ij}||. \tag{A.4}$$

A. Upper bound of the trace norm of the master equation

In the next step, we extend the right side by a $\dot{\rho}_j$- term which leads to

$$||\dot{\rho}^{prod}|| \leq \sum_i ||\mathcal{R}\dot{\rho}_i + \sum_{\langle j \rangle} \mathcal{R}\left(\rho_i\dot{\rho}_j + \dot{C}_{ij}\right)||. \tag{A.5}$$

The value of the variational norm will not be lowered by this extension as $\dot{\rho}_i$ and $\dot{\rho}_j$ act on different parts of the Hilbert space.
Applying the triangle inequality a second time we get

$$||\dot{\rho}^{prod}|| \leq \sum_{\langle ij \rangle} ||\mathcal{R}\left(\dot{\rho}_i\rho_j + \rho_i\dot{\rho}_j + \dot{C}_{ij}\right)|| = \sum_{\langle ij \rangle} ||\dot{\rho}_{ij}||. \tag{A.6}$$

As result, the upper bound reduces the intractable problem of calculating $||\dot{\rho}||$ to a sum of single bonds $||\dot{\rho}_{ij}||$.

A.1.2. Correlated states

Including nearest neighbours, the density matrix can be written as

$$\rho^{corr} = \Pi_i\rho_i + \sum_{\langle ij \rangle} C_{ij} \tag{A.7}$$

where the first part $\Pi_i\rho_i$ corresponds to product states introduced in the previous section and C_{ij} stands for the correlation between adjacent sites i and j. Differentiating ρ^{corr} with respect to time, one obtains [142]

$$\dot{\rho}^{corr} = \sum_i \mathcal{R}\dot{\rho}_i + \sum_{\langle ij \rangle} \mathcal{R}\dot{C}_{ij} + \sum_{\langle ijk \rangle} \mathcal{R}\left(\dot{\rho}_i C_{jk} + \dot{C}_{ijk}\right) \tag{A.8}$$

where three particle correlations of the form C_{ijk} are created by the differentiation of the correlations in the ansatz (A.7). The trace norm reads

$$||\dot{\rho}^{corr}|| = ||\sum_i \mathcal{R}\dot{\rho}_i + \sum_{\langle ij \rangle} \mathcal{R}\dot{C}_{ij} + \sum_{\langle ijk \rangle} \mathcal{R}\left(\dot{\rho}_i C_{jk} + \dot{C}_{ijk}\right)|| \tag{A.9}$$

As a next step, we apply the triangle inequality which results in

$$||\dot{\rho}^{corr}|| \leq \sum_i ||\mathcal{R}\dot{\rho}_i + \sum_j \mathcal{R}\dot{C}_{ij} + \sum_{\langle jk \rangle} \mathcal{R}\left(\dot{\rho}_i C_{jk} + \dot{C}_{ijk}\right)||. \tag{A.10}$$

Analogue to the product state case, we can now extend the expression in the trace norm according to

$$||\dot{\rho}^{corr}|| \leq \sum_i ||\mathcal{R}\dot{\rho}_i + \sum_j \mathcal{R}\left(\rho_i\dot{\rho}_j + \dot{C}_{ij}\right) + \sum_{\langle jk \rangle} \mathcal{R}\left(\dot{\rho}_i C_{jk} + \dot{C}_{ijk}\right)||. \tag{A.11}$$

and apply the triangle inequality with respect to the j-sum. Then, the upper bound reads

$$||\dot{\rho}^{corr}|| \leq \sum_{\langle ij \rangle} ||\mathcal{R}\dot{\rho}_i\rho_j + \mathcal{R}\left(\rho_i\dot{\rho}_j + \dot{C}_{ij}\right) + \sum_k \mathcal{R}\left(\dot{\rho}_i C_{jk} + \dot{C}_{ijk}\right)||. \tag{A.12}$$

In the next step, we again make use of the fact that the $\dot{\rho}_\nu$, with $\nu \in \{i, j, k\}$, act on different parts of the Hilbert space, whereas correlation terms C_{ij} aswell as their derivatives are traceless. Therefore extending the right side of Eq. (A.12) with therms like $\dot{\rho}_i C_{jk}$ will never decrease the trace norm. Consequently, we can write

$$||\dot{\rho}^{corr}|| \leq \sum_{\langle ij \rangle} ||\mathcal{R}\dot{\rho}_i\rho_j + \mathcal{R}\left(\rho_i\dot{\rho}_j + \dot{C}_{ij}\right) \tag{A.13}$$

$$+ \sum_k \mathcal{R}\left(\rho_i\rho_j\dot{\rho}_k + \dot{\rho}_i C_{jk} + \dot{\rho}_j C_{ik} + C_{ij}\dot{\rho}_k + \rho_i\dot{C}_{jk} + \dot{\rho}_i\dot{C}_{jk} + \dot{C}_{ijk}\right)||. \tag{A.14}$$

As a last step, we pull out the k-sum and obtain

$$||\dot{\rho}^{corr}|| \leq \sum_{\langle ijk \rangle} ||\mathcal{R}(\dot{\rho}_i\rho_j\rho_k + \rho_i\dot{\rho}_j\rho_k + \rho_i\rho_j\dot{\rho}_k + \dot{C}_{ij}\rho_k + \rho_i\dot{C}_{jk} \tag{A.15}$$

$$+ \dot{\rho}_i\dot{C}_{jk} + \dot{\rho}_i C_{jk} + \dot{\rho}_j C_{ik} + C_{ij}\dot{\rho}_k + \dot{C}_{ijk})|| \tag{A.16}$$

$$= \sum_{\langle ijk \rangle} ||\dot{\rho}_{ijk}||. \tag{A.17}$$

One notices that the problem is now reduced to a three-site problem, which is different to the sum of two-site problems in the upper bound for product states.

A.2. Time evolution

In this section, we will derive an upper bound for the variational norm of the time evolution. We start with the trace norm

$$||\rho(t + \tau) - \rho(t) - \tau\mathcal{L}\rho(t)|| \tag{A.18}$$

where the term in the trace norm brackets corresponds to the explicit euler integration. The derivation of the upper bound for the midpoint integration works analogue. Using the superoperator $\mathcal{R}$ and assuming a product state for ρ, we can write

$$||\mathcal{R}(t + \tau) - \mathcal{R}(t) - \tau\left(\sum_i \mathcal{R}\dot{\rho}_i + \sum_{\langle ij \rangle} \mathcal{R}\dot{C}_{ij}\right)||. \tag{A.19}$$

A. Upper bound of the trace norm of the master equation

Making the same steps as in the chapters (A.1.1), i.e. exploiting the triangle inequality and adding a $\dot{\rho}_j$-term, we arrive at

$$||\rho(t+\tau) - \rho(t) - \tau\dot{\rho}(t)|| \leq \sum_{ij} ||\rho_{ij}(t+\tau) - \rho_{ij}(t) - \tau\dot{\rho}_{ij}||. \tag{A.20}$$

For density matrices including nearest-neighbour correlations, one starts again with Eq. (A.18) and makes the step discussed in chapter (A.1.2). Correspondingly to the steady state, one ends up at a sum of three-site terms

$$||\rho(t+\tau) - \rho(t) - \tau\dot{\rho}(t)|| \leq \sum_{ijk} ||\rho_{ijk}(t+\tau) - \rho_{ijk}(t) - \tau\dot{\rho}_{ijk}||. \tag{A.21}$$

B Comparison between the variational time evolution and the full solution

In chapter (5.1.2), we noticed a good agreement between the variational time evolution and the quantum trajectory method on a 4×4 lattice with periodic boundary conditions for $\Omega = \gamma$ and $V = 2\gamma$. Close to the liquid-gas transition for larger Ω, however, the deviation between the two solutions becomes larger. This can be traced back to long-range correlations becoming more important. On the other hand, finite size effects become stronger close to the phase transition. Here, we show a comparison between the variational states including nearest-neighbour correlations and the full solution according to the quantum trajectory method for different values of Ω and V. While we still find a good agreement for $\Omega = 3\gamma$ and 4γ and lower values of V, the solutions deviate in general.
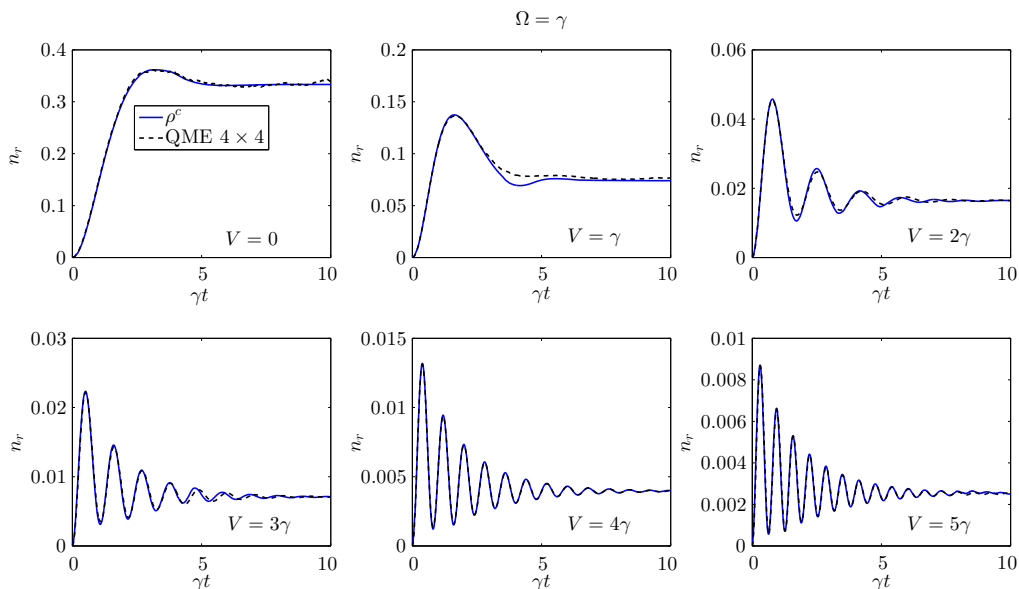
Figure B.1.: Time evolution calculated via the quantum trajectory method (dashed line) and the variational principle (solid line) for $\Omega = \gamma$.

B. Comparison between the variational time evolution and the full solution
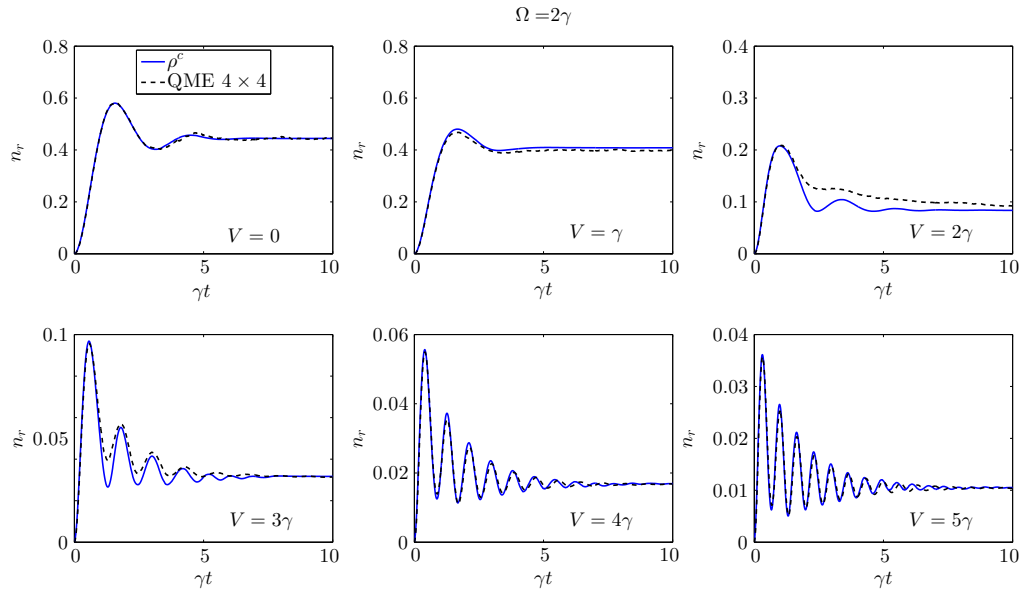
Figure B.2.: Time evolution of the Rydberg density n_r for $\Omega = 2\,\gamma$ and $V = \gamma$ to $V = 5\gamma$.
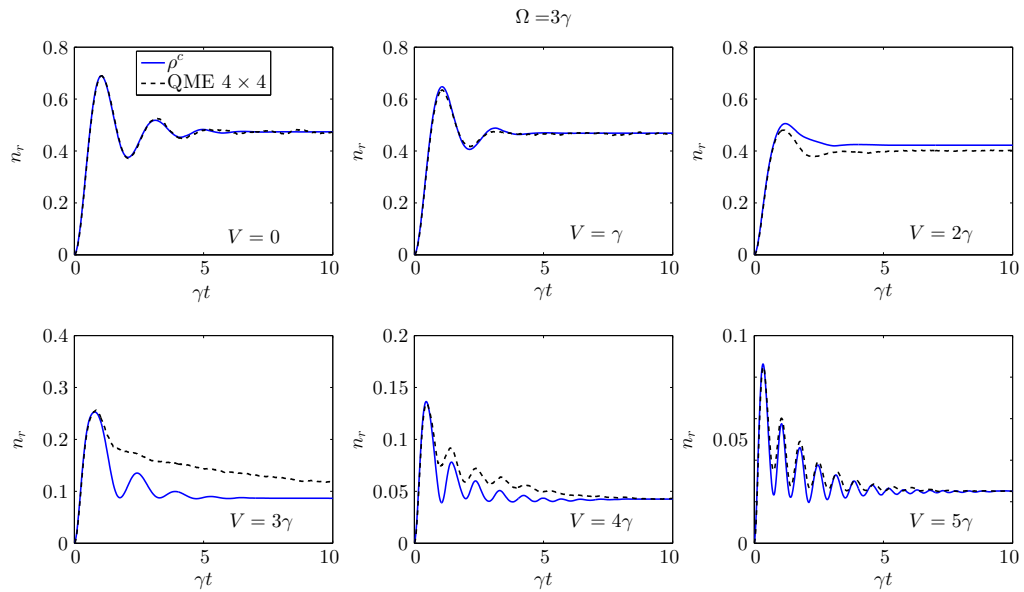
Figure B.3.: Time evolution of the Rydberg density n_r for $\Omega = 3\,\gamma$ and $V = \gamma$ to $V = 5\gamma$.
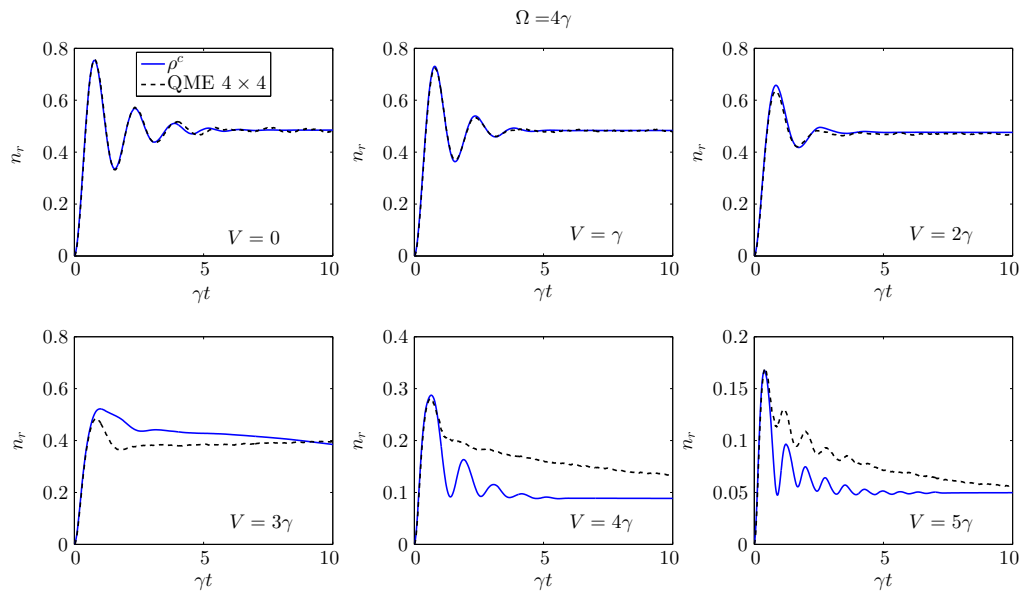
Figure B.4.: Time evolution of the Rydberg density n_r for $\Omega = 4\,\gamma$ and $V = \gamma$ to $V = 5\gamma$.

C   Generalized form of the quantum master equation

Via the time-convolutionless projection operator method [172, 173], it has been shown that even if non-Markovian effects are present, the time evolution can often be expressed in time-local form as

$$\dot{\rho}(t) = \Lambda_t \left[\rho(t) \right] \tag{C.1}$$

where Λ_t is a linear map and $\Lambda_t \left[\rho(t) \right]$ hermitian and traceless. In the following, all quantities will be time dependent and we will not explcitly write down the time dependence. One can now expand the expression in operators B_k and A_k, so that we can write [94]

$$\dot{\rho}(t) = \sum_k A_k \rho B_k^{\dagger}. \tag{C.2}$$

The operators A_k and B_k can be written in terms of basis operators G_n that fullfil

$$G_0 = \hat{1}\sqrt{d}; \quad G_m = G_m^{\dagger}; \quad \text{Tr}\{G_m G_n\} = \delta_{mn} \tag{C.3}$$

with $\hat{1}$ being the identity. In our case, d is equal to 4 and the G_m are all possible combinations of the Pauli matrices.
The expansion of A_k and B_k gives

$$A_k = \sum_j G_j a_{jk}; \quad A_k = \sum_j G_j a_{jk}. \tag{C.4}$$

Then, we get for $\dot{\rho}$ [102]

$$\dot{\rho} = \sum_{i,j=0}^{N-1} c_{ij} G_i \rho G_j. \tag{C.5}$$

Exploiting the hermiticity of ρ, one can show that the matrix $\mathbf{c}$ with the the entries c_{ij} is also hermitian so that $c_{ij} = c_{ji}^*$ [94].

C. Generalized form of the quantum master equation

Seperating out the c_{0j} and c_{i0}-terms, the right side of Eq. (C.5) can be rewritten as

$$\dot{\rho} = C\rho + \rho C + \sum_{i,j=1}^{N-1} d_{ij} G_i \rho G_j. \tag{C.6}$$

with the decoherence $(N-1) \times (N-1)$-matrix $d_{ij} \equiv c_{ij}$ for $i, j > 0$.
In the next step, we make use of the fact that $C + C^\dagger = -\sum_{i,j=1}^{N-1} d_{ij} G_j G_i$ and define the time dependent operator $H \equiv \frac{1}{2} i\hbar \left(C - C^\dagger \right)$. This leads to the expression

$$\dot{\rho} = -\frac{i}{\hbar} [H, \rho] + \sum_{i,j=1}^{N-1} d_i j(t) \left(G_i \rho G_j - \frac{1}{2} \{ G_j G_i, \rho \} \right). \tag{C.7}$$

Finally, we make use of the fact that $\mathbf{d}$ is hermititan and rewrite it as

$$d_{ij} = \sum_k U_{ik} \gamma_k U_{jk}^* \tag{C.8}$$

with the time dependent eigenvalues $\gamma_k(t)$ of $\mathbf{d}$ and unitary $\mathbf{U}$ matrix that is constructed by the eigenvectors of $\mathbf{d}$ and fullfils $\sum_k U_{ik} U_{jk}^* = \delta_{ij}$. Together with the definition

$$L_k \equiv \sum_i U_{ik} G_j G_i \tag{C.9}$$

we eventually arrive at the canonical form of the master equation given by in Eq. (2.24).

D   Effective Hamiltonian within degenerate perturbation theory

In this chapter, we derive an effective Hamiltonian according to level scheme (4.2) based on a perturbation theory of almost degenerate states. As a start, the full Hamiltonian is decomposed into two parts:

$$H = H_0 + H_1, \tag{D.1}$$

where H_1 is considered as the (small) perturbation. Considering the two ground states $|\uparrow\rangle$ and $|\downarrow\rangle$ and the rydberg state $|r\rangle$, the unperturbed part of the two-atom Hamiltonian can be written as

$$H_0 = \begin{pmatrix} \Delta & \Omega & 0 \\ \Omega & 0 & 0 \\ 0 & 0 & \delta_r \end{pmatrix} \otimes \mathbb{I} + \mathbb{I} \otimes \begin{pmatrix} \Delta & \Omega & 0 \\ \Omega & 0 & 0 \\ 0 & 0 & \delta_r \end{pmatrix} + V|rr\rangle\langle rr|, \tag{D.2}$$

where Δ is the detuning of the $|\uparrow\rangle$-state, Ω is the coupling between the ground states $|\uparrow\rangle$ and $|\downarrow\rangle$, δ_r is the Rydberg dressing and V is the interaction strength between two excited atoms. The perturbative part H_1 of the Hamiltonian from formula (D.1) describing the transition between the subspaces $\mathcal{D}$ and $\mathcal{H}/\mathcal{D}$ of the Hilbert space $\mathcal{H}$ reads

$$H_1 = \begin{pmatrix} 0 & 0 & \Omega_r \\ 0 & 0 & \Omega_r \\ \Omega_r & \Omega_r & 0 \end{pmatrix} \otimes \mathbb{I} + \mathbb{I} \otimes \begin{pmatrix} 0 & 0 & \Omega_r \\ 0 & 0 & \Omega_r \\ \Omega_r & \Omega_r & 0 \end{pmatrix} \tag{D.3}$$

The eigenenergies of H_0 assigned to the low-energy subspace (or model space) $\mathcal{D}$ of the Hilbert space, where no energy scale connected to the Rydberg state appears, are given by

$$E_{p_1} = E_{p_2} = \Delta \tag{D.4}$$
$$E_{p_3} = \Delta - \sqrt{\Delta^2 + 4\Omega^2}$$
$$E_{p_4} = \Delta + \sqrt{\Delta^2 + 4\Omega^2}$$

D. Effective Hamiltonian within degenerate perturbation theory

with the corresponding eigenstates

$$|p_1\rangle = \left(-\frac{1}{\sqrt{\frac{\Delta^2}{\Omega^2}+2}};\frac{\Delta}{\sqrt{\frac{\Delta^2}{\Omega^2}+2\Omega}};0;0;\frac{1}{\sqrt{\frac{\Delta^2}{\Omega^2}+2}};0;0;0;0\right)^T \tag{D.5}$$

$$|p_2\rangle = \left(-\frac{\Delta\Omega\sqrt{2-\frac{\Delta^2}{\Delta^2+2\Omega^2}}}{\Delta^2+4\Omega^2};-\frac{2\Omega^2\sqrt{2-\frac{\Delta^2}{\Delta^2+2\Omega^2}}}{\Delta^2+4\Omega^2};0;\frac{1}{\sqrt{2-\frac{\Delta^2}{\Delta^2+2\Omega^2}}};\frac{\Delta\Omega\sqrt{2-\frac{\Delta^2}{\Delta^2+2\Omega^2}}}{\Delta^2+4\Omega^2};0;0;0;0\right)^T$$

$$|p_3\rangle = \left(\frac{\Omega^2\Gamma}{\sqrt{2}\left(\Delta^2+4\Omega^2\right)};\frac{\Delta-\sqrt{\Delta^2+4\Omega^2}}{\sqrt{2}\Omega\Gamma};0;\frac{\Delta-\sqrt{\Delta^2+4\Omega^2}}{\sqrt{2}\Omega\Gamma};\frac{\sqrt{2}}{\Gamma};0;0;0;0\right)^T$$

$$|p_4\rangle = \left(\frac{\Omega^2\Xi}{\sqrt{2}\left(\Delta^2+4\Omega^2\right)};\frac{\Omega\Lambda\Xi}{2\sqrt{2}\left(\Delta^2+4\Omega^2\right)^{3/2}};0;\frac{\Omega\Lambda\Xi}{2\sqrt{2}\left(\Delta^2+4\Omega^2\right)^{3/2}};\frac{\sqrt{2}}{\Xi};0;0;0;0\right)^T$$

with $\Gamma = \sqrt{\frac{\left(\Delta^2+4\Omega^2\right)\left(\Delta^2-\sqrt{\Delta^2+4\Omega^2}\Delta+2\Omega^2\right)}{\Omega^4}}$, $\Xi = \sqrt{\frac{\left(\Delta^2+4\Omega^2\right)\left(2\Omega^2+\Delta\left(\Delta+\sqrt{\Delta^2+4\Omega^2}\right)\right)}{\Omega^4}}$ and
$\Lambda = \left(\Delta^2 - \sqrt{\Delta^2+4\Omega^2}\Delta + 4\Omega^2\right)$.
For the complementary high-energy subspace $\mathcal{H}/\mathcal{D}$ we find the eigenenergies

$$E_{q_1} = V + 2\delta_r \tag{D.6}$$

$$E_{q_2} = E_{q_3} = \frac{1}{2}\left(\Delta + 2\delta_r - \sqrt{\Delta^2+4\Omega^2}\right)$$

$$E_{q_4} = E_{q_5} = \frac{1}{2}\left(\Delta + 2\delta_r + \sqrt{\Delta^2+4\Omega^2}\right)$$

where the energy scale of the Rydberg state, δ_r, appears. The correponding eigenstates
of H_0 in the high energy subspace are given by

$$|q_1\rangle = (0;0;0;0;0;0;0;0;1)^T \tag{D.7}$$

$$|q_2\rangle = \left(0;0;0;0;0;0;-\frac{\sqrt{2}\Omega\Sigma}{\sqrt{\Delta^2+4\Omega^2}};\frac{1}{\sqrt{2}\Sigma};0\right)^T$$

$$|q_3\rangle = \left(0;0;-\frac{\sqrt{2}\Omega\Sigma}{\sqrt{\Delta^2+4\Omega^2}};0;0;\frac{1}{\sqrt{2}\Sigma};0;0;0\right)^T$$

$$|q_4\rangle = \left(0;0;0;0;0;0;\frac{\Delta+\sqrt{\Delta^2+4\Omega^2}}{\Omega\sqrt{2}\Theta};\frac{1}{\Theta};0\right)^T$$

$$|q_5\rangle = \left(0;0;\frac{\Delta+\sqrt{\Delta^2+4\Omega^2}}{\Omega\sqrt{2}\Theta};0;0;\frac{1}{\Theta};0;0;0\right)^T$$

with the abbreviations $\Sigma = \sqrt{\frac{1}{\frac{\Delta}{\sqrt{\Delta^2+4\Omega^2}}+1}}$ and $\Theta = \sqrt{\frac{\Delta\left(\Delta+\sqrt{\Delta^2+4\Omega^2}\right)}{\Omega^2}+8}$. We see that the energy difference in the eigenstates of the two subspaces are essentially δ_r (per atom). In our perturbation analysis, we assume that all other energy scales (except the interaction V) are small compared to δ_r, so that the use of an perturbation theory for almost degenerate states is well justified [156].

The projections onto the subspaces are given by [174]

$$P = \sum_{p\in\mathcal{D}} |p\rangle\langle p| \tag{D.8}$$

$$Q = \sum_{q\in\mathcal{H}/\mathcal{D}} |q\rangle\langle q|$$

for the low-energy and the high-energy subspace, respectively. With these projectors, the effective Hamiltonian derrived within our perturbation can be written as [174]

$$H_{\text{eff}}^{(i)} = PH_0P + PH_1\left(\Omega^{(0)} + \Omega^{(1)} + \Omega^{(2)} + ... + \Omega^{(i-1)}\right) \tag{D.9}$$

with the wave operator Ω given by the recursion formula [156]

$$\Omega^{(0)} = P; \quad \left[\Omega^{(l)}, H_0\right] = QH_1\Omega^{(l-1)} - \sum_{m=1}^{l-1} \Omega^{l-m}H_1\Omega^{(m-1)} \tag{D.10}$$

In our case, the expansion of the Hamiltonian in Ω according to formula (D.9) corresponds to an expansion in $\frac{\Omega_r}{\delta_r}$. Here, we will go to the fourth order, i.e. $H_{\text{eff}}^{(4)}$. Note that $H_{\text{eff}}^{(i)}$ fullfils hermiticity only up to the $i'th$ order in $\frac{\Omega_r}{\delta_r}$. The wave operators needed for that can be extracted from Lindgren's formula (D.10) and read

$$\Omega^{(1)} = \sum_j \sum_i |q_j\rangle\langle p_i| \frac{\langle q_j|H_1|p_i\rangle}{E_{p_i} - E_{q_j}} \tag{D.11}$$

$$\Omega^{(2)} = \sum_j \sum_i |q_j\rangle\langle p_i| \frac{\langle q_j|H_1\Omega^{(1)} - \Omega^{(1)}H_1|p_i\rangle}{E_{p_i} - E_{q_j}}$$

$$\Omega^{(3)} = \sum_j \sum_i |q_j\rangle\langle p_i| \frac{\langle q_j|H_1\Omega^{(2)} - \Omega^{(1)}H_1\Omega^{(1)} - \Omega^{(2)}H_1|p_i\rangle}{E_{p_i} - E_{q_j}}$$

The resulting $H_{\text{eff}}^{(3)}$ can be written as

$$H_{\text{eff}}^{(3)} = \Delta'\sum_i \sigma_z^{(i)} + \Omega'\sum_i \sigma_x^{(i)} - \sum_{ij} J_{ij}\sigma_x^{(i)}\sigma_x^{(j)} + \text{const.} \tag{D.12}$$

The σ_x term breaks the Z_2 symmetry. Choosing $\delta_r = -1$, $V = 3\delta_r$, $\Omega_r = \delta_r/10$ and $\Delta = \Omega_r^4/\delta_r^3$, we can get rid of the Z_2-symmetry breaking term by tuning Ω. For $\Omega \approx 0.0092\delta_r$, we find that Ω' becomes small compared to Δ' and J_{ij}. Therefore the σ_x-part is negligible and the Z_2 symmetry is restored.

E The coefficients of the Landau expansion

Here, we are showing the full expression of the variational norm in the Z_2-preserving dissipative Ising model described chap. (4.2). The expansion coefficients of the variational norm according to

$$||\dot{\rho}_{ij}|| = u_0 + u_2\phi^2 + u_4\phi^4 + u_6\phi^6 \tag{E.1}$$

are given by

$$u_0 = 2J, \tag{E.2}$$

$$u_2 = \frac{\frac{\gamma^2}{16} + \Delta^2}{J} + J\left(\frac{16\Delta^2 z^2}{\gamma^2 + 16\Delta^2} - 1\right) - 2\Delta z, \tag{E.3}$$

$$u_4 = -\frac{1}{512J^3\left(\gamma^2 + 16\Delta^2\right)^4}\Big[\left(\gamma^2 + 16\Delta^2\right)^6 + 8192\gamma^5 J^7 z^4 + 131072\gamma^4\Delta^2 J^6 z^4 \tag{E.4}$$

$$-1024\gamma^2 J^5 z^2\left(\gamma^2 + 16\Delta^2\right)^2\left(8\Delta z - \gamma\right) + 16384\Delta^2 J^4 z^2\left(\gamma^2 + 16\Delta^2\right)^2\left(\gamma^2 + 4\Delta^2 z^2\right)$$

$$+32J^3\left(\gamma^2 + 16\Delta^2\right)^3\left(\gamma^3 + 16\gamma\Delta^2 + 256\Delta^3 z\left(1 - 2z^2\right) + 16\gamma^2\Delta z\right)$$

$$-64J^2\left(\gamma^2 + 16\Delta^2\right)^4\left(\gamma^2 + 8\Delta^2\left(1 - 3z^2\right)\right) - 64\Delta Jz\left(\gamma^2 + 16\Delta^2\right)^5\Big],$$

E. The coefficients of the Landau expansion

$$u_6 = -\frac{1}{24576 J^5 (\gamma^2 + 16\Delta^2)^6} \Big[-(\gamma^2 + 16\Delta^2)^9 + 1048576\gamma^7 J^{11} z^6 \tag{E.5}$$
$$- 524288\gamma^6 J^{10} z^6 (\gamma^2 - 16\Delta^2)$$
$$- 65536\gamma^4 J^9 z^4 (\gamma^2 + 16\Delta^2)(-3\gamma^3 + 16\gamma\Delta^2(2z^2 - 3) + 8\gamma^2\Delta z + 128\Delta^3 z)$$
$$- 131072\gamma^4 J^8 z^4 (\gamma^2 + 16\Delta^2)(\gamma^4 - 8\gamma^2\Delta^2 + 128\Delta^4(2z^2 - 3) - 2\gamma^3\Delta z - 32\gamma\Delta^3 z)$$
$$+ 4096\gamma^2 J^7 z^2 (\gamma^2 + 16\Delta^2)^2 (\gamma^5(3 - 2z^2) - 96\gamma^3\Delta^2(z^2 - 1) + 1536\gamma^2\Delta^3 z(z^2 - 1)$$
$$+ 256\gamma\Delta^4(3 - 4z^2) + 4096\Delta^5 z(2z^2 - 3) - 48\gamma^4\Delta z)$$
$$- 2048 J^6 z^2 (\gamma^2 + 16\Delta^2)^3 (5\gamma^6 + 64\gamma^4\Delta^2(3z^2 - 1)$$
$$+ 256\gamma^2\Delta^4(14z^2 - 9) + 8192\Delta^6 z^2(z^2 - 1) - 16\gamma^5\Delta z - 256\gamma^3\Delta^3 z)$$
$$- 256 J^5 (\gamma^2 + 16\Delta^2)^4 (\gamma^5(4z^2 - 1) - 8\gamma^4\Delta z(4z^2 + 3) + 32\gamma^3\Delta^2(3z^2 - 1)$$
$$- 256\gamma^2\Delta^3 z(4z^2 + 3) + 256\gamma\Delta^4(2z^2 - 1) - 6144\Delta^5 z(1 - 2z^2)^2)$$
$$- 256 J^4 (\gamma^2 + 16\Delta^2)^5 (5\gamma^4 + 16\gamma^2\Delta^2(7 - 10z^2) + 256\Delta^4(15z^4 - 12z^2 + 2)$$
$$- 4\gamma^3\Delta z - 64\gamma\Delta^3 z)$$
$$- 32 J^3 (\gamma^2 + 16\Delta^2)^6 (\gamma^3 + 16\gamma\Delta^2 + 1280\Delta^3 z(1 - 2z^2) + 112\gamma^2\Delta z)$$
$$+ 16 J^2 (\gamma^2 + 16\Delta^2)^7 (5\gamma^2 + 48\Delta^2(1 - 5z^2)) + 96\Delta J z(\gamma^2 + 16\Delta^2)^8 \Big].$$

F   NV center and ^{13}C spin bath

In this part of the appendix, we will introduce in detail the hyperfine interaction terms of the NV-^{13}C interaction and transform the Hamiltonian of the NV-nuclei system to derive the Hamiltonian (7.1), which includes a rotating wave approximation. In the last part, we investigate in detail the effects of the state mixing due to the hyperfine interaction close to the GSLAC, particularly on the RF irradiation and laser illumination. The content of this chapter follows the calculations done in [170].

F.1. Hyperfine interaction of the NV-nucleus Hamiltonian

The main contributions to the electron-nucleus interaction are the Fermi contact interaction [175] and the dipole-dipole interaction.
The Fermi contact interaction occurs if an electron is very close to the nucleus. In that case, the magnetic field of the nucleus is no longer dipolar. Thus the interaction of the magnetic moments of the electron and the nucleus is very different from dipolar interaction.
The corresponding interaction Hamiltonian including both kinds of interaction can be expressed as [176]

$$H_{hf} = SAI \tag{F.1}$$

with the hyperfine interaction matrix A. S refers to the spin angular momentum of the electron, I to that one of the nucleus.
As we assume a large distance between the nuclei and the NV center, we only take the traceless T-matrix into account, which corresponds to the dipole-dipole interaction.
The dipole-tdipole interaction can be written as

$$H_{DD} = -\frac{\mu_0}{4\pi}\gamma_I\gamma_S h \left(\frac{I \cdot S}{\mathbf{r}^3} - \frac{3(I \cdot \mathbf{r})(S \cdot \mathbf{r})}{\mathbf{r}^5} \right) \equiv -\frac{\mu_0}{4\pi}\frac{\gamma_e\gamma_n}{r^3}\left[A + B + C + D + E\right] \tag{F.2}$$

F. NV center and ^{13}C spin bath

The single parts of the dipol-dipol interaction can be expressed as [177]

$$A = S_z I_z \left(3\cos 2\theta - 1\right) \tag{F.3}$$

$$B = -\frac{1}{4}\left(S^- I^+ + S_x I_-\right)\left(3\cos 2\theta - 1\right)$$

$$C = -\frac{3}{2} - \left(I_z + S_+ + S_z I_+\right)\sin\theta\cos\theta e^{-i\phi}$$

$$D = -\frac{3}{2} - \left(I_z + S_- + S_z I_-\right)\sin\theta\cos\theta e^{i\phi}$$

$$E = -\frac{3}{4}\left(S_+ I_+\right)\sin^2\theta e^{-2i\phi}$$

$$F = -\frac{3}{4}\left(S_- I_-\right)\sin^2\theta e^{2i\phi}$$

The A term and under certain conditions also the B term are secular, i.e. they commute with the Zeeman Hamiltonian. The other terms C-F are always non-secular. Close to the GSLAC condition, the Zeeman splitting of the NV center and the nucleus are equal, i.e. in this case B is secular. All other terms can be neglected due to the weak interaction $a \ll \gamma_n B, \gamma_e B - D$ with $a = -\frac{\mu_0}{8\pi}\frac{\gamma_e \gamma_n \hbar}{r^3}$. The resulting hyperfine interaction Hamiltonian reads

$$H_{DD} = a\left(2S_z I_z - \frac{1}{2}(S_- I_+ + S_+ I_-)\right) \tag{F.4}$$

F.2. Rotating frame and rotating wave approximation of the Hamiltonian

For the denotion of the ^{13}C atoms we use a spin one-half representation with the Pauli matrices $I_\mu^{(j)}$ at site j and $\mu \in \{x, y, z\}$. The S_μ operators represent the NV's electron in spin one description. Close to the GSLAC condition, the Hamiltonian can be written as

$$H = D_G S_z^2 + B_0\left(\gamma_e S_z + \gamma_n \sum_j I_z^{(j)}\right) + \sum_j SAI^{(j)} + 2B_1\cos(\omega_{RF}t)\left(\gamma_e S_x + \gamma_n \sum_j I_x^{(j)}\right) \tag{F.5}$$

with the zero field splitting $D_G = 2.87\text{GHz}$. The Zeeman effect concerning the ^{13}C atoms and the NV center contributes to the Hamiltonian with the gyromagnetic ratios of $\gamma_e = 2.802\text{MHz/Gauss}$ for the NV electron and $\gamma_n = -10.705 \cdot 10^{-4}\text{MHz/Gauss}$ for the nuclei. The interaction between the ^{13}C nuclei and the NV center is given in terms of a hyper-fine interaction $SAI^{(j)}$ with the hyperfine tensor A. Additionally, we have irradation acting on the NV center and the nuclei. Here, we omit the $|1\rangle$ state of the NV ground state subspace, so that S_μ represents the $\{|0\rangle; |-1\rangle\}$-subspace. The S_μ read

$$S_x = \frac{1}{\sqrt{2}}\begin{pmatrix} 0 & 1 \\ 1 & 0 \end{pmatrix}; \quad S_y = i\frac{1}{\sqrt{2}}\begin{pmatrix} 0 & -1 \\ 1 & 0 \end{pmatrix}; \quad S_z = \frac{1}{\sqrt{2}}\begin{pmatrix} 0 & 0 \\ 0 & -1 \end{pmatrix} \tag{F.6}$$

F.2. Rotating frame and rotating wave approximation of the Hamiltonian

There is no interaction with the ^{14}N or ^{15}N included which we consider to be fully polarized.

We will now transform the Hamiltonian to the rotating frame of the drive w_{RF} following the calculation done in [170] H is transformed according to

$$H_R = R^\dagger(t)H_L(t)R() - iR^\dagger(t)\frac{d}{dt}R(t) \tag{F.7}$$

with the unitary transformation

$$R(t) = e^{i\omega_{RF}t(S_z+I_z)}. \tag{F.8}$$

We use $R^\dagger(t)\frac{1}{2}(I_+S_- + I_-S_+)R(t) = (I_xS_x + I_yS_y)$ and $R^\dagger(t)\cos(\omega_{RF}t)R(t) = (S_x - \cos(2\omega_{RF}tS_x) - \sin(2\omega_{RF}t)S_y) + (I_x - \cos(2\omega_{RF}tI_x) - \sin(2\omega_{RF}t)I_y)$ [170]. This procedure leads to

$$H_R = DS_z^2 + (\gamma_e B_0 + \omega_{RF})S_z + (\gamma_n B_0 + \omega_{RF})\sum_j I_z^{(j)} \tag{F.9}$$

$$+ \sum_j a_j\left(2S_z I_z^{(j)} - \frac{1}{2}(S_- I_+^{(j)} + S_+ I_-^{(j)})\right) + B_1(\gamma_e S_x + \gamma_n \sum_j I_x^{(j)}).$$

$$- B_1\left(\cos(2w_{RF}t)(\gamma_e S_x + \gamma_n \sum_j I_x^{(j)}) + \sin(2\omega_{RF}t)(\gamma_e S_y + \sum_j I_y^{(j)})\right).$$

H_R is the Hamiltonian in the rotating frame of the $|0\rangle \leftrightarrow |-1\rangle$ transition, as the RF irradiation is far away from the $|0\rangle \leftrightarrow |1\rangle$ transition. The fast rotating parts going like $2\omega_{RF}$ average out to zero and are therefore neglected (rotating wave approximation). Then, the Hamiltonian reads

$$H_R = DS_z^2 + (\gamma_e B_0 + \omega_{RF})S_z + (\gamma_n B_0 + \omega_{RF})\sum_j I_z^{(j)} \tag{F.10}$$

$$+ \sum_j a_j\left(2S_z I_z^{(j)} - \frac{1}{2}(S_- I_+^{(j)} + S_+ I_-^{(j)})\right) + B_1(\gamma_e S_x + \gamma_n \sum_j I_x^{(j)}).$$

As the RF irradiation only acts on the $|0\rangle \leftrightarrow |-1\rangle$ transition and the $|1\rangle$ state is unpopulated through the laser illumination, we can restrict ourselves to the $|0\rangle - |1\rangle$ subspace. As a result, H can be written as

$$H = \Delta_e S_z + \Delta_n \sum_j I_z^{(j)} + \sum_j a_j\left(2S_z I_z^{(j)} - S_x I_x^{(j)} - S_y I_y^{(j)}\right)$$

$$+ \frac{1}{\sqrt{2}}\Omega(S_x + \frac{\sqrt{2}\gamma_n}{\gamma_e}\sum_j I_x^{(j)}) \tag{F.11}$$

with $\Delta_e = \gamma_e B_0 - D + \omega_{RF}$ being the off resonant irradiation of the $|0\rangle \leftrightarrow |-1\rangle$ transition and $\Delta_n = \gamma_n B_0 + \Omega_{RF}$ being the off resonant nuclear transition. $\Omega = B_1\gamma_e$ is the Rabi frequency of the NV transition.

Bibliography

[1] H.-P. Breuer and F. Petruccione, *The Theory of Open Quantum Systems* (Oxford University Press, Oxford, 2002).

[2] S. Diehl, A. Micheli, A. Kantian, B. Kraus, H. P. Büchler, and P. Zoller, Quantum states and phases in driven open quantum systems with cold atoms, Nature Phys. **4**, 878 (2008).

[3] F. Verstraete, M. M. Wolf, and J. Ignacio Cirac, Quantum computation and quantum-state engineering driven by dissipation, Nature Phys. **5**, 633 (2009).

[4] S. Diehl, W. Yi, A. J. Daley, and P. Zoller, Dissipation-Induced d-Wave Pairing of Fermionic Atoms in an Optical Lattice, Phys. Rev. Lett. **105**, 227001 (2010).

[5] A. F. Alharbi and Z. Ficek, Deterministic creation of stationary entangled states by dissipation, Phys. Rev. A **82**, 054103 (2010).

[6] G. Watanabe and H. Mäkelä, Dissipation-induced squeezing, Phys. Rev. A **85**, 023604 (2012).

[7] D. D. B. Rao and K. Mølmer, Dark Entangled Steady States of Interacting Rydberg Atoms, Phys. Rev. Lett. **111**, 033606 (2013).

[8] C. Carr, R. Ritter, C. G. Wade, C. S. Adams, and K. J. Weatherill, Nonequilibrium Phase Transition in a Dilute Rydberg Ensemble, Phys. Rev. Lett. **111**, 113901 (2013).

[9] H. Weimer, N. Y. Yao, and M. D. Lukin, Collectively Enhanced Interactions in Solid-State Spin Qubits, Phys. Rev. Lett. **110**, 067601 (2013).

[10] J. Otterbach and M. Lemeshko, Dissipative Preparation of Spatial Order in Rydberg-Dressed Bose-Einstein Condensates, Phys. Rev. Lett. **113**, 070401 (2014).

[11] N. Syassen, D. M. Bauer, M. Lettner, T. Volz, D. Dietze, J. J. García-Ripoll, J. I. Cirac, G. Rempe, and S. Dürr, Strong Dissipation Inhibits Losses and Induces Correlations in Cold Molecular Gases, Science **320**, 1329 (2008).

[12] K. Baumann, C. Guerlin, F. Brennecke, and T. Esslinger, Dicke quantum phase transition with a superfluid gas in an optical cavity, Nature **464**, 1301 (2010).

Bibliography

[13] J. T. Barreiro, M. Müller, P. Schindler, D. Nigg, T. Monz, M. Chwalla, M. Hennrich, C. F. Roos, P. Zoller, and R. Blatt, An open-system quantum simulator with trapped ions, Nature **470**, 486 (2011).

[14] H. Krauter, C. A. Muschik, K. Jensen, W. Wasilewski, J. M. Petersen, J. I. Cirac, and E. S. Polzik, Entanglement Generated by Dissipation and Steady State Entanglement of Two Macroscopic Objects, Phys. Rev. Lett. **107**, 080503 (2011).

[15] G. Barontini, R. Labouvie, F. Stubenrauch, A. Vogler, V. Guarrera, and H. Ott, Controlling the Dynamics of an Open Many-Body Quantum System with Localized Dissipation, Phys. Rev. Lett. **110**, 035302 (2013).

[16] W. H. Louisell, *Quantum Statistical Properties of Radiation* (Wiley, 1973).

[17] C. Cohen-Tannoudji, *Atom-Photon interactions* (Wiley, 1992).

[18] H. J. Carmichael, *Statistical Methods in Quantum Optics* (Springer, 1999).

[19] R. Puri, *Mathematical Methods of Quantum Optics* (Springer, 2001).

[20] A. J. Leggett, S. Chakravarty, A. T. Dorsey, M. P. A. Fisher, A. Garg, and W. Zwerger, Dynamics of the dissipative two-state system, Rev. Mod. Phys. **59**, 1 (1987).

[21] K. Blum, *Density Matrix Theory and Applications* (Plenum Press, 1996).

[22] O. K. V. May, *Charge and Energy Transfer Dynamics in Molecular Systems* (Wiley-VCH, 2004).

[23] A. Nitzan, *Chemical Dynamics in Condensed Phases: Relaxation Transfer, and Reactions in Condensed Molecular Systems* (Oxford University Press, 2006).

[24] K. Huang, *Statistical Mechanics* (John Wiley and Sons, New York, 1987).

[25] A. Tomadin, S. Diehl, and P. Zoller, Nonequilibrium phase diagram of a driven and dissipative many-body system, Phys. Rev. A **83**, 013611 (2011).

[26] T. E. Lee, H. Häffner, and M. C. Cross, Antiferromagnetic phase transition in a nonequilibrium lattice of Rydberg atoms, Phys. Rev. A **84**, 031402 (2011).

[27] J. Qian, L. Zhou, and W. Zhang, Quantum phases of strongly interacting Rydberg atoms in triangular lattices, Phys. Rev. A **87**, 063421 (2013).

[28] T. E. Lee, S. Gopalakrishnan, and M. D. Lukin, Unconventional Magnetism via Optical Pumping of Interacting Spin Systems, Phys. Rev. Lett. **110**, 257204 (2013).

[29] K. Liu, L. Tan, C.-H. Lv, and W.-M. Liu, Quantum phase transition in an array of coupled dissipative cavities, Phys. Rev. A **83**, 063840 (2011).

[30] J. Jin, D. Rossini, R. Fazio, M. Leib, and M. J. Hartmann, Photon Solid Phases in Driven Arrays of Nonlinearly Coupled Cavities, Phys. Rev. Lett. **110**, 163605 (2013).

[31] M. Hoening, W. Abdussalam, M. Fleischhauer, and T. Pohl, Antiferromagnetic long-range order in dissipative Rydberg lattices, Phys. Rev. A **90**, 021603 (2014).

[32] M. F. Maghrebi and A. V. Gorshkov, Nonequilibrium many-body steady states via Keldysh formalism, Phys. Rev. B **93**, 014307 (2016).

[33] J. J. Mendoza-Arenas, S. R. Clark, S. Felicetti, G. Romero, E. Solano, D. G. Angelakis, and D. Jaksch, Beyond mean-field bistability in driven-dissipative lattices: Bunching-antibunching transition and quantum simulation, Phys. Rev. A **93**, 023821 (2016).

[34] M. Höning, D. Muth, D. Petrosyan, and M. Fleischhauer, Steady-state crystallization of Rydberg excitations in an optically driven lattice gas, Phys. Rev. A **87**, 023401 (2013).

[35] M. Marcuzzi, E. Levi, S. Diehl, J. P. Garrahan, and I. Lesanovsky, Universal Nonequilibrium Properties of Dissipative Rydberg Gases, Phys. Rev. Lett. **113**, 210401 (2014).

[36] R. Löw, H. Weimer, J. Nipper, J. B. Balewski, B. Butscher, H. P. Büchler, and T. Pfau, An experimental and theoretical guide to strongly interacting Rydberg gases, J. Phys. B **45**, 113001 (2012).

[37] B. Zhao, A. W. Glaetzle, G. Pupillo, and P. Zoller, Atomic Rydberg Reservoirs for Polar Molecules, Phys. Rev. Lett. **108**, 193007 (2012).

[38] H. Weimer, M. Müller, I. Lesanovsky, P. Zoller, and H. P. Büchler, A Rydberg quantum simulator, Nature Phys. **6**, 382 (2010).

[39] J. E. Johnson and S. L. Rolston, Interactions between Rydberg-dressed atoms, Phys. Rev. A (2010).

[40] G. Pupillo, A. Micheli, M. Boninsegni, I. Lesanovsky, and P. Zoller, Strongly Correlated Gases of Rydberg-Dressed Atoms: Quantum and Classical Dynamics, Phys. Rev. Lett. **104**, 223002 (2010).

[41] Y.-Y. Jau, A. M. Hankin, T. Keating, I. H. Deutsch, and G. W. Biedermann, Entangling atomic spins with a Rydberg-dressed spin-flip blockade, Nat. Phys. **12**, 71 (2016).

[42] U. Raitzsch, R. Heidemann, H. Weimer, B. Butscher, P. Kollmann, R. Löw, H. P. Büchler, and T. Pfau, Investigation of dephasing rates in an interacting Rydberg gas, New J. Phys. **11**, 055014 (2009).

Bibliography

[43] H. Schempp, G. Günter, M. Robert-de Saint-Vincent, C. S. Hofmann, D. Breyel, A. Komnik, D. W. Schönleber, M. Gärttner, J. Evers, S. Whitlock, and M. Weidemüller, Full Counting Statistics of Laser Excited Rydberg Aggregates in a One-Dimensional Geometry, Phys. Rev. Lett. **112**, 013002 (2014).

[44] A. Urvoy, F. Ripka, I. Lesanovsky, D. Booth, J. P. Shaffer, T. Pfau, and R. Löw, Strongly Correlated Growth of Rydberg Aggregates in a Vapor Cell, Phys. Rev. Lett. **114**, 203002 (2015).

[45] J. Honer, R. Löw, H. Weimer, T. Pfau, and H. P. Büchler, Artificial Atoms Can Do More Than Atoms: Deterministic Single Photon Subtraction from Arbitrary Light Fields, Phys. Rev. Lett. **107**, 093601 (2011).

[46] S. D. Huber and H. P. Büchler, Dipole-Interaction-Mediated Laser Cooling of Polar Molecules to Ultracold Temperatures, Phys. Rev. Lett. **108**, 193006 (2012).

[47] C. Ates, B. Olmos, W. Li, and I. Lesanovsky, Dissipative Binding of Lattice Bosons through Distance-Selective Pair Loss, Phys. Rev. Lett. **109**, 233003 (2012).

[48] M. Lemeshko and H. Weimer, Dissipative binding of atoms by non-conservative forces, Nature Commun. **4**, 2230 (2013).

[49] A. Amo, D. Sanvitto, F. P. Laussy, D. Ballarini, E. d. Valle, M. D. Martin, A. Lemaître, J. Bloch, D. N. Krizhanovskii, M. S. Skolnick, C. Tejedor, and L. Vina, Collective fluid dynamics of a polariton condensate in a semiconductor microcavity, Nature **457**, 291 (2009).

[50] M. J. Hartmann, Polariton Crystallization in Driven Arrays of Lossy Nonlinear Resonators, Phys. Rev. Lett. **104**, 113601 (2010).

[51] D. Nagy, G. Kónya, G. Szirmai, and P. Domokos, Dicke-Model Phase Transition in the Quantum Motion of a Bose-Einstein Condensate in an Optical Cavity, Phys. Rev. Lett. **104**, 130401 (2010).

[52] N. Malossi, M. M. Valado, S. Scotto, P. Huillery, P. Pillet, D. Ciampini, E. Arimondo, and O. Morsch, Full Counting Statistics and Phase Diagram of a Dissipative Rydberg Gas, Phys. Rev. Lett. **113**, 023006 (2014).

[53] C. Joshi, F. Nissen, and J. Keeling, Quantum correlations in the one-dimensional driven dissipative XY model, Phys. Rev. A **88**, 063835 (2013).

[54] L. M. Sieberer, S. D. Huber, E. Altman, and S. Diehl, Dynamical Critical Phenomena in Driven-Dissipative Systems, Phys. Rev. Lett. **110**, 195301 (2013).

[55] B. Horstmann, J. I. Cirac, and G. Giedke, Noise-driven dynamics and phase transitions in fermionic systems, Phys. Rev. A **87**, 012108 (2013).

[56] A. Faraon, C. Santori, Z. Huang, V. M. Acosta, and R. G. Beausoleil, Coupling of Nitrogen-Vacancy Centers to Photonic Crystal Cavities in Monocrystalline Diamond, Phys. Rev. Lett. **109**, 033604 (2012).

[57] I. Aharonovich, A. D. Greentree, and S. Prawer, Diamond photonics, Nature Photonics **5**, 397 (2011).

[58] J. L. O'Brien, A. Furusawa, and J. Vučković, Photonic quantum technologies, Nature Photonics **3**, 687 (2009).

[59] F. Jelezko and J. Wrachtrup, Single defect centres in diamond: A review, physica status solidi (a) **203**, 3207 (2006).

[60] L. Childress, J. M. Taylor, A. S. Sørensen, and M. D. Lukin, Fault-tolerant quantum repeaters with minimal physical resources and implementations based on single-photon emitters, Phys. Rev. A **72**, 052330 (2005).

[61] C. Degen, Scanning magnetic field microscope with a diamond single-spin sensor, Applied Physics Letters **92**, 243111 (2008).

[62] J. Taylor, P. Cappellaro, L. Childress, L. Jiang, D. Budker, P. Hemmer, A. Yacoby, R. Walsworth, and M. Lukin, High-sensitivity diamond magnetometer with nanoscale resolution, Nature Physics **4**, 810 (2008).

[63] F. Dolde et al., Electric-field sensing using single diamond spins, Nature Physics **7**, 459 (2011).

[64] J. Zeiher, R. van Bijnen, P. Schauß, S. Hild, J.-y. Choi, T. Pohl, I. Bloch, and C. Gross, Many-body interferometry of a Rydberg-dressed spin lattice, arXiv:1602.06313 (2016).

[65] A. Deriglazov, *Classical Mechanics* (Springer, 2010).

[66] J. M. Jauch, *Foundations of Quantum Mechanics* (Addison-Wesley, 1968).

[67] N. I. Akhiezer, *The calculus of variations* (Blaisdell publishing company, 1962).

[68] L. N. Hand and J. D. Finch, *Analytical mechanics* (Cambridge University Press, 2001).

[69] V. García-Morales, J. Pellicer, and J. A. Manzanares, Thermodynamics based on the principle of least abbreviated action: Entropy production in a network of coupled oscillators, Annals of Physics **323**, 1844 (2008).

[70] K. Gottfried, *Quantum Mechanics, Vol.1, Fundamentals* (W. A. Benjamin, 1966).

[71] J. Gazquez and J. Keller, *Density Functional Theory* (Springer-Verlag, 1983).

Bibliography

[72] M. L. Wall, *Quantum Many-Body Physics of Ultracold Molecules in Optical Lattices* (Springer, 2015).

[73] G. Carleo and M. Troyer, Solving the quantum many-body problem with artificial neural networks, Science **355**, 602 (2017).

[74] R. Bhatia, *Matrix analysis* (Springer Science & Business Media, 2013).

[75] M. A. Nielsen and I. L. Chuang, *Quantum computation and quantum information* (Cambridge University Press, Cambridge, 2000).

[76] A. Gilchrist, N. K. Langford, and M. A. Nielsen, Distance measures to compare real and ideal quantum processes, Phys. Rev. A **71**, 062310 (2005).

[77] J. W. Gibbs, *Elementary Principles of Statistical Mechanics* (Charles Scribners Sons, 1902).

[78] J. W. Gibbs, *Scientific Papers of J Willard Gibbs* (Longmans, Green and co, 1906).

[79] S. Sachdev, *Quantum Phase Transitions* (Cambridge University Press, Cambridge, 1999).

[80] P. Ehrenfest, Phasenumwandlungen im üblichen und erweiterten Sinn, classifiziert nach den entsprechenden Singularitäten des thermodynamischen Potentiales, Proceedings Koninklijke Akademie van Wetenschappen **36**, 153 (1933).

[81] G. H. Wannier, *Statistical Physics* (John Wiley & Sons, 1966).

[82] G. Jaeger, The Ehrenfest Classification of Phase Transitions: Introduction and Evolution, Archive for History of Exact Sciences **53**, 51 (1998).

[83] N. Goldenfeld, *Lectures on Phase Transitions and the Renormalization Group* (Addison-Wesley, Reading, MA, 1992).

[84] M. P. A. Fisher, P. B. Weichman, G. Grinstein, and D. S. Fisher, Boson localization and the superfluid-insulator transition, Phys. Rev. B **40**, 546 (1989).

[85] D. Ter Haar, *Collected papers of LD Landau* (Elsevier, 2013).

[86] J. M. Kosterlitz and D. J. Thouless, Ordering, metastability and phase transitions in two-dimensional systems, J. Phys. C **6**, 1181 (1973).

[87] A. J. Leggett and F. Sols, On the concept of spontaneously broken gauge symmetry in condensed matter physics, Foundations of Physics **21**, 353 (1991).

[88] L. P. Kadanoff, More is the same; Phase Transitions and Mean Field Theories, arXiv:0906.0653v2 (2009).

[89] J. Zinn-Justin, *Quantum field theory and critical phenomena* (Oxford: Clarendon Press, 1996).

[90] H. M. Wiseman and G. J. Milburn, *Quantum measurement and control* (Cambridge university press, 2010).

[91] A. Rivas, S. F. Huelga, and M. B. Plenio, Entanglement and Non-Markovianity of Quantum Evolutions, Phys. Rev. Lett. **105**, 050403 (2010).

[92] S. Luo, S. Fu, and H. Song, Quantifying non-Markovianity via correlations, Phys. Rev. A **86**, 044101 (2012).

[93] S. Lorenzo, F. Plastina, and M. Paternostro, Role of environmental correlations in the non-Markovian dynamics of a spin system, Phys. Rev. A **84**, 032124 (2011).

[94] M. J. W. Hall, J. D. Cresser, L. Li, and E. Andersson, Canonical form of master equations and characterization of non-Markovianity, Phys. Rev. A **89**, 042120 (2014).

[95] S. Hou, S. Liang, and X. Yi, Non-Markovianity and memory effects in quantum open systems, Phys. Rev. A **91**, 012109 (2015).

[96] H.-P. Breuer, E.-M. Laine, and J. Piilo, Measure for the Degree of Non-Markovian Behavior of Quantum Processes in Open Systems, Phys. Rev. Lett. **103**, 210401 (2009).

[97] E.-M. Laine, J. Piilo, and H.-P. Breuer, Measure for the non-Markovianity of quantum processes, Phys. Rev. A **81**, 062115 (2010).

[98] A. Rivas, S. F. Huelga, and M. B. Plenio, Quantum non-Markovianity: characterization, quantification and detection, Rep. Prog. Phys. **77**, 094001 (2014).

[99] X.-M. Lu, X. Wang, and C. Sun, Quantum Fisher information flow and non-Markovian processes of open systems, Phys. Rev. A **82**, 042103 (2010).

[100] W. Zhong, Z. Sun, J. Ma, X. Wang, and F. Nori, Fisher information under decoherence in Bloch representation, Phys. Rev. A **87**, 022337 (2013).

[101] M. Fisz, *Wahrscheinlichkeitsrechnung und mathematische Statistik* (VEB Deutscher Verlag der Wissenschaften, 1962).

[102] V. Gorini, A. Kossakowski, and E. C. G. Sudarshan, Completely positive dynamical semigroups of N-level systems, J. Math. Phys. **17**, 821 (1976).

[103] G. B. Arfken and H. J. Weber, *Mathematical Methods for Physicists, Fourth Edition* (Academic Press, San Diego, 4 edition edition, 1995).

[104] M. Ohya and D. Petz, *Quantum entropy and its use* (Springer, 1993).

Bibliography

[105] T. F. Gallagher, *Rydberg Atoms* (Cambridge University Press, Cambridge, 1994).

[106] E. Urban, T. A. Johnson, T. Henage, L. Isenhower, D. Yavuz, T. Walker, and M. Saffman, Observation of Rydberg blockade between two atoms, arXiv preprint arXiv:0805.0758 (2008).

[107] C. Ates, T. Pohl, T. Pattard, and J. M. Rost, Many-body theory of excitation dynamics in an ultracold Rydberg gas, Phys. Rev. A **76**, 013413 (2007).

[108] L. Isenhower, E. Urban, X. L. Zhang, A. T. Gill, T. Henage, T. A. Johnson, T. G. Walker, and M. Saffman, Demonstration of a Neutral Atom Controlled-NOT Quantum Gate, Phys. Rev. Lett. **104**, 010503 (2010).

[109] M. Saffman, T. G. Walker, and K. Mølmer, Quantum information with Rydberg atoms, Rev. Mod. Phys. **82**, 2313 (2010).

[110] T. G. Walker and M. Saffman, Consequences of Zeeman degeneracy for the van der Waals blockade between Rydberg atoms, Phys. Rev. A **77**, 032723 (2008).

[111] C. Cohen-Tannoudji, J. Dupont-Roc, and G. Grynberg, *Atom-Photon Interactions: Basic Processes and Applications* (John Wiley & Sons, 1992).

[112] N. Henkel, R. Nath, and T. Pohl, Three-Dimensional Roton Excitations and Supersolid Formation in Rydberg-Excited Bose-Einstein Condensates, Phys. Rev. Lett. **104**, 195302 (2010).

[113] J. Honer, H. Weimer, T. Pfau, and H. P. Büchler, Collective Many-Body Interaction in Rydberg Dressed Atoms, Phys. Rev. Lett. **105**, 160404 (2010).

[114] A. W. Glaetzle, M. Dalmonte, R. Nath, C. Gross, I. Bloch, and P. Zoller, Designing Frustrated Quantum Magnets with Laser-Dressed Rydberg Atoms, Phys. Rev. Lett. **114**, 173002 (2015).

[115] R. M. W. van Bijnen and T. Pohl, Quantum Magnetism and Topological Ordering via Rydberg Dressing near Förster Resonances, Phys. Rev. Lett. **114**, 243002 (2015).

[116] S. Helmrich, A. Arias, and S. Whitlock, Scaling of a driven atomic gas from the weakly-dressed to the quantum critical regime, arXiv:1605.08609 (2016).

[117] R. Schirhagl, K. Chang, M. Loretz, and C. L. Degen, Nitrogen-Vacancy Centers in Diamond: Nanoscale Sensors for Physics and Biology, Annual Review of Physical Chemistry **65**, 83 (2014), PMID: 24274702.

[118] A. Gruber, A. Dräbenstedt, C. Tietz, L. Fleury, J. Wrachtrup, and C. v. Borczyskowski, Scanning Confocal Optical Microscopy and Magnetic Resonance on Single Defect Centers, Science **276**, 2012 (1997).

[119] G. Balasubramanian, P. Neumann, D. Twitchen, M. Markham, R. Kolesov, N. Mizuochi, J. Isoya, J. Achard, J. Beck, J. Tissler, V. Jacques, P. R. Hemmer, F. Jelezko, and J. Wrachtrup, Ultralong spin coherence time in isotopically engineered diamond, Nature Mater. **8**, 383 (2009).

[120] B. Naydenov, F. Dolde, L. T. Hall, C. Shin, H. Fedder, L. C. L. Hollenberg, F. Jelezko, and J. Wrachtrup, Dynamical decoupling of a single-electron spin at room temperature, Phys. Rev. B **83**, 081201 (2011).

[121] N. Bar-Gill, L. M. Pham, A. Jarmola, D. Budker, and R. L. Walsworth, Solid-state electronic spin coherence time approaching one second, Nature communications **4**, 1743 (2013).

[122] F. Jelezko, T. Gaebel, I. Popa, A. Gruber, and J. Wrachtrup, Observation of Coherent Oscillations in a Single Electron Spin, Phys. Rev. Lett. **92**, 076401 (2004).

[123] F. Jelezko and J. Wrachtrup, Read-out of single spins by optical spectroscopy, Journal of Physics: Condensed Matter **16**, R1089 (2004).

[124] M. V. G. Dutt, L. Childress, L. Jiang, E. Togan, J. Maze, F. Jelezko, A. S. Zibrov, P. R. Hemmer, and M. D. Lukin, Quantum Register Based on Individual Electronic and Nuclear Spin Qubits in Diamond, Science **316**, 1312 (2007).

[125] P. Neumann, N. Mizuochi, F. Rempp, P. Hemmer, H. Watanabe, S. Yamasaki, V. Jacques, T. Gaebel, F. Jelezko, and J. Wrachtrup, Multipartite Entanglement Among Single Spins in Diamond, Science **320**, 1326 (2008).

[126] J. Wrachtrup and F. Jelezko, Processing quantum information in diamond, Journal of Physics: Condensed Matter **18**, S807 (2006).

[127] J. R. Maze, J. M. Taylor, and M. D. Lukin, Electron spin decoherence of single nitrogen-vacancy defects in diamond, Phys. Rev. B **78**, 094303 (2008).

[128] S. Takahashi, R. Hanson, J. van Tol, M. S. Sherwin, and D. D. Awschalom, Quenching Spin Decoherence in Diamond through Spin Bath Polarization, Phys. Rev. Lett. **101**, 047601 (2008).

[129] F. Dolde, M. W. Doherty, J. Michl, I. Jakobi, B. Naydenov, S. Pezzagna, J. Meijer, P. Neumann, F. Jelezko, N. B. Manson, and J. Wrachtrup, Nanoscale Detection of a Single Fundamental Charge in Ambient Conditions Using the NV⁻ Center in Diamond, Phys. Rev. Lett. **112**, 097603 (2014).

[130] G. Waldherr, J. Beck, M. Steiner, P. Neumann, A. Gali, T. Frauenheim, F. Jelezko, and J. Wrachtrup, Dark States of Single Nitrogen-Vacancy Centers in Diamond Unraveled by Single Shot NMR, Phys. Rev. Lett. **106**, 157601 (2011).

Bibliography

[131] V. M. Acosta, *Optical Magnetometry with Nitrogen-Vacancy Centers in Diamond*, PhD thesis, University of California, Berkeley, 2011, Copyright - Database copyright ProQuest LLC; ProQuest does not claim copyright in the individual underlying works; Last updated - 2016-03-10.

[132] L. I. Childress, *Coherent manipulation of single quantum systems in the solid state*, PhD thesis, Harvard University, 2007.

[133] N. Reddy, N. Manson, and E. Krausz, Two-laser spectral hole burning in a colour centre in diamond, Journal of Luminescence **38**, 46 (1987).

[134] J. Loubser and J. van Wyk, Electron spin resonance in the study of diamond, Reports on Progress in Physics **41**, 1201 (1978).

[135] P. Neumann et al., Excited-state spectroscopy of single NV defects in diamond using optically detected magnetic resonance, New Journal of Physics **11**, 013017 (2009).

[136] M. F. H. G. Davies, Optical studies of the 1.945 eV vibronic band in diamond, Proceedings of the Royal Society of London A: Mathematical, Physical and Engineering Sciences **348**, 285 (1976).

[137] L. Rogers, S. Armstrong, M. Sellars, and N. Manson, Infrared emission of the NV centre in diamond: Zeeman and uniaxial stress studies, New Journal of Physics **10**, 103024 (2008).

[138] L. Robledo, L. Childress, H. Bernien, B. Hensen, P. F. A. Alkemade, and R. Hanson, High-fidelity projective read-out of a solid-state spin quantum register, Nature **477**, 574 (2011).

[139] K. Morigaki, Optically detected magnetic resonance, in *Semiconductors and Semimetals*, volume 21, pages 155–191, Elsevier, 1984.

[140] X.-F. He, N. B. Manson, and P. T. H. Fisk, Paramagnetic resonance of photoexcited N-V defects in diamond. I. Level anticrossing in the ^{3}A ground state, Phys. Rev. B **47**, 8809 (1993).

[141] H. Weimer, Variational Principle for Steady States of Dissipative Quantum Many-Body Systems, Phys. Rev. Lett. **114**, 040402 (2015).

[142] H. Weimer, Variational analysis of driven-dissipative Rydberg gases, Phys. Rev. A **91**, 063401 (2015).

[143] E. Jones et al., SciPy: Open source scientific tools for Python, 2001, [Online; http://www.scipy.org/].

[144] M. Powell, Direct search algorithms for optimization calculations, Acta numerica **7**, 287 (1998).

[145] D. Kraft, A software package for sequential quadratic programming, Forschungsbericht- Deutsche Forschungs- und Versuchsanstalt fur Luft- und Raumfahrt (1988).

[146] F. W. G. Transchel, A. Milsted, and T. J. Osborne, A Monte Carlo Time-Dependent Variational Principle, arXiv:1411.5546 (2014).

[147] E. Mascarenhas, H. Flayac, and V. Savona, Matrix-product-operator approach to the nonequilibrium steady state of driven-dissipative quantum arrays, Phys. Rev. A **92**, 022116 (2015).

[148] J. Cui, J. I. Cirac, and M. C. Bañuls, Variational Matrix Product Operators for the Steady State of Dissipative Quantum Systems, Phys. Rev. Lett. **114**, 220601 (2015).

[149] E. Süli and D. F. Mayers, *An introduction to numerical analysis* (Cambridge university press, 2003).

[150] W. H. Press, S. A. Teukolsky, and W. T. Vetterling, *Numerical Recipes in C* (Cambridge University Press, Cambridge, 1992).

[151] V. R. Overbeck, M. F. Maghrebi, A. V. Gorshkov, and H. Weimer, Multicritical behavior in dissipative Ising models, Phys. Rev. A. **95**, 042133 (2017).

[152] J. Sanders, R. van Bijnen, E. Vredenbregt, and S. Kokkelmans, Wireless Network Control of Interacting Rydberg Atoms, Phys. Rev. Lett. **112**, 163001 (2014).

[153] M. Marcuzzi, M. Buchhold, S. Diehl, and I. Lesanovsky, Absorbing State Phase Transition with Competing Quantum and Classical Fluctuations, Phys Rev. Lett. **116**, 245701 (2016).

[154] B. McCoy and T. T. Wu, *The Two-Dimensional Ising-Model* (Harvard University Press, 1973).

[155] B. H. Brandow, Linked-Cluster Expansions for the Nuclear Many-Body Problem, Rev. Mod. Phys. **39**, 771 (1967).

[156] I. Lindgren, The Rayleigh-Schrödinger perturbation and the linked- diagram theorem for a multi-configurational model space, J. Phys. B **7**, 2447 (1974).

[157] D. A. Steck, Rubidium 87 D Line Data, available online at http://steck.us/alkalidata (revision 2.1.5, 13 January 2015).

[158] P. M. Chaikin and T. C. Lubensky, *Principles of condensed matter physics* (Cambridge University Press, Cambridge, 1995).

[159] H. Kleinert and V. Schulte-Frohlinde, *Critical Properties of Φ^4-Theories* (World Scientific, Singapore, 2001).

Bibliography

[160] R. Kenna, Finite size scaling for $O(N)$ φ^4-theory at the upper critical dimension, Nucl. Phys. B **691**, 292 (2004).

[161] K. G. Wilson and J. Kogut, The renormalization group and the ϵ expansion., Phys. Rep. **12**, 75 (1974).

[162] V. R. Overbeck and H. Weimer, Time evolution of open quantum many-body systems, Phys. Rev. A **93**, 012106 (2016).

[163] A. J. Daley, Quantum trajectories and open many-body quantum systems, Adv. Phys. **63**, 77 (2014).

[164] J. Johansson, P. Nation, and F. Nori, QuTiP 2: A Python framework for the dynamics of open quantum systems, Comp. Phys. Comm. **184**, 1234 (2013).

[165] R. M. Angelo, S. A. Vitiello, M. A. M. de Aguiar, and K. Furuya, Quantum linear mutual information and classical correlations in globally pure bipartite systems, Physica A **338**, 458 (2004).

[166] A. Hu, T. E. Lee, and C. W. Clark, Spatial correlations of one-dimensional driven-dissipative systems of Rydberg atoms, Phys. Rev. A **88**, 053627 (2013).

[167] A. Kshetrimayum, H. Weimer, and R. Orús, A simple tensor network algorithm for two-dimensional steady states, Nature communications **8**, 1291 (2017).

[168] H. B. Callen, *Thermodynamics and an Introduction to Thermostatistics, second edition* (Wiley & Sons, 1985).

[169] B. Øksendal, *Stochastic Differential Equations An Introduction with Applications* (Springer, 2003).

[170] H. Inbar, Toward robust spin-bath polarization utilizing dissipative dynamics in a NV- ^{13} C system in diamond, Master's thesis, The Hebrew University of Jerusalem, 2017.

[171] E. M. Kessler, G. Giedke, A. Imamoglu, S. F. Yelin, M. D. Lukin, and J. I. Cirac, Dissipative phase transition in a central spin system, Phys. Rev. A **86**, 012116 (2012).

[172] S. Chaturvedi and F. Shibata, Time-convolutionless projection operator formalism for elimination of fast variables. Applications to Brownian motion, Z. Phys. B **35**, 297 (1979).

[173] F. Shibata, Y. Takahashi, and N. Hashitsume, A generalized stochastic liouville equation. Non-Markovian versus memoryless master equations, J. Stat. Phys. **17**, 171 (1977).

[174] R. Frésard, C. Hackenberger, and T. Kopp, Magnetic transitions in strong coupling expansions for nearly degenerate states, Ann. Phys. **524**, 411 (2012).

[175] M. Bucher, The electron inside the nucleus: an almost classical derivation of the isotropic hyperfine interaction, European Journal of Physics **21**, 19 (2000).

[176] G. J. Gerfen and D. J. Singel, Determination of hyperfine interaction matrix principal values and principal axis orientations in an orientationally disordered solid: A multifrequency electron spin echo envelope modulation study of nitrogen$-$15 in a copper(ll)$-$15N-imidazole complex, The Journal of Chemical Physics **100**, 4127 (1994).

[177] N. Bloembergen, E. M. Purcell, and R. V. Pound, Relaxation Effects in Nuclear Magnetic Resonance Absorption, Phys. Rev. **73**, 679 (1948).

List of Symbols

γ .... Decay rate

H .... Hamiltonian

Ω .... Rabi frequency

Δ .... Detuning

T .... Temperature

Z .... Partition function

k_B .... Boltzmann constant

β .... Thermodynamic beta

A .... Helmhotz free energy

S .... Entropy

$S(\rho)$ .... Quantum entropy dependend on the density matrix

$P(A)$ .... Probability for event A

$\Psi(\mathbf{r})$ .... Spatial dependend order parameter

ξ .... Correlation length

ν .... Critical exponent

ρ .... Density matrix

$\mathcal{H}$ .... Hilbert space

Tr_i .... Partial trace over subsystem i

ρ_i .... Reduced density matrix

$\mathcal{H}_S$ .... Hilbert space of the subsystem S

$\mathcal{H}_E$ .... Hilbert space of the subsystem E

$\mathcal{L}$ .... Liouvillian

γ_k .... Decay rate of the k'th channel

A_k .... Lindblad operator of channel k

$\Lambda_t[\rho]$ .... Linear map

$\gamma_k(t)$ .... Generalized decay rates

$L_k(t)$ .... Generalized Lindblad operators

$H(t)$ .... Time dependent hermitian operator

$||...||_1$ .... Trace norm

ρ^{var} .... Result of the variational optimization for the density matrix

C_{ij} .... Correlation between site i and j

α_μ .... Variational parameters

c_i .... Jump operators acting on site i

σ_μ .... Pauli matrices

H^{loc} .... Local part of the Hamiltonian

H^{eff} .... Mean-field part of the Hamiltonian

ρ^c_{ij} .... Two-site density matrix including a correlation between sites i and j

τ .... Integration time step

τ' .... Dimensionless integration time step

D .... Variational norm of the time evolution

J .... Interaction strength of the Ising Hamiltonian

Ω_r .... Coupling between ground state and Rydberg state

δ_r .... Rydberg dressing

H_{eff} .... Effective Hamiltonian

u_n .... Coefficients of the Landau expansion with $u \in \{0, 2, 4, 6\}$

ϕ .... Order parameter

c .... Variational parameter

T_{eff} .... Effective Temperature

v_2 .... Coefficient of the gradient term

z .... Two times spatial dimension

c_3 .... Renormalization coefficient of the u_4 term

$\delta\phi$ .... Value of the order parameter at the first order transition

b .... Proportional factor of $\delta\phi$

g .... Transverse field

h .... Longitudinal field

$\mathbf{d}$ .... Decoherence matrix

$f(t)$ .... Non-Markovianity

I .... Quantum linear mutual information

S_l .... Linear entropy

I_{VN} .... Von Neumann mutual informtion

$n_\uparrow$ .... Rydberg density

D_i .... Variational norm with respect to site i

$\mathcal{D}_{\mathbf{ij}}(t)$ .... Midpoint expression at the variational minimum of site i

$W(t)$ .... Wiener process

Z_t .... Normally distributed random number

$\zeta_\mu^{(i)}$ .... Noise terms applied to site i in direction μ

Λ' .... Normalization factor

Δ_e .... NV off resonance term

Δ_n .... Nucleus off resonance term

ω_{RF} .... Radiao frequency

S_μ .... Spin operators for the $|-1\rangle - |0\rangle$ subspace

I_μ .... Spin operators for the ^{13}C nuclei

D .... Zero field splitting

r_L .... Laser illumination rate

Acknowledgement

The past three years have been rich of new experiences for me. I learned a lot of new things, got to know new people, had experiences of success and also faced challenges. Luckily, during all that time I could rely on the support of my colleagues, friends and family.

My special thanks goes to my supervisor Hendrik Weimer, who made this work possible and who did not mind taking all the time he could afford discussing with me and giving me advice. With all his knowledge and experience, he was able to show the way through scientific aberrations.

I had the pleasure to work together with members of other research groups, among them Alexey Gorshkov and Mohammad Maghrebi from the University of Maryland, Yonatan Hovav, Hadas Inbar and Nir Bar-Gill from the University of Jerusalem aswell as Augustine Kshetrimayum and Roman Orus from Universität Mainz. Thanks for your immense support, I really enjoyed our collaboration and I am proud of what we achieved.

My thank also goes to all members of the Weimer group and the Santos group of the ITP of the Leibniz University. I always had the feeling of being surrounded not only by colleagues, but also by friends. I enjoyed working and and sharing my time with you, I will deeply miss the great atmosphere here.

Among these I want to mention the postdoc of our group, Maryam Roghani. Beside a lot of laughter and shared experiences, we had fruitful scientific discussions and she always offered help whenever I asked for it.

During these years, some ties to Berlin endured. My gratitude goes to Faris Kadi, whom I know from my Master's time at TU Berlin. With his fresh experience in doing a Ph.D. in theoretical physics, he was always able to give me advice on how to deal with problems. Moreover, his encouraging and motivating words never failed to cheer me up. I cannot thank enough for the emotional support I recieved from my parents and my siblings.

My last and most hearty thanks goes to Lara. During the past three years, she proved to be a good listener and a great supporter. How did I deserve you?

Publications

V. R. Overbeck, H. Weimer, Time evolution of open quantum systems, Phys, Rev. A **93**, 012106 (2016)

V. R. Overbeck, M. F. Maghrebi, A. V. Gorshkov and H. Weimer, Multicritical behaviour in dissipative Ising models, Phys, Rev. A **95**, 042133 (2017)

Curriculum vitae

Vincent Raphael Overbeck
Fössestraße 48
30451 Hannover
Lower saxony, Germany

E-mail : vincent.overbeck@web.de
Mobile : +(49) 15771583842

Education

since 02/2015	:	Doctoral student in physics, Leibniz University of Hannover
04/2013-01/2015	:	Master's programme in physics, Technical University of Berlin
04/2010-03/2013	:	Bachelor's programme in physics, Technical University of Berlin
06/2009	:	Abitur, Kaserin Auguste Viktoria Gymnasium in Celle

Selbstständigkeitserklärung

Hiermit versichere ich, die vorliegende Doktorarbeit selbstständig und unter ausschließlicher Verwendung der angegebenen Hilfsmittel angefertigt zu haben.

Hannover, März 2018

Vincent Overbeck